Structural, Electrical and Optical Properties of $Zn_{1-x}Cd_xO$ Alloys using Density Functional Theory

SUBMITTED BY

WASEEM AHMAD QURESHI

Reg. # 159-FET/MSEE/F08

Department of Electronic Engineering (DEE),

Faculty of Engineering and Technology (FET),

International Islamic University (IIU), Islamabad

SUPERVISOR

DR. AFAQ AHMAD

Associate Professor, COE in Solid State Physics (CSSP),

University of the Punjab (PU), Quaid-i-Azam Campus, Lahore

2014

Structural, Electrical and Optical Properties of $Zn_{1-x}Cd_xO$ Alloys using Density Functional Theory

Waseem Ahmad Qureshi

(Reg. # 159-FET/MSEE/F08)

This dissertation is submitted to Faculty of Engineering and Technology, International Islamic University, Islamabad, Pakistan for partial fulfillment of the degree of **MS Electronic Engineering** with specialization in **Signal & Image Processing** at the Department of Electronic Engineering.

Faculty of Engineering and Technology (FET),

International Islamic University (IIU), Islamabad, Pakistan

Supervisor:

Dr. Afaq Ahmad

CSSP, PU, Lahore

June 2014

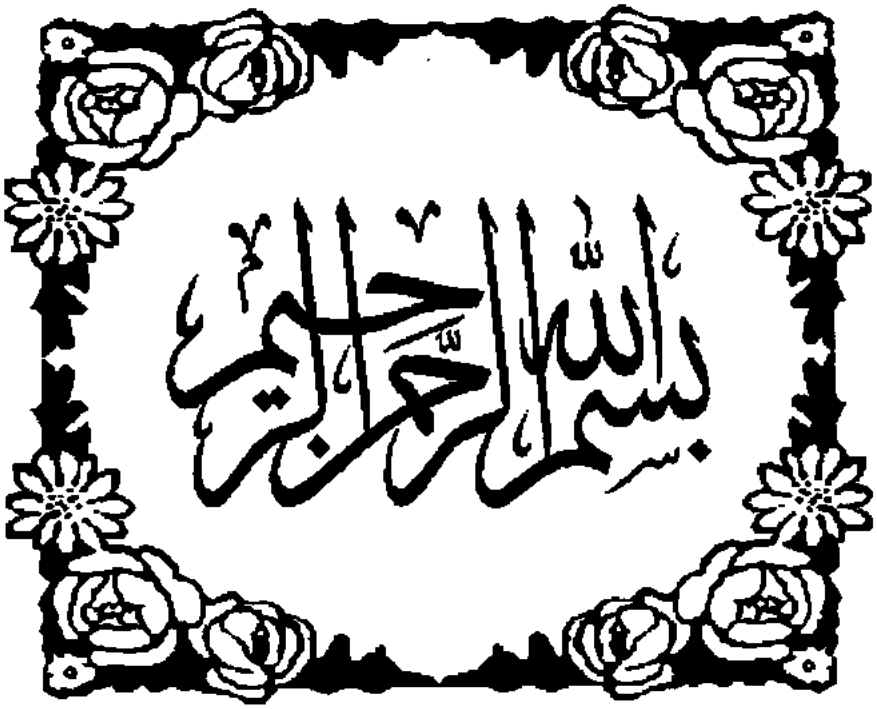

In the name of Allah (SWT) the most beneficent and the most merciful

DUAA

My Allah! Grant me that I should be grateful for Thy favor which Thou have bestowed on me and on my parents, and that I should do good such as Thou art pleased with, and make me enter by Thy mercy into Thy servants, the good ones.

[Para 27, Surah Al-Naml, Ayah 19]

DEDICATED TO MY PROJECT SUPERVISOR, PARENTS, SISTERS, BROTHERS, RELATIVES AND FRIENDS

DECLARATION

I certify that the research work titled, "Structural, Electrical and Optical Properties of $Zn_{1-x}Cd_xO$ Alloys using Density Functional Theory" is my own work and has not been presented elsewhere for assessment. Moreover, the material taken from the other sources has also been acknowledged properly.

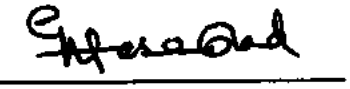

WASEEM AHMAD QURESHI

Reg. # 159-FET/MSEE/F08

CERTIFICATE OF APPROVAL

Title of Thesis: Structural, Electrical and Optical Properties of $Zn_{1-x}Cd_xO$ Alloys using Density Functional Theory

Name of Student: Waseem Ahmad Qureshi

Registration No: 159-FET/MSEE/F08

Accepted by the Faculty of Engineering and Technology, International Islamic University, Islamabad, Pakistan in partial fulfillment of the requirements for the Master of Science (MS) Degree in Electronic Engineering.

VIVA VOICE COMMITTEE:

Dean Engineering
Dr. Aqdas Naveed Malik
DEE, FET, IIU, Islamabad

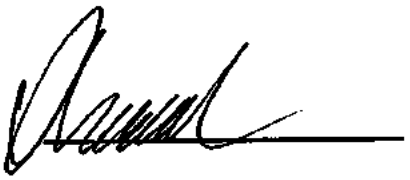

Chairman / HOD
Dr. Muhammad Amir
DEE, FET, IIUI

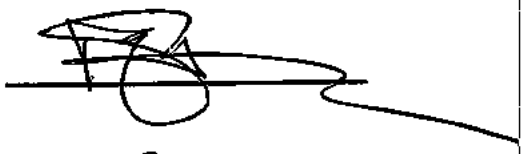

External Examiner
Dr. M. M. Talha
KRL, Islamabad

Internal Examiner
Dr. Adnan Umer
DCE, FET, IIUI

Supervisor
Dr. Afaq Ahmad
CSSP, PU, Lahore

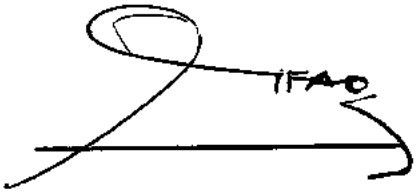

June 2014

ACKNOWLEDGEMENT

All praise and glory goes to Allah Almighty (Subhanahu Wa Ta'ala) who gave me courage and patience to carry out this research work. Peace and blessings of Allah be upon his last prophet Mohammad (Sallulaho Alaihe Wassalam) and all his Sahaba (Razi Allaho Anhum) who devoted their lives for the prosperity and spread of Islam.

First of all I would like to thank my Supervisor, **Dr. Afaq Ahmad**, Associate Professor, Center of Excellence in Solid State Physics (CSSP), University of the Punjab (PU), Quaid-i-Azam Campus, Lahore, with help of him this thesis could be possible. I'm also grateful to the other staff for their meritorious services. Then, I would like to thank the Director CSSP, **Prof. Dr. Shahzad Naseem**, who facilitated me work in the WIEN2K Lab and provided with the fully supportive research environment. I extend my gratitude to the Center-fellows, **Mr. Bakhtiar Jadoon**, and **Mr. Muhammad Ashraf**, who helped me a lot during my thesis. I am also thankful to the Computer Lab Administrator, **Mr. Abid**, for all the possible helps.

I would also like to thank Department of Electronic Engineering (DEE), International Islamic University (IIU), Islamabad, for all the possible services. I would also like to thank the Dean of Electronic Engineering, **Dr. Ahmad Shuja Syed**, and the Focal Person, **Dr. Ihsanul Haq**, for their nicest behaviors and guidance. I'm also thankful to the Engineering faculty staff. I'm also grateful to my class-fellows **Mr. Syed Fazil Bin Farrukh** and **Mr. Baqir Ali** for their guidance, and most thankful to my senior, **Mr. Qaiser Mushtaq**, who helped me compose the thesis.

I would like to thank my beloved parents and family members, especially my brother, **Mr. Naeem Ahmed Qureshi**. Their prayers and encouragement have always helped me take the right steps in life. There is no way and no words to express my love and gratitude.

Waseem Ahmad Qureshi

ABSTRACT

The first principle calculations established on density functional theory (DFT) are the most contemporary influential techniques to study the ground state properties of solid materials. In this research work, we analyzed the structural, electrical and optical properties for $Zn_{1-x}Cd_xO$ alloys for x = 0 to 75% in the zinc blende (ZB) phase. For this purpose, we adopted the full-potential linearized augmented plane wave plus local orbitals (FP-LAPW + lo) method based on the DFT within the generalized gradient approximation (GGA) scheme, especially the Wu-Cohen GGA formalism.

In the structural properties, we find that the lattice constant 'a', bulk modulus 'B' and its derivative with respect to pressure 'B′' are in enough accordance with the experimental results for ZnO. In electrical properties, the density of states (DOS) and the direct band gap (BG) are very close to the experimental results showing that ZnO is a semiconductor.

The structural properties of the $Zn_{1-x}Cd_xO$ alloys reveal that the lattice constant in these alloys goes on increasing with the increase in the cadmium (Cd) concentration into ZnO while the bulk modulus decreases correspondingly and its derivative as well. In electrical properties, we calculate the electron charge density 'ρ(r)', DOS and BG of the $Zn_{1-x}Cd_xO$ alloys to analyze the bonding character, orbital hybridization and energy states. The bonding character of $Zn_{1-x}Cd_xO$ alloys reveals that the $Zn_{0.75}Cd_{0.25}O$ alloy possesses the semiconductor behavior while the BG calculations indicate that the $Zn_{0.50}Cd_{0.50}O$ and $Zn_{0.25}Cd_{0.75}O$ alloys are metallic in nature. The optical analysis of the $Zn_{1-x}Cd_xO$ alloys reveals that the imaginary part '$\varepsilon_2(\omega)$' of the dielectric function decreases with the increase in energy while the real one '$\varepsilon_1(\omega)$' increases correspondingly. The joint density of states (JDOS) and the conductivity 'C' decrease with the fall in the energy. The energy loss function 'L' and the refractive index 'n' increase with the increase in the energy. The optical transition between the uppermost valence band and the lowest conduction band was found to be shifted towards the low energy range with the increasing concentration x of cadmium.

TABLE OF CONTENTS

LIST OF FIGURES

LIST OF TABLES

Chapter 1

INTRODUCTION

This dissertation comprises the Structural, Electrical and Optical properties and their statistics in the zinc blende (ZB) phase for the zinc oxide (ZnO) binary compound and changes produced in its properties by its substitution with cadmium (Cd) to make $Zn_{1-x}Cd_xO$ tertiary alloys. As zinc belongs to Group II of the Periodic Table while oxygen does Group VI, so ZnO is called a Group II-VI compound having semiconductor properties due to consisting of a direct and wide band gap (BG). Changes in the BG of the $Zn_{1-x}Cd_xO$ compounds have also been investigated and it is observed that the BG of a ternary alloy decreases as we increase the doping of Cd in the range x = 0 – 75%. However, the optical properties concerned with the contraction of the band gap of the $Zn_{1-x}Cd_xO$ alloys have not fully been determined and we still have not unveiled an optical transition completely. In this respect, the First-Principles formalism is charming to research on the optical properties of the $Zn_{1-x}Cd_xO$ compounds. In our calculation procedure, the full potential linearized augmented plane wave (FP-LAPW) method in the WIEN2k software package [1] will be used for our solid material under the first principles method.

There are immense applications of ZnO in many fields. It is used as a substrate in solar cells, varistors, heterojunctions, transparent conductors, thin film gas sensors, surface electroacoustic wave devices, light emitting diodes (LEDs), ultraviolet (UV) solid state emitters and detectors, UV LASERs, LASER diodes, etc. [2]. There is marvelous attraction for the optical properties of ZnO in the commercial fields which require the optoelectronic instruments that can be operated in the spectral or deep blue region. In the optoelectronic applications, there is the great importance of heterostructures of ZnO formed with the Group II-B oxides (CdO, HgO, etc.) having the little band gaps than that of ZnO [3]. We hope that our theoretical results would help the experimentalists in the optoelectronic industry for the fabrication of devices.

1.1. Zinc Oxide

The chemical properties of zinc oxide indicate that it is an inorganic compound. It is also called Plaster of Paris. It is found in the form of white powder which rarely dissolves in water. The powder is usually used as an additive into various things and products like glass, ceramics, plastics, rubbers, paints, lotions, ointments, cosmetics, lubricants [4], adhesives, pigments, sealants, batteries, fire retardants, food, and the first-aid equipment, etc. It is found in the natural form as Zincite – a mineral, but its major production is commercially [5]. ZnO is inflammable.

Table 1.1 - Experimental calculations about zinc oxide

STATISTICS ABOUT ZINC OXIDE	
ELEMENT	VALUE
Appearance	White Solid
Smell	Odorless
Molar Mass	81.41 g/mol
Density (Specific Gravity)	5.607 g/cm^3 at 20 °C [6]
Aqueous Solubility	0.16 mg/100 mL at 30 °C
Melting Point	1975 °C [7]
Boiling Point	2360 °C
Refractive Index	2.004
Band Gap (Direct)	3.37 eV
European Union Classification	Dangerous to Atmosphere

1.1.1. Properties

1.1.1.1. Structural Properties

Hexagonal Wurtzite Structure

It is the most found common compound due to having a stable structure under the confined conditions [8]. The centers of both zinc and oxide lie at a tetrahedral. The polymorphs of the hexagonal wurtzite have no inversion symmetry which means that the reflection of this crystal about a certain point cannot convert it into itself. This property along with other symmetry properties of the lattice concludes the Piezoelectricity and Pyroelectricity of the hexagonal structure of ZnO. The piezoelectricity means the

generation of electricity when a crystal or a specific substance is compressed and the pyroelectricity is the production of the electricity through a material due to change in its temperature.

Due to the ionic bonding in ZnO with the Zn^{+2} radius of 0.074 nm and 0.140 nm of O^{-2}, the major formation is of the wurtzite structure rather than the zincblende one [9] and a high value of piezoelectricity can be detected. Due to the polar bonding in ZnO, the zinc and oxygen planes contain positive and negative electric charges respectively, which are naturally smooth, constant and they don't need to reform themselves to keep electrical neutrality like the other materials whose surfaces themselves rebuild at the atomic level in order to maintain the electrical neutrality. Hence, we need to completely describe this inconsistent behavior of ZnO [10].

The point group of the structure is 6 mm according to the Hermann-Mauguin notation or C_{6v} in the Schoenflies notation and the space group is $P6_3mc$ or C_{6v}^4. Its Strukturbericht designation is B4 [11].

The lattice constants are a = 3.2501 Å and c = 5.2071 Å and their ratio c/a of the hexagonal cell as 1.6021 is near to the ideal c/a ratio equal to 1.633 [12]. A unit cell of the Wurtzite ZnO phase with the atomic positions Zn (1/3, 2/3, 0) & (2/3, 1/3, 1/2) and O (1/3, 2/3, μ) & (2/3, 1/3, μ + 1/2) having μ = c/a as a certain parameter is shown below:

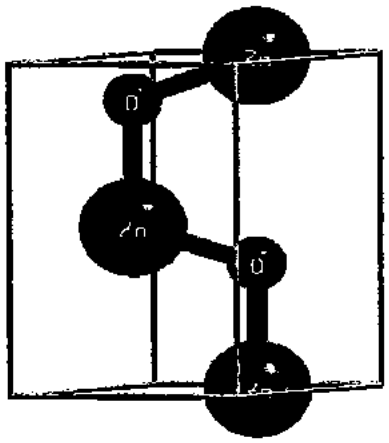

Figure 1 - Unit cell structure of ZnO in the Wurtzite phase

Cubic Zincblende Structure

It is a temporary structure appearing during the fabrication of the wurtzite structure of ZnO and was named by the mineral Sphalerite, also called Zincblende [13]. It can be alleviated by mounting ZnO on substrates with the cubical lattice shapes. The centers of both zinc and oxygen position at the tetrahedral and this property along with other symmetry properties of the lattice, results in the piezoelectricity of the zincblende structure of ZnO. The closest neighbors of every atom comprise four contrary atoms placed at the four corners of the systematic tetrahedral. In this structure, the arrangement of atoms is that of the diamond cubic structure but the atom types at lattice sites lie alternately. Also, the polymorphs of zinc blende have no inversion symmetry.

Its space group is F43m according to the Herman-Mauguin notation or "number 216" according to International Tables for Crystallography [14, 15]. Its Strukturbericht designation is B3 [11]. A ZnO zincblende unit cell with the atomic positions Zn (0, 0, 0) and O (1/4, 1/4, 1/4) has been shown in the following figure:

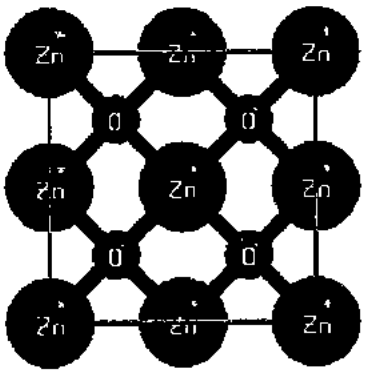

Figure 1.2 - Unit cell structure of ZnO Zincblende

Cubic Rocksalt Structure

This structure is like that of sodium chloride (NaCl) or Halite and is visible at high pressure of 10 GPa [16]. In this structure, each of two atom types builds a detached face-centered lattice and two lattices pierce mutually to construct a 3-dimentional checkerboard arrangement. The structure can be formed more possibly if the size of the

cation is little bit smaller than that of the anion such that the ratio of the radii of cation and anion may have a value from 0.414 to 0.732. The interatomic distance between the cation and anion (half the length of the unit cell) is 2.8 Å for NaCl [17]. Every atom in this structure has a coordination number of 6, i.e., every cation is organized with 6 anions and every anion is coordinated to 6 cations on the corners of an octahedron.

Its space group according to the Herman-Mauguin notation is Fm3m or 225 in International Tables for Crystallogarphy. Its Strukturbericht designation is B1 [11]. A unit cell of the rocksalt structure with atomic positions Zn (0, 0, 0) and O (1/2, 1/2, 1/2) is shown below:

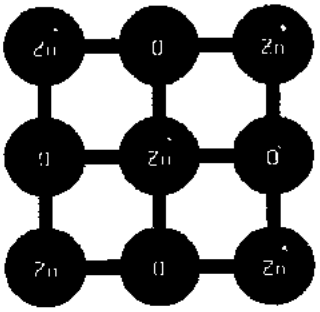

Figure 1.3 - Unit cell structure of Rocksalt ZnO

The crystal structure of ZnO in three phases has been shown below:

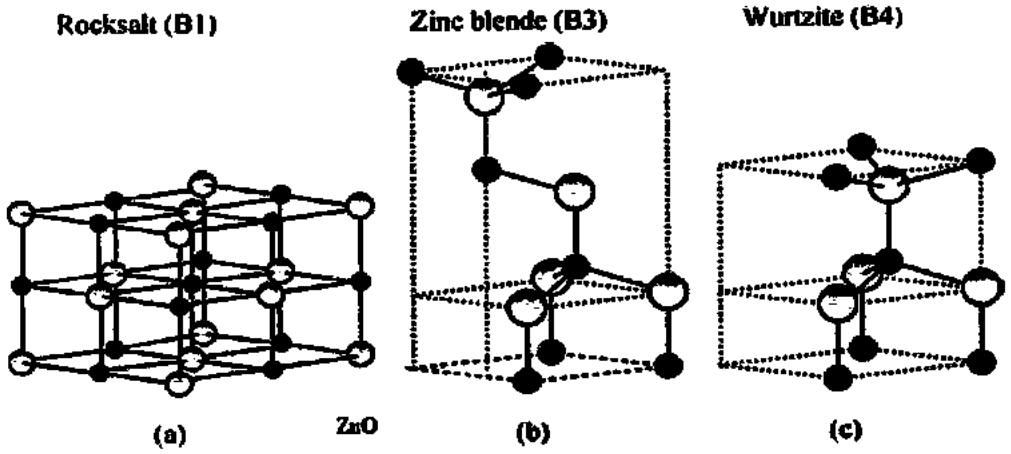

Figure 1.4 - ZnO structure in three phases B1, B3 and B4 [16]

1.1.1.2. Electrical Properties

ZnO being a semiconductor is high electron mobile, vast band gapped, transparent and intensively luminescent at room-temperature. At this temperature, the value of the ZnO band gap (BG) is 3.37 eV or 375 nm which facilitates us attain low noise in electronics, high values of breakdown voltage, persistent wide electric fields, higher temperatures and bigger power operations. The BG can be upgraded to 4 eV by alloying ZnO with cadmium oxide (CdO) or any other binary compound [16].

ZnO compounds often behave as N-type materials even we don't perform its planned doping. The N-type behavior appears due to non-Stoichiometry, but the matter is debatable [18]. A substitute grounded on the theoretical measurements has been described for this controversy indicating that the unintentional hydrogen impurities cause this behavior [19]. We can also obtain the manageable N-type doping simply on the substitution of Zn in the Group III elements like aluminum (Al), gallium (Ga), Indium (In), etc. or oxygen with the Group VII elements as chlorine (Cl) or iodine (I) [20].

A P-type doping of ZnO is unreliable because P-type dopants are less soluble and have less reimbursement with abundant N-type impurities. In intrinsic N-type materials, measurement of the P-type doping is obscure due to inhomogeneity of the sample materials [21]. Electronic and optoelectronic uses of ZnO, which normally need PN-Junctions, are not limited by the constrained P-doping. The discovered P-type dopants comprise of the Group-I elements [lithium (Li), sodium (Na), potassium (K), etc.] and the Group-XV elements [nitrogen (N), phosphorus (P), arsenic (As), etc.] as well as the Group-XI elements [copper (Cu), silver (Ag), etc.]. Among these dopants several being deep acceptors are unable to generate apparent conduction of P-type at room temperature [16]. In ZnO, mobility of the electrons is highly temperature dependent having maximum value of 2000 $cm^2/(V.s)$ at 80 K [22]. The mobility of holes has meager calculations and some determined values range 5–30 $cm^2/(V.s)$ [23].

1.1.2. Applications

1.1.2.1. Optical Usage

Diodes

Because of the wide direct band gap of ZnO, this compound is mostly applicable in the light emitting diodes (LEDs) and LASER diodes [24, 25] which are emerging technologies of the past year, 2009.

Bright Emission

The exciton binding energy (EBE) of ZnO is 60 meV. It is 2.4 times of its thermal energy at room temperature which causes a bright emission from ZnO as compared to GaN having a band gap of 3.4 eV near that of ZnO but with the lower EBE at room temperature. Therefore, due to resemblance a few optoelectronic uses of ZnO superimpose with those of GaN and we can mix GaN in ZnO for different applications of the LEDs [26].

Radiation Resistor

ZnO being highly stable is a good resistive target for high energy radiations [27]. It is also applicable to researches in Space Science [28]. It decomposes at 1975 °C [7] into Zn vapours and O_2 molecules showing its high stability.

Random LASERS

The electronically pumped ultra-violet (UV) LASER sources in the area of Random LASERS [29, 30] are generated by ZnO.

Transparent Electrodes

The ZnO layers doped with Al work as transparent electrodes. Commercially, ZnO is used as transparent electrode in liquid crystal displays (LCDs) [31], face contacts for solar cells and energy saving windows.

Photocopying

The largest application of ZnO was in photocopy in which ZnO of high quality manufactured by the French process was used as a filter in the photocopying paper but was soon replaced [32].

1.1.2.2. Electrical Usage

Electric Field Emitters

Nano-rods of ZnO are used as field emitters because their point tips work as levers of the intense electric field [33].

Field Effect Transistors

ZnO having the negligible P-type doping can be used in the formation of field-effect transistors (FETs) because they don't need a PN-junction. A few of the FETs use ZnO nano-rods as the conducting media [34].

Spintronics

If we dope ZnO with 1-10% of magnetic ions of iron (Fe), manganese (Mn), cobalt (Co), etc., then it becomes a ferromagnetic substance even at room temperature. The ferromagnetism of ZnO and Mn occurs at room temperature but is doubtful about its origin whether it is from the matrix itself or from the phases of a secondary oxide [35].

Piezoelectricity

In semiconductors, bonded tetrahedral, ZnO has the highest piezoelectric tensor which makes it important technologically for several piezoelectrical applications demanding large electromechanical couplings [36]. Fibers coated with ZnO are able to fabricate "self-powered nano-systems" [37] and generate piezoelectricity by activities of our body or every day mechanical stresses caused by wind [38].

Biosensors

ZnO having fast kinetics to transport the electrons and high bio-compatibility is applied as a bio-mimic membrane to halt and transform bio-molecules [39].

1.2. Cadmium

It is a bluish-white, ductile, malleable and soft bivalent metal. It is diamagnetic [40]. It resembles zinc and mercury in various aspects but forms complex compounds [41]. The electronic configuration of Cd is $1s^2$, $2s^2$, $2p^6$, $3s^2$, $3p^6$, $3d^{10}$, $4s^2$, $4p^6$, $4d^{10}$, $5s^2$.

Table 1.2 - Statistics about cadmium

DATA ABOUT CADMIUM	
Classification	Transitional Metal & Toxic
Atomic Number	48
Periodic Group	12
Block	d
Space Group	194, P63/mmc
Atomic Mass	
Density	8.65 g/cm^3 at 293 K
Oxidation State	+2
Melting Point	320.9 °C
Boiling Point	765 °C
Lattice Constants	a = b = 297.94 & c = 561.86 pm
Crystal Angles	$\alpha = \beta = 90°$ & $\gamma = 120°$

Its structure is hexagonal closed pack (HCP) [42] as shown in the following figure:

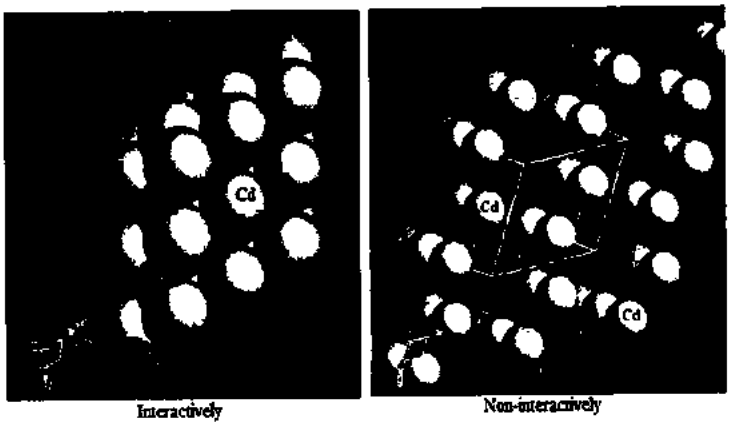

Figure 1.5 - Structure of cadmium [42]

1.2.1. Applications

1.2.1.1. Electrical Applications

Batteries

Cd is mostly used in batteries, especially in the rechargeable Ni-Cd batteries. In 2009, the world used 86% of Cd in batteries. A nickel-cadmium cell is made up of a nickel hydroxide anode and a cadmium cathode separated by a potassium hydroxide (KOH) alkaline electrolyte. The European Union (EU) forbade the cadmium usage in Electronics in 2004 with numerous exemptions but permitted the quantity of the Cd usage in Electronics up to 0.002% [43].

Electroplating

In electroplating, 6% cadmium is used. The Cd electroplating is often used in the Aircraft Industry because the Cd-plated steel objects offer the excellent corrosion resistance [44]. The passivation can occur in the Cd coating by using the chromate salts [45]. The hydrogen embrittlement of the high-strength steels is restricted by the Cd plating which occurs during the electroplating method. The steels, having the tensile strength above 1300 MPa/200 ksi obtained after the heat treatment, must be coated by the physical vapor deposition method or the special low-embrittlement cadmium electroplating technique. The titanium (Ti) embrittlement, produced due to the cadmium-plated tool residues, was banished due to these tools and the routine tool testing programs for finding the Cd contamination were also banned by U-2; 12/SR-71 and the successive aircraft programs consuming Ti [46].

Soldering

Cadmium is used in solders [44]. A solder is an alloy of metals having the melting point ranging from 90 to 450 °C. The solder is fused to join the metallic surfaces and is especially used in Electronics and Plumbing.

Solar Cells

A few compound semiconductors used for light detection contain Cd as a constituent in the forms of cadmium selenide, cadmium telluride and cadmium sulfide materials [44]. When light falls on these materials, they start conducting currents.

1.2.1.2. Optical Applications

LASER and Lab Experiments

The helium-cadmium (He-Cd) LASERs, operating at 325 or 422 nm, are a good mutual source of the blue UV LASER light. They are applied in fluorescence microscopes and several laboratory experiments [47, 48].

Quantum Dots

Quantum dots (QDs) of cadmium selenide under the ultraviolet (UV) excitation in the He-Cd LASER produce an intense luminescence which may have yellow, green or red colour depending upon the sizes of the particles. The QDs are the solid state structures consisting of metals or semiconductors which contain a countable small quantity of electrons in a narrow space. The electrons are confined by introducing the insulating materials which surround the central conducting areas. The QDs colloidal solutions are used for imaging purposes in Biology, and make solutions by a fluorescence microscope [49].

Television Picture Tubes

The black and white television picture tubes use cadmium oxide (CdO) as the black and white phosphors and the coloured television picture tubes comprise CdO as red, green and blue (RGB) phosphors [50].

Photocopier

The surfaces of photocopier drums are coated by cadmium sulfide (CdS) for the photoconductive purposes [51].

Infra-Red Light Detectors

Sensitivity of mercury cadmium telluride (HgCdTe) to the infra-red light applies that it can be used as an infra-red light detector in [52] or it can be a switch in the remote control devices.

Stabilizer

In the Polyvinyl Chloride Industry, cadmium is used as the heat, light, and weathering stabilizer [44, 53].

Blocker

In Molecular Biology, Cd is used to block voltage-dependent calcium channels from fluxing calcium ions.

1.3. $Zn_{1-x}Cd_xO$ Alloys

1.3.1. Photoluminescent Properties of the $Zn_{1-x}Cd_xO$ Alloys

The $Zn_{1-x}Cd_xO$ alloys are considered as the ideal solids for making instruments based on ZnO. On alloying with CdO having a narrow BG of 2.3 eV, we can red-shift the band gap (BG) of ZnO to the blue and green light spectral regions. Resemblance of Zn and Cd in their radii and the other fundamental properties demands a suitable constituent of CdO into ZnO for the fabrication of $Zn_{1-x}Cd_xO$ or ZnO heterojunctions or super-lattices which are the main entities in the ZnO based light emitting and light detecting devices. However, the most researches on thin films of the $Zn_{1-x}Cd_xO$ alloys are not congenial because there coexist multiphases or polycrystalline shapes with the undesired orientations. Hence, there are a very few reports on the photoluminescence properties of the $Zn_{1-x}Cd_xO$ alloys [54].

1.3.2. Optical Behavior of the $Zn_{1-x}Cd_xO$ Alloys Developed by the Molecular Beam Epitaxy (MBE)

During the formation of $Zn_{1-x}Cd_xO$ alloys, the heterostructures and quantum structures are produced which are the indicators of the energy E_g of the band structures. The $Zn_{1-x}Cd_xO$ compounds are the proper nominees for realization of the band gap engineering (BGE) due to the slight energy value of the direct band gap of the CdO compound. If we want to get the full recognition of the BGE of the $Zn_{1-x}Cd_xO$ compounds, then we will have to get comprehensive knowledge of the basic parameters (compositional and temperature dependences of energy bands) of these compounds.

As the Cd content x is increased, Eg decreases and the compositional dependences have been found deviating prominently among the different researches. Also effects on the temperature dependences of the band gaps of the $Zn_{1-x}Cd_xO$ alloys with the increasing Cd concentration x are rarely known.

Now we will use the temperature depending reflection and optical absorption statistics to study the compositional and temperature dependences of the BGs of the $Zn_{1-x}Cd_xO$ compounds with Cd compositions x up to 15.7% [55]. The following figure shows the absorption spectrum for epilayers of the $Zn_{1-x}Cd_xO$ alloys at room temperature in $(\alpha h\nu)^2$ versus hv coordinates:

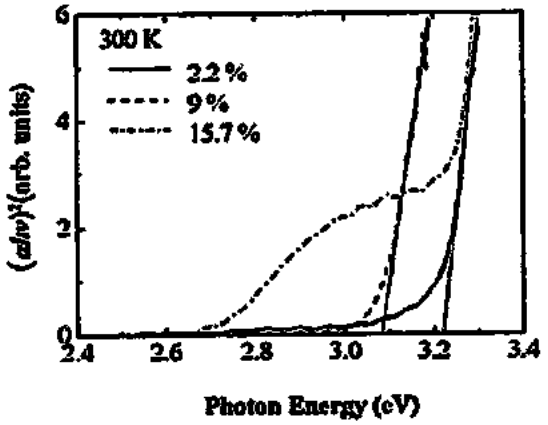

Figure 1.6 - Spectral dependences of the absorption coefficient for the ZnCdO alloys under the certain Cd concentrations at room temperature [55]

The linear part of the plot has been inferred to zero to get BG energies in the $Zn_{1-x}Cd_xO$ alloys. The alloys which absorb the Cd contents of 2.2% or 9%, their spectra display the desired linear dependence, otherwise the alloys with Cd content x = 15.7% exhibit a strong deviation from the linear relation. It occurs due to the tough compositional non-uniformity or the phase separation for the Cd composition x with high quantity which makes it uncertain to find the BG energy E_g for the alloys. Figure 1.6 expresses the compositional dependence of the calculated fundamental E_g of the $Zn_{1-x}Cd_xO$ alloys.

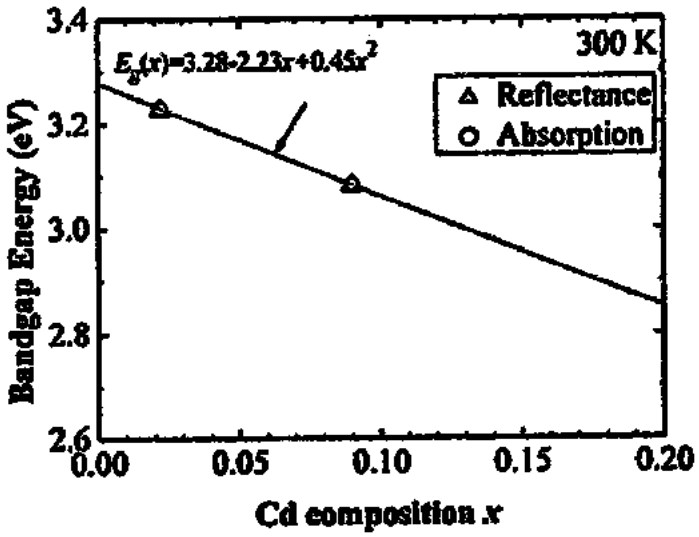

Figure 1.7 - Changes in the band energy of ZnCdO as a function of the Cd doping x [55]

Here, the circles describe the values derived from the absorption calculations. The triangles display consequences of the performed complementary reflectance statistics. The results from two measurements are in accordance with one another and spotlight the reliability of the preassumed values. The bowing parameter in the BG energy of the alloys is found when the experimental measurements fit in the conventional equation as given below:

$$E_g^{ZnCdO} = (1-x)E_g^{CdO} + xE_g^{ZnO} - bx(1-x). \quad (1.1)$$

Here, E_g^{ZnCdO}, E_g^{ZnO} and E_g^{CdO} are the BG energies of the $Zn_{1-x}Cd_xO$, ZnO and CdO compounds respectively and 'b' is called the bowing coefficient. The equivalent results have been shown in the above figure by the solid line. $E_g^{CdO} = 1.5$ eV for the Wurtzite phase of CdO has been assumed theoretically which gives b = 0.45 eV because we don't know the properties of CdO in this phase. The experimental value computed for b is specific for the semiconducting compounds having a short difference in the electronegativity of the end binaries and is acceptable for the $Zn_{1-x}Cd_xO$ alloys [55].

The absorption and reflectance data was also used to observe the effects of the Cd substitution x in the ZnO compound on the variations in temperature in the elementary band gap of the investigated ZnCdO compounds. The alloys with high Cd contents showed a decrease in the variation of the BG energy with the increase in the temperature.

We applied the optical absorption and reflectance data to compute the compositional and temperature dependences of the energies of the band gaps in the $Zn_{1-x}Cd_xO$ alloys developed by the MBE. The compositional dependence of the BG energy of a ZnCdO compound was exposed to follow the style [55] given by:

$$E_g(x) = 3.28 - 2.23x + 0.45x^2. \quad (1.2)$$

The inferiority in the quality of a $Zn_{1-x}Cd_xO$ alloy because of the proper phase separation produced a quicker red shift of absorption edge. It was also revealed that the Cd concentration slightly slowed down the variation in the BG energies with respect to the changes in temperature and it might be valuable for future applications of ZnO-based instruments [55].

Chapter 2

DENSITY FUNCTIONAL THEORY

2.1. Introduction

Density functional theory (DFT) is a quantum mechanical modeling tool by which we examine the electronic structure, energy states and optical properties of many-body system models (atoms, molecules and condensed matter phases) in Physics, Chemistry and Materials Science. Especially, the ground-states of solids are investigated by the DFT. It is adaptable and being most popular, it is contemporarily widely applicable in Computational Physics, Condensed Matter Physics and Computational Chemistry. The DFT is generally applied for the interacting Fermions (quarks, electrons, muons and neutrinos) but we will consider here the electrons only.

The electrons are not expressed by their many-body wave functions but by their densities only. A solid consisting of N electrons which obey Pauli's exclusion principle (PEP) and undergo Coulomb's repulsive potential (CRP), depends on the spatial fundamental variables x, y and z only despite the 3N degrees of freedom.

This theory comprises functionals (functions of the other functions) for revealing properties of the many-electron sample materials. The functional used here is the electron density depending on space. Therefore, the title "Density Functional Theory" was proposed due to the consumption of the functionals of the electron density. This technique comprises dual rewards of being capable of solving various issues up to satisfactory accuracy and being computationally easy.

2.1.1. History of the DFT

The DFT has been dormant in simulations of the periodic phenomena in Quantum Mechanics since last 35 years about. Since 1970, the DFT has become a charismatic technique for computations in Solid State Physics and Electronics. It has been probated in severe cases and was found that the calculations by the DFT under the local density approximation (LDA) displayed the desired results at lower computational prices than the

other methods used to solve the quantum mechanical many-body problems based on the complex wave functions. However, the DFT was found sufficiently imprecise in deriving satisfactory results in Quantum Chemistry till 1990s. Then approximations used in the DFT were sophisticated to describe effective models of exchange and correlation interactions for calculations of solids to verify experimental results.

In these days, the DFT has excelled in both the fields for structural, electrical and optical properties of solids. Although the DFT has been given various improvements, yet it comprises a few ambiguities like the proper expression of intermolecular interactions e.g., Van der Waal's forces, band gap calculations in semiconductors [56], excitations in charge transfer, transition states, global potential energy surfaces, intense correlated systems, systems ruled by dispersion, e.g., interacting atoms of noble gases [57] and overwhelming of dispersion on the other effects as in biomolecules [58].

Contemporarily, construction of better approximations, changes in functionals [59], inclusion of additive terms and modernization of the DFT methods with sound applications to control these issues is a major field of the current research [60, 61, 62].

2.1.2. Methodology of the DFT

The Electronic structure theory (EST) comprises the formal methods based on the complex many-electron wave function like the Hartree-Fock theory (HFT) and its posterities but the motto of the DFT encloses a replacement of the wave function of a many-electron system by its electron density being a basic entity in the computations of properties of solids.

Also, the many-body wave function depends on 3N variables according to Lagrangian Mechanics, i.e., there are three spatial variables (x, y, z) for everyone of N electrons, that is, xN, yN, zN = (x, y, z)N independent coordinates are required, while the electron density depends only on the spatial variables x, y and z under the use of the functionals of the electron density.

The Ancient theory of molecules in a solid contains the non-uniform electron clouds, also called the inhomogeneous electron gases. According to the Born-Oppenheimer approximation (BOA), an inhomogeneous electron gas consists of a combination of interacting electrons which travel quantum mechanically through a potential field produced by the collection of the stationary nuclei of atoms. A solution of such a model bases on the approximation patterns, like the independent electron approximation (IEA), Hartree theory (HT) and HFT but the DFT has become extremely widespread method for the solution of such an issue [63] as supported by the following figure:

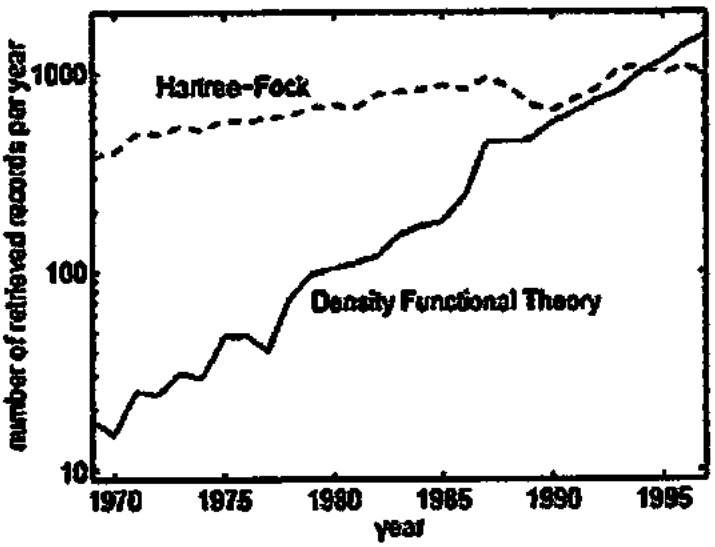

Figure 2.1 - Graph for the increased use of the DFT by a number of the Information Services for Physics, Electronics and Computing (INSPEC) databases, IET, UK for a certain year [63]

The Hohenberg-Kohn (HK) first theorem expresses properties of the ground state of a many-electron system model calculated by the help of the electron density depending on three spatial coordinates only. It provides us with a milestone for converting a problem of N electrons having 3N spatial coordinates to 3 spatial coordinates on using the electron density functional.

We can enhance the theorem to an arena depending on time in order to model time-dependent density functional theory (TDDFT) which can be applied to demonstrate

the excited states. The HK second theorem describes a functional for the energy of the system and verifies that this energy functional is minimized by an accurate electron density of the ground state.

The DFT basically runs on the Kohn-Sham (KS) method also called the Kohn-Sham density functional theory (KSDFT) as its best pillar. In the KSDFT, we reduce a stubborn problem of many interacting electrons undergone a static potential field into a controllable many non-interacting electrons issue experiencing an affective potential. The effective potential is a combination of the external potential (EP) due to the nuclei and Coulomb's potential (CP) due to the electrons. It means that we concern with both the exchange and correlation interactions. The KSDFT suffers from troubles in shaping the exchange and correlation interactions. To overcome these issues, an easy approximation based on the exact exchange energy for a uniform electron gas called the LDA was developed from the Thomas-Fermi model (TFM) and the fittings to the correlation energy for a homogeneous electron gas system.

Recently, the DFT is being formulated without the HK theorems on the basis of the Legendre theory (LT) which transforms the external potential into the electron density [63]. There is a book "The Fundamentals of Density Functional Theory" by Helmut Eschrig (2003) comprising the detailed mathematical deliberations about the DFT. In it, the mathematical problems in a finite periodic system do not occur but the problems appear when we deal with an N-particle system having infinite volume.

2.2. DFT - A Solution of Quantum Many-Body Problems

A solid is considered to be an assembly of the massive positively charged particles (Nuclei) and the slight negatively charged particles (Electrons). For N nuclei, we have to deal with N+NZ particles which interact electromagnetically, termed as a many-body problem. The Hamiltonian for such a system is described by the following equation:

$$\hat{H} = -\frac{\hbar^2}{2}\sum_I^N \frac{\nabla^2 \vec{R}_I}{M_I} - \frac{\hbar^2}{2}\sum_I^N \frac{\nabla^2 \vec{r}_I}{m} - \frac{1}{4\pi\varepsilon_\circ}\sum_{I,J}^N \frac{e^2 Z_I}{|\vec{R}_I - \vec{r}_J|} + \frac{1}{8\pi\varepsilon_\circ}\sum_{i\neq j}^N \frac{e^2}{|\vec{r}_i - \vec{r}_j|} + \frac{1}{8\pi\varepsilon_\circ}\sum_{I\neq J}^N \frac{e^2 Z_I Z_J}{|\vec{R}_I - \vec{R}_J|} \quad (2.1)$$

Here M_i is mass of any nucleus lying at a displacement $\vec{R_i}$ and m is the mass of any electron at a position $\vec{r_i}$ where $\vec{r_i} = \vec{r_1}, \vec{r_2}, \vec{r_3}, \ldots, \vec{r_N}$. Z is charge on a nucleus. We will write all the vectors in the bold notation throughout the thesis.

In the above equation, the first term is an operator form for the kinetic energy (KE) of the nuclei; the second term is the KE of the electrons and the remaining three terms specify the Coulomb interaction between the nuclei and electrons, among the electrons themselves and with the electrons of the other atoms, and the nucleus of one atom with the other nuclei.

We are unable to solve this problem truly, but we will determine the suitable approximate eigenstates for which we will have to make approximations.

2.2.1. Born-Oppenheimer Approximation

"As the nuclei are too much massive and the electrons are slight, therefore the nuclei are supposed to freeze at the specific positions due to slow motion and the electrons are supposed to be in a sudden dynamic equilibrium with them."

In this Born and Oppenheimer approximation (BOA) [64], the nuclei are dispossessed of being actors in this many-body problem and concluded only as a certain source of positive charge exterior to the electron cloud which is a true player in this problem. Therefore, we have to deal with NZ electrons moving through the external potential produced by N nuclei.

As nuclei don't displace, so they have zero KE and the first term in equation (2.1) vanishes. The last term adopts a shape of a constant. So, Eq. (2.1) reduces to:

$$\hat{H} = -\frac{\hbar^2}{2}\sum_i^N \frac{\nabla^2 r_i}{m} - \frac{1}{4\pi\varepsilon_\circ}\sum_{i,j}^N \frac{e^2 Z_j}{|R_i - r_j|} + \frac{1}{8\pi\varepsilon_\circ}\sum_{i\neq j}^N \frac{e^2}{|r_i - r_j|}, \tag{2.2}$$

or

$$\hat{H} = \hat{T} + \hat{V}_{ext} + \hat{V}_{ee}. \tag{2.3}$$

The above equation shows that the KE and the electron-electron interactions are due to the many-electron system, not due to the many-proton system, experiencing an external nuclear potential due to the protons. The first two terms in the above equation are independent of a specific many-electron system to constitute a universal part being independent of the electrons of any solid material and a particular information about the system arrives us totally from the second term, $\hat{V}_{ext}$.

Our main focus is on the features of the DFT. Therefore, we are neglecting the spin coordinate throughout this topic for the simplification purposes.

2.2.2. Solution by the DFT

The many-body problem received after the BOA is too simpler than the original one but is still complicated to be solved. There are various methods to solve Eq. (2.2) to an approximate but a manageable form. The historic HF method, described in the condensed matter literature, performs nicely for atoms and molecules and is thus widely used in Quantum Chemistry but it is less precise for solids. Therefore, in spite of the HF method, we are going to apply a more sophisticated and influential method called the density functional theory DFT. It is a common technique to elucidate many-body problems. It is applicable to the electron gas but also to the proton and neutron gases for constructing the nuclear models or to the nucleus and the electron gas without the BOA to define solids with light elements as well.

2.2.3. Hohenberg-Kohn Theorems

In 1964, Hohenberg and Kohn provided us with two theorems called the Hohenberg-Kohn (HK) theorems [65] as discussed below:

Theorem 1

"Electron density under an additive constant, determines external potential."

In the other words, there is one to one correspondence between the ground state charge density $\rho(\mathbf{r})$ of a many-electron system and the external potential, V_{ext}. Its abrupt

outcome reveals that the expectation value of any observable quantity $\hat{Q}$ at the ground state is a unique functional of the exact ground state electron density as follows:

$$\langle \Psi | \hat{Q} | \Psi \rangle = Q[\rho]. \tag{2.4}$$

The statement of the first theorem indicates that the 1-1 correspondence between the density ρ at ground state and the external potential V_{ext} is fascinating. It emphasizes on the electron density which retrieves the Hamiltonian operator. The Hamiltonian is identified by the external potential and the total number of electrons N which may be determined by the density simply on integrating it over the whole space. We know that a certain many-electron system has a sole external potential that produces a many-particle ground state wave function Ψ with the Hamiltonian in Eq. (2.2). The wave function reveals us all the material properties. We can easily find the respective electron density $\rho(\mathbf{r})$ from the wave function Ψ. Thus, the external potential helps us calculate its equivalent unique ground-state density, but it seems as the density confines less informations than the wave function does.

If it is true, then it is impossible to compute a unique external potential from a given ground-state density only unless more parameters are given. This 1st theorem of Hohenberg and Kohn gives us an exact possibility that the density contains all the informations as the wave function does. Therefore, informations can be derived uniquely from the density and they may be expressed as functionals of the density $\rho(\mathbf{r})$.

A straight forward proof of the First HK theorem was generalized to add systems having the degenerate states by Levy in 1979 [66]. The theoretical spectroscopist, EB Wilson, introduced a direct proof of this theorem in 1962 which described that the electron density ρ revealed positions and charges of the nuclei uniquely resulting in the computation of the Hamiltonian trivially [67]. The reality behind this proof bases on the electron density which suffers a cusp near a nucleus such that:

$$Z_l = \frac{-\hbar^2}{2\rho_0} \left[\frac{\partial \overline{\rho(r_l)}}{\partial r_l} \right]_{r_l=0}. \tag{2.5}$$

Here, $\bar{\rho}$ is the spherical average of $\rho(\mathbf{r}_i)$ whose careful analysis gives the external potential from which the Hamiltonian can be computed. The Wilson's proof has less generalization than that of Levy, but is valid for the interactions among the electrons and nuclei.

From this discussion, we conclude that the energy is a functional of the charge density $E[\rho]$.

Theorem 2

For $\hat{Q}$ being $\hat{H}$, the ground state total energy functional $\hat{H}[\rho] \equiv E_{V_{ext}}[\rho]$ will shape as:

$$E_{V_{ext}}[\rho] = \langle \Psi | \hat{T} + \hat{V} | \Psi \rangle + \langle \Psi | \hat{V}_{ext} | \Psi \rangle \tag{2.6}$$

$$= F_{HK}[\rho] + \int \rho(\mathbf{r}) V_{ext}(\mathbf{r})\, d\mathbf{r}. \tag{2.7}$$

Here, $F_{HK}[\rho]$ is the Hohenberg-Kohn density functional defined by:

$$\langle \Psi | \hat{T} + \hat{V} | \Psi \rangle \equiv F_{HK}[\rho], \qquad \text{(Hohenberg-Kohn density functional)}$$

and

$$\langle \Psi | \hat{V}_{ext} | \Psi \rangle \equiv \int \rho(\mathbf{r}) V_{ext}(\mathbf{r})\, d\mathbf{r}. \qquad \text{(External potential)}$$

The Hohenberg-Kohn density functional is universal for all the many-electron systems because it is free from the informations about nuclei and their locations. Therefore, its obvious description has to be revealed. $E_{V_{ext}}[\rho]$ attains its minimum value which is the ground state total energy for the ground state density corresponding to V_{ext}.

The first HK theorem also indicates that after finding a positive definite trial density ρ_t, a unique Hamiltonian can be determined if $\int \rho_t(\mathbf{r})\, d\mathbf{r} = N$, which can give the corresponding trial wave function Ψ_t and we can get the relevant energy functional as follows:

$$E[\rho_t] = \langle \Psi_t | \hat{H} | \Psi_t \rangle \geq E_o. \quad (2.8)$$

The second HK theorem is invalid for the DFT to analyze the ground state but a small addition in it can cause variation in the excited states of the electrons which are surely perpendicular to the ground state. We can study this variation exactly from the statistics of the wave function which describes the ground state.

Using the density operator for N particles, and assuming that the ground state density has been determined, a contribution to the total energy from the external potential can accurately be computed. The density operator for N electrons is:

$$\hat{\rho}(r) = \sum_{i=1}^{N} \delta(r_i - r). \quad (2.9)$$

If we estimate this density operator for a many-particle wave function Ψ, then we get the density as follows:

$$\rho(r) = \langle \Psi(r_1, r_2, r_3, \ldots\ldots, r_N) | \hat{\rho}(r) | \Psi(r_1, r_2, r_3, \ldots\ldots, r_N) \rangle \quad (2.10)$$

$$= \langle \Psi(r_1, r_2, r_3, \ldots\ldots, r_N) | \sum_{i=1}^{N} \delta(r_i - r) | \Psi(r_1, r_2, r_3, \ldots\ldots, r_N) \rangle \quad (2.11)$$

$$= \sum_{i=1}^{N} \int \Psi^*(r_1, r_2, \ldots, r_i \equiv r, \ldots, r_N)\, \Psi(r_1, r_2, \ldots, r_i \equiv r, \ldots, r_N)$$

$$dr_1\, dr_2 \ldots dr_i \ldots dr_N. \quad (2.12)$$

This second theorem also generates a possibility of using the Variational principle - the Rayleigh-Ritz approximation [68] to compute the ground state density. We get numerous values of the conceivable densities but the density value which minimizes $E_{V_{ext}}[\rho]$ happens as the ground state density equivalent to the external potential, $V_{ext}(r)$. We can find it if we know an approximation to $F_{HK}[\rho]$. But after finding $\rho(r)$, all the informations about the system can be grasped.

When $E_{V_{ext}}[\rho]$ is determined for $\rho(r)$ relating to a specific V_{ext} for a solid, we get the ground state energy and when it is derived for any other density, the result is vague. A density $\rho_i(r)$ which maximizes $E_{V_{ext}}[\rho]$ is an excited state density other than the ground

state one with the corresponding energy $E_i = E_{V_{ext}}[\rho = \rho_i]$. Its converse is false because all the excited states don't extremalize $E_{V_{ext}}[\rho]$. If $\rho_j(\mathbf{r})$ is this density, then $E_j = E_{V_{ext}}[\rho = \rho_j]$ is a lower bound for the energy in an excited state.

These theorems together conclude the basic statement of the DFT as follows:

$$\delta[E[\rho] - \mu(\int \rho(\mathbf{r})\, d\mathbf{r} - N)] = 0. \tag{2.13}$$

Here the density and energy of the ground state represent the lowest value of $E[\rho]$ under the constraint which confines the density to have the correct quantity of electrons. The Lagrange multiplier of this constraint gives the electrochemical potential μ. At the end, we conclude that we may have a universal functional $E[\rho]$ independent of the external potential and which denotes a specific system of interest. If we know the form of $E[\rho]$, we can reduce the above equation to receive the exact ground state density and energy.

2.2.4. Kohn-Sham Equations

The approximations for the KE and electron-electron interactions were proposed by Kohn and Sham in 1965 which paved the DFT as a practical gadget and were termed as Kohn-Sham (KS) equations which helped in determining the ground-state density [69]. These equations provide us with the practical solution of the Hohenberg-Kohn functional $F_{HK}[\rho]$ as described in Eq. (2.7).

We start by rewriting the Hohenberg-Kohn functional in the proper form such that the correlation energy is a part of the total energy which lies in the exact solution but vanishes in the HF solution. The functionals of the total energy $E_{tot}[\rho]$ and that of the HF energy $E_{HF}[\rho]$ compatible with the Exact and HF Hamiltonians are given by:

$$\hat{H}_{tot}[\rho] = E_{tot}[\rho] = T + V, \tag{2.14}$$

and

$$\hat{H}_{HF}[\rho] = E_{HF}[\rho] = T_o + V_H + V_x,$$

$$= T_o + V, \tag{2.15}$$

where

$$V = V_H + V_x. \tag{2.16}$$

Here T, V and T_o are respectively the exact KE of the interacting electrons, the electron-electron PE and the KE of the non-interacting electrons functionals while V_H and V_x are the Hartree and the Exchange potential contributions respectively. Subtracting Eq. (2.15) from (2.14), we get the following functional for the correlation contribution potential:

$$E_{tot} - E_{HF} = T - T_o, \tag{2.17}$$

or

$$V_c = T - T_o, \tag{2.18}$$

where

$$E_{tot} - E_{HF} = V_c.$$

Here V_c is the correlation energy.

Now the exchange energy is a contribution to the total energy to be occurring in the HF solution but lacking of the Hartree solution. The Hartree energy functional is given by:

$$E_H[\rho] = T_o + V_H \tag{2.19}$$

The corresponding exchange PE is:

$$V_x = V - V_H. \tag{2.20}$$

With help of the above data, we can rearrange the Hohenberg-Kohn functional as follows:

$$F_{HK}[\rho] = (T + V) + T_o - T_o.$$

$$= T_o + V + (T - T_o).$$

$$= T_o + V + V_c.$$

$$= T_o + V + V_c + V_H - V_H.$$

$$= T_o + V_H + V_c + (V - V_H).$$

$$= T_o + V_H + V_c + V_x.$$

$$= T_o + V_H + (V_x - V_c).$$

$$\Rightarrow \quad F_{HK}[\rho] = T_o[\rho] + V_H[\rho] + V_{xc}[\rho]. \tag{2.21}$$

Here the energy functional $V_{xc}[\rho]$ is accurately unknown because it comprises only the complex exchange and correlation contributions.

Now using the second HK theorem to calculate the ground state density, we will achieve nothing from our alteration but we may deduce the above equation which will be the energy functional of a non-interacting classical electron gas undergone two external potentials: one of which is due to the nuclei and the other is because of the exchange and correlation effects.

The respective Hamiltonian, termed as the KS Hamiltonian, is given by:

$$\hat{H}_{KS} = \hat{T}_o + \hat{V}_H + \hat{V}_{xc} + \hat{V}_{ext}. \tag{2.22}$$

$$= -\frac{\hbar^2}{2m}\nabla_i^2 + \frac{e^2}{4\pi\epsilon_o}\int \frac{\rho(r')}{|r-r'|}dr' + V_{xc} + V_{ext}. \tag{2.23}$$

Here the exchange-correlation potential V_{xc} is defined by the exchange-correlation potential functional $\hat{V}_{xc}$ as follows:

$$\hat{V}_{xc} = \frac{\delta V_{xc}[\rho]}{\delta\rho}. \tag{2.24}$$

According to the above computations, the KS theorem can be framed by presenting a fictitious system model of N non-interacting electrons, which was denoted

by a single determinant wave function in N orbitals $\phi_i(\mathbf{r})$. These KS orbitals are expanded to get a pure numerical solution but in practice the most applications of Kohn-Sham density functional theory (KSDFT) use an expansion of $\phi_i(\mathbf{r})$ into the basis functions φ_b given by:

$$\phi_i(\mathbf{r}) = \sum_{b=1}^{L} c_{ib}\, \varphi_b, \tag{2.25}$$

where

$$\varphi_b \equiv \frac{1}{\sqrt{V}} e^{i(\mathbf{k}+\mathbf{K})\cdot\mathbf{r}}. \tag{2.26}$$

Here $\mathbf{k}$ is the wave propagation vector within the first Brillouin zone (BZ), $\mathbf{K}$ is the reciprocal lattice vector, $\mathbf{r}$ is the position vector and $e^{i\mathbf{k}.\mathbf{r}}$ and $e^{i\mathbf{K}.\mathbf{r}}$ represent plane waves in the real and reciprocal spaces respectively. V is the volume of the unit cell.

Actually, the expansion of $\phi_i(\mathbf{r})$ truncates and the number of φ_b really needed to get the nice expression of ϕ_i potently depends upon the basis set which is constructed according to the problem. The startle of calculations also depends upon whether the boundary conditions are applied.

From these orbitals, the wave function, KE and electron density are completely acknowledged as:

$$\Psi_{HF} = \frac{1}{\sqrt{N!}} \det[\phi_1\, \phi_2\, \phi_3 \dots\dots\dots \phi_N]. \tag{2.27}$$

$$T_s[\rho] = -\frac{\hbar^2}{2} \sum_{i=1}^{N} \langle \phi_i | \nabla^2 | \phi_i \rangle. \tag{2.28}$$

This KE is not real and is only of the non-interacting electrons to regenerate the real density at the ground state as follows:

$$\begin{aligned} \rho(\mathbf{r}) &= \sum_{i=1}^{N} \phi_i^*(\mathbf{r})\, \phi_i(\mathbf{r}) \\ &= \sum_i |\phi_i(\mathbf{r})|^2. \end{aligned} \tag{2.29}$$

The single-particle wave functions $\phi_i(\mathbf{r})$ being the lowest energy solutions of the KS equations are given by:

$$\hat{H}_{KS}\phi_i = \varepsilon_i\phi_i, \tag{2.30}$$

where $\varepsilon_i(\mathbf{r})$ represents the energy per electron, i.e., energy density of the uniform electron gas.

The explicit setup of the density from these orbitals favors the legality that it has been built from an anti-symmetric wave function Ψ. For finding the ground-state density, we are leaving the use of the second HK theorem further and are solving the Schrodinger-like non-interacting single-body equations. This alternate of the SWE results in a complex system of the coupled differential equations due to the electron-electron interactions. $\phi_i(\mathbf{r})$ are not only the wave functions of the single-electrons but they also secretly define the mathematical quasi-particles. It is believed that the entire density of the particles may only be equal to the electron density, ρ. Further, energies ε_i of the single-particles are not the energies of the single-electrons. $\hat{V}_H$ and $\hat{V}_{xc}$ depend upon $\rho(\mathbf{r})$ which internally depend upon ϕ_i to be calculated. It means that our problem is self-consistent in which the solutions $\phi_i(\mathbf{r})$ shape Eq. (2.22) which is impossible to write and solve unless its solution is known.

We suppose an initial density $\rho_o(\mathbf{r})$ and construct a Hamiltonian H_{KS1} with it. Then we solve the eigenvalue problem which yields a set of ϕ_1 from which we derive a density $\rho_1(\mathbf{r})$ such that ρ_1 differs from ρ_o. Now from ρ_1, we construct H_{KS2} which will generate $\rho_2(\mathbf{r})$ and so on. The process is managed such that the series converges to $\rho_f(\mathbf{r})$ which produces H_{KSf} that generates ρ_f again as a solution which is consistent with the Hamiltonian [70]. Moreover, we notice that an apparent part of an electron-electron interaction is the classical Coulomb interaction or the Hartree energy. Therefore, the Hartree potential can be expressed as follows:

$$V_H[\rho] = \frac{\hbar^2}{2}\int \frac{\rho(\mathbf{r}_1)\rho(\mathbf{r}_2)}{|\mathbf{r}_1-\mathbf{r}_2|}d\mathbf{r}_1 d\mathbf{r}_2 \tag{2.31}$$

The energy functional is being managed as follows:

$$E[\rho] = T_o[\rho] + V_H[\rho] + V_{ext}[\rho] + E_{xc}[\rho], \tag{2.32}$$

where $E_{xc}[\rho]$ is the functional of the exchange-correlation energy given by:

$$E_{xc}[\rho] = (T[\rho] - T_s[\rho]) + (V_{ee}[\rho] - V_H[\rho]). \tag{2.33}$$

E_{xc} is only the addition of the error occurred in the use of the non-interacting KE and the error appeared in reckoning the electron-electron interaction classically. If we express the functional of the above equation in place of the density constructed explicitly from the non-interacting orbitals of Eq. (2.29) and implementing the VT from Eq. (2.13), we get the orbitals which minimize the total energy and satisfy the following equation:

$$\left[-\frac{\hbar^2}{2}\nabla_i^2 + V_{ext}(\mathbf{r}) + \int \frac{\rho(\mathbf{r}')}{|\mathbf{r}-\mathbf{r}'|}d\mathbf{r}' + V_{xc}(\mathbf{r})\right]\phi_i(\mathbf{r}) = \varepsilon_i(\rho)\,\phi_i(\mathbf{r}) \tag{2.34}$$

This combination of equations is termed as Kohn-Sham (KS) equations. In these equations, a local multiplicative potential $V_{xc}(\mathbf{r})$ has been described, which is the derivative of the functional of the exchange-correlation energy with respect to the electron density and is given by:

$$V_{xc}(\mathbf{r}) = \frac{\delta E_{xc}[\rho]}{\delta \rho} \tag{2.35}$$

The set of the KS equations represents behavior of the non-interacting electrons in the effective local potential. So, on choosing an accurate functional and the exact local potential, the orbitals result the true ground-state density through Eq. (2.13) and the true ground-state energy via the Eq. (2.31). The structure of the KS equations resembles that of the HF equations rejecting the non-local exchange potential substituted by the local exchange-correlation potential V_{xc}. This is a vague use and vulgar reproduction of the structure but we have already approximated that V_{xc} is not an addition of the exchange and correlation energies as considered in case of the HFT and correlated wave function theory (WFT) but it only comprises a component of the KE.

The KS density functional theory (KSDFT) exactly corresponds to the ground-state density, energy of the non-interacting Fermions and realistic many-body systems defined by the SWE [71] as shown in Figure 2.2:

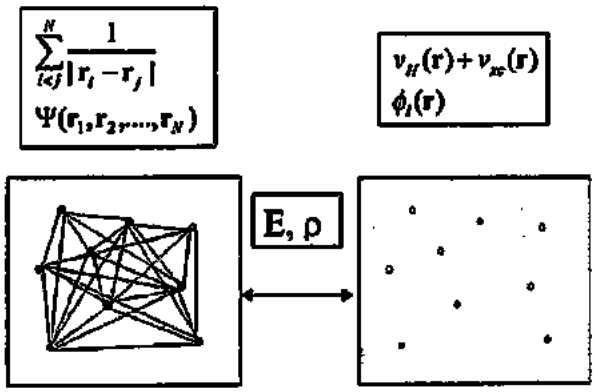

Figure 2.2 - Relation between the real many-body system (Leftwards) and the non-interacting system of the KSDFT (Rightwards) [71]

The correspondence is true only if we know the accurate functional of the charge density and energy of the non-interacting many-body system which implies that the KSDFT is an empirical tool, not a systematic theory because we have still not determined the exact functional. Although the KSDFT is realistic, yet the functional is universal, i.e., independent of the materials under observation. Hence, in principle, we solve the SWE precisely and calculate the total energy functional and its respective potential.

In these calculations, we make a tiring utmost as compared to that made in the direct energy solution. Ability of finding the true properties, often related to the ab initio formalism, of the Universal functional in several systems never permitted the admirable approximations to the functional under construction and was applied in the unbiased and analytical studies of a large quantity of materials. Due to this reason, approximations made in the DFT are considered as the "ab initio" or "first principles" techniques.

The solution of the KS equations (2.34) bears a computational cost scaling initially as N^3 in order to preserve the orthogonality of N orbitals but in the recent methods, this cost descends towards N^1 via the abuse of the locations of the orbitals. For

the initial energy surface computations, the DFT represents a practical and exact potential substitute to the wave function methodology but practically the theory depends upon the approximation imposed for $E_{xc}[\rho]$.

The DFT suffers from the main problem of unknowing the exact functional for the exchange and correlation functions. These are known only for the free electron gas but there occur approximations that allow the computations of the specific physical quantities precisely. Although the DFT reveals sound information about the ground-state properties in principle, yet the practical applications of the DFT reside in the exchange and correlation potentials.

An exchange-correlation potential expresses the effects of Coulomb potential (CP) and Pauli Exclusion Principle (PEP) far from the pure electrostatic interactions of the electrons. A solid can't represent its true inner picture, so we can't solve the many-body problems in solids exactly. To find an exact solution of a many-body problem, we get the exact exchange-correlation potential which can be applied in parallel to the free electron gas in which the electrons don't interact with one another.

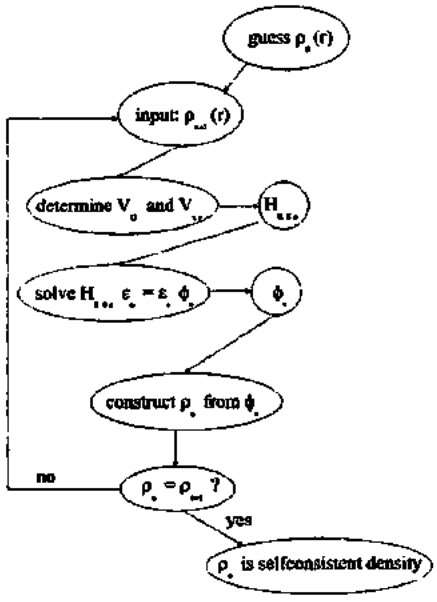

Flow chart for the Hartree-Fock or Kohn-Sham equations

Figure 2.3 - Flow chart for the Hartee-Fock or Kohn Sham equations during the n^{th} iteration [70]

2.2.5. Local Density Approximation

In the DFT, we vastly use an approximation to hypothesize the exchange-correlation functional called local density approximation (LDA). Approximation structures for $E_{xc}[\rho]$ are a large and quickly growing field of research in the DFT. In literature, there exist several tangs of this functional which are suitable or less proper for a specific field of the research, yet the greatest importance is that we need to be familiar with the derivation and structure of a functional to be selected for a certain research. The homogeneous electron gas system was an initial conception paving the way of the practical implementation of the DFT.

The homogeneous electron gas, uniform electron gas or Jellium model (JM) comprises a fictional solid in which charge of nuclei has uniformly been distributed over the whole space. The system electrons are imposed to an invariant external potential such that the electronic charge density is also constant. This charge density completely describes the homogeneous electron gas.

In the early 1920s, Thomas and Fermi researched independently on the homogeneous electron gas by considering the orbitals of the system as plane waves under the symmetry formalism [71]. If we estimate the interactions among the electrons with the classical Hartree potential (CHP) in which the exchange and correlation effects have been neglected, we can easily calculate the total energy functional [72]. These constraints show that the dependency of the kinetic and exchange energies on the charge density of the electron gas can be determined and described in terms of a local density function [73, 74, 75].

From here, we conclude that we can approximate the energy functional by integrating it over this local density function. We can solve the free electron gas analytically in the direct manner and it is very tough for an interacting electron gas. The arithmetical computations for the total energy can be done with the Variational Quantum Monte Carlo approach (VQMCA) only [76]. The subtraction of the non-interacting kinetic and Hartree energies yields a numerical value for the exchange-correlation energy

per particle $\varepsilon_{xc}(\rho)$ of a system with the uniform charge density and is achieved after working for various densities $\rho(\mathbf{r})$.

We conclude the kinetic and exchange energy densities of a system of the non-interacting uniform electron gas as follows:

$$T[\rho] = (2.87) \int \rho^{\frac{5}{3}}(\mathbf{r})d\mathbf{r}, \tag{2.36}$$

and

$$E_x[\rho] = (0.74) \int \rho^{\frac{4}{3}}(\mathbf{r})d\mathbf{r}. \tag{2.37}$$

These two equations can help in determining $E_{xc}[\rho]$ in a non-uniform system.

Here, we are approximating the local exchange-correlation energy per electron as a function of the local charge density $\varepsilon_{xc}(\rho)$ as described below:

$$E_{xc}^{LDA}[\rho(\mathbf{r})] \approx \int \rho(\mathbf{r})\, \varepsilon_{xc}^{LDA}(\rho)\, d\mathbf{r} \tag{2.38}$$

The above equation shows that we have to vividly adopt the function ε_{xc}^{LDA} as the exchange-correlation energy density of the homogeneous electron gas of the charge density $\rho(\mathbf{r})$. The postulate described by Eq. (2.38) is the LDA.

This assumption for the LDA is a little bit realistic because we see that the exchange-correlation energy due to a certain density $\rho(\mathbf{r})$ can be calculated on apportioning the specimen material into a large number of infinitesimal volumes each having an invariant density. Every infinitesimal volume element donates the total exchange-correlation energy a quantity equal to the exchange-correlation energy of a similar volume element stuffed with the uniform electron gas. This quantity has the same entire charge density as that of the genuine material in this volume element [70].

It is only a sensible idea that the law of nature assures that the real $E_{xc}^{LDA}[\rho]$ is of the form mentioned above. Further construction of the LDA is expected to accomplish well for the systems with slowly fluctuating densities. Also, it has been found that the

LDA has shown surprising results proving its accuracy in the several other realistic systems.

In the LDA, $\varepsilon_{xc}^{LdA}(\rho)$ is only the function of the local density and can be split into the exchange and correlation contributions as follows:

$$\varepsilon_{xc}^{LdA}(\rho) = \varepsilon_{x}^{LdA}(\rho) + \varepsilon_{c}^{LdA}(\rho) \tag{2.39}$$

We can express $\varepsilon_{xc}(\rho)$ in the Dirac formalism with reference to Eq. (2.37) as follows:

$$\varepsilon_{x}^{LDA}(\rho) = -C\,\rho(r)^{1/3} \tag{2.40}$$

This functional is largely applicable and can be set up from the ascending opinions [71]. C is a free constant other than that computed for the Jellium model.

The functional of the correlation energy density $\varepsilon_c(\rho)$ is determinable and its simulation for the uniform electron gas in the quantum Monte Carlo computations displays the accurate results [77]. The subsequent $\varepsilon_{xc}(\rho)$ has been adjusted by several analytical forms [78, 79, 80] and all of them practically showed the similar consequences. All these forms were collectively termed as the LDA functionals.

2.2.6. Generalized Gradient Approach

The LDA runs on the exchange-correlation energy at every point in the homogeneous system of the electrons irrespective of homogeneity of the real charge density but this energy can deviate apparently from the calculated homogeneous results. The systems in which the charge density varies slowly the generalized gradient approximation (GGA) excels over the LDA. Generalized means that a straightforward gradient may conclude a functional that deviates from the certain relationships whose precision may be verified for the genuine functional and for the LDA as well. In the GGA, a certain form of a functional depending upon both the charge density and its gradient is taken to ensure the normalization [81].

A distinctive GGA functional is given below:

$$E_{xc}^{GGA} \approx \int \rho(\mathbf{r})\, \varepsilon_{xc}^{GGA}(\rho, \nabla\rho)\, d\mathbf{r} \qquad (2.41)$$

The LDA is deliberated as the Zeroth order approximation (ZOA) to the semi-classical progression of the density matrix in place of the density and its derivatives [82]. An improvement in the LDA demands logical stages under which we can cause the exchange and correlation contributions of each tiny volume element depend on the local density in that volume but also on the densities in the neighboring volume elements. Although the GGA acts generally somewhat superior to the LDA, yet it comprises some demerits as mentioned below:

"There is a unique exchange and correlation functional for the LDA because there is a sole demarcation for $\varepsilon_{xc}^{LdA}(\rho)$. However, there is freedom to include something in the density gradient and hence, various savors of the GGA exist. Usually, a nominee GGA functional with free parameters is fitted to a vast set of experimental statistics on atoms, molecules and solids. Then these parameters are bound by the fixed values and the functional is finished for applying to the solids in routine. Such a GGA computation is restricted not to be called an Ab Initio computation because the particular experimental information is used. Moreover, the GGAs never happen without a parameter."

Here, we cover up the discussion by concluding that the GGA is significantly better than the LDA in explaining the binding energy (BE) of the molecules and hence, the DFT was widely accepted in early 1990's. The bond dissociation energies were overestimated at most 10% by the LDA whereas the GGA gave ambiguities specifically about order of 10% or less. Many functionals have been constructed in the GGA family and their performances have been probated on the different systems [83, 84, 85, 86].

2.3. General Remarks on the DFT

We see that the DFT is a proficient and impartial technique to calculate the ground state energy of the solid materials in the bulk phases and their surfaces as well. By knowing the ground state energy being the function of the positions of the atomic

nuclei, we can compute the molecular and crystal structures and the forces acting on the nuclei when they leave their mean positions. The truthfulness of these computations bases on the approximations of the exchange-correlation energy functional depending on the local density gradients and the semi-local calculations of the density.

In Atomic and Molecular Physics, the DFT is contemporarily being used to solve issues like the computations of ionization potentials [87], investigation of chemical reactions, vibrational spectra structure of biomolecules [88] and nature of dynamic places in catalysts [89].

In Condensed Matter Science, the DFT helps to examine problems as the lattice structures [90], phase transitions in solids [91], liquid metals [92] and evolution of the true molecular dynamics patterns in which the forces are reckoned quantum mechanically [93] by the practical applications of the DFT founded on uncontrolled applications like the LDA method whose validity lies in its capability of regenerating the experimental results. For the atoms and tiny molecules, the simplest LDA has already shown the nice qualitative and semi-quantitative results. It is a surprising success over the Thomas-Fermi model (TFM) and the Hartree-Fock (HF) method which overestimate the strength of the molecular bonds. An improvement can be made if an isolated atom or molecule is considered as an inhomogeneous electron system in which the electronic correlations are poor and resemble averagely to those of a homogeneous electron gas.

The Configuration Interaction (CI) method [94] of Quantum Chemistry can solve the many-body quantum states with high accuracy. So, the quantum chemists don't recommend the use of the DFT at the initial stage. Such techniques use the locally controlled approximations and the accuracy in results can be enhanced. For the bigger molecules, the DFT is an essential tool [95]. In traditional Quantum Chemistry, the computational method comprises the expansion of a variable exponentially with the number of electrons under process, while in the DFT this variable grows roughly about the third power of this number. It concludes that the DFT is applicable to the bigger molecules with hundreds of atoms and fails for smaller ones, while with the CI method, we are confined by a few atoms.

In Solid State Physics, the DFT can determine the lattice constants of the simple crystals with an accuracy of about 1% under the LDA in which the electronic structure of a single unit cell is studied under the periodic boundary conditions [96]. The GGA gives the nice manifestation of the structural and electronic properties of the most solids like the lattice parameters within 1-2%, qualitatively accurate band structure, metal-insulator and magnetism, etc. This application can also be used for the investigation of a super cell which comprises several unit cells with a single defect or impurity [97]. This super cell approach (SCA) is also applicable for more complicated issues like the anti-ferromagnetism and systems suffering from intense electronic correlation. The local approximations can't find the work-functions of metals because of the displacement of the exchange-correlation hole from the original position and the production of image forces which are $1/r$ performance of $V_{xc}(r, r')$ that is non-local where r is a small distance from the metal surface. We can diminish this discrepancy [98].

In general, the LDA and GGA have shown a consistent level of accuracy and inaccuracy in various problems contrary to the approximations using the free parameters which are optimized empirically to fit a specific data and thus we can use them reliably for interpolation. For dealing with the image and Vander Waal's forces [99], especially in biomolecules, these approximations fail because both of these forces are the descriptions of the non-local correlations (non-locality) which are absent from the LDA and its instantaneous extensions.

This failure along with the uncontrolled approximations paves the research towards the modern and precise exchange-correlation energy functionals. The consistency of the DFT computations bases on the progress in the approximations for the functionals of the exchange and correlation energy. The evident advancements in the quality of the exchange-correlation functionals depending upon the gradients of the local charge density, semi-local measurements of the charge density and non-local exchange functionals. The approximation of the local charge density is simple and significantly truthful for the structure, elastic moduli, phase stability and transition states but is less reliable for the binding energy (BE).

In Electronics, the Time-dependent density functional theory (TDDFT) links the interacting and non-interacting systems undergoing the time dependent potentials, and the Relativistic density functional theory (RDFT) calculates the Kohn-Sham states by using the Dirac equation (DE) instead of the Schrodinger wave equation (SWE) [100].

In Nuclear Physics, the DFT calculates the densities of the protons and neutrons and their corresponding energies are studied [101].

Chapter 3

FULL POTENTIAL AUGMENTED PLANE WAVE METHODS

A Full potential augmented plane wave (FP-APW) method comprises the developed augmented plane wave (APW) methods which start from the Slater's APW method to the Linearized augmented plane wave (LAPW) method and the fresh Augmented plane wave plus Local orbitals (APW + lo) method mentioned in the Schwarz et al. (2001) and will run under the WIEN2k software package [102]. First, we will discuss the Plane wave (PW) method.

3.1. Plane Wave Method

In a crystalline solid, the electrons travel through a periodic effective potential V_{eff} produced by the electron-nuclei and electron-electron interactions. The nuclei are periodically managed in the crystal and reflect the symmetry of the crystal as given below:

$$V_{eff}(\mathbf{r} + \mathbf{R_n}) = V_{eff}(\mathbf{r}), \tag{3.1}$$

where

$$\mathbf{R_n} = n_1\mathbf{a_1} + n_2\mathbf{a_2} + n_3\mathbf{a_3}.$$

$\mathbf{R_n}$ is called the translational lattice vector; n is the number of the Brillouin zone (BZ) where **R** lies and as are the unit cell vectors in the crystal.

According to Andre Bloch, the eigenfunctions which are actually the wave functions of the electrons deduced from the SWE comprising the periodic potential in the Hamiltonian, are expressed by a product of a symmetric lattice periodic function $u_k^n(\mathbf{r})$ and a plane wave $e^{i\mathbf{k}.\mathbf{r}}$ as follows:

$$\psi_k^n(\mathbf{r}) = u_k^n(\mathbf{r})\, e^{i\mathbf{k}.\mathbf{r}}, \tag{3.2}$$

where

$$u_k^n(r) = \sum_K c_K^{n,k} e^{iK.r}.$$

Now Eq. (3.2) becomes:

$$\psi_k^n(r) = \left(\sum_K c_K^{n,k} e^{iK.r}\right) e^{ik.r}$$

$$= \sum_K c_K^{n,k} e^{i(k+K).r}. \qquad (3.3)$$

Here, **k** is the wave propagation vector within the first Brillouin zone (BZ), **K** is the reciprocal lattice vector, **r** is the position vector and $e^{ik.r}$ and $e^{iK.r}$ represent plane waves in the real and reciprocal spaces respectively. $c_K^{n,k}$ are coefficients to be determined. Eq. (3.2) reveals that the selection of a basis set comprising the basis functions to expand the Kohn-Sham (KS) wave functions comprises the PWs.

These PWs are periodic and mathematically easy but the expansion of the PWs demands a huge number of the basis functions for a suitable representation of the wave functions of the valence electrons. The valence electrons are distributed spatially in a vast region and are the major entities of the bonding among the atoms while the core electrons are confined intensely by the nuclei and are restricted in a smaller core region.

The wave functions within the core region are oscillating forcefully while in the valence region they are much smoother. The strong oscillations are produced due to the orthogonalization of the wave functions of the valence electrons to those of the core electrons. This problem can be solved by applying the Pseudopotential (PP) method [103] according to which the core electrons are not treated separately but are considered to be merged with the nuclei to form the PP. The wave functions of the valence electrons travelling through this PP are enough smoother and can be expressed by a tiny number of the PWs.

There is another method, except the PP method, which can involve all the electrons. This approach splits up the real space into a number of regions near the nucleus and in between each region. The KS orbitals are expanded differently in every region. These expansions are done under the APW method coming next.

3.2. Augmented Plane Wave Method

Although the augmented plane wave (APW) method has been founded on the basis set of the APWs, yet it has been discarded from the practical use these days. Here, we are using it only for the devotion to the LAPW and APW + lo methods.

The APW method was developed by J. C. Slater in 1937 [104]. Its basis set was constructed on the concepts which were behind the formation of the pseudopotential. He started setting up the basis set from the Muffin-Tin approximation (MTA) [104] which comprises a combination of the PWs in the regions where the potential varies slowly and the atomic-like functions in these regions where the wave functions vary fast. Far from the nucleus, the electrons are loosely bound or can move freely and these free electrons are manifested by the PWs being the eigenfunctions of the Hamiltonian having zero potential. Near the nucleus, the electrons are so tightly bound that they are believed to be in a free atom and can be represented by the atomic-like functions.

Therefore, according to the MTA, space around an atom in the crystal has been divided into two regions: the first region is a sphere of radius R_α around every atom, called the MT sphere denoted by S_α and a portion of space under S_α is termed as the MT region denoted by II. We label different atoms in a unit cell by α which differs for all the atoms in that unit cell, and not only for unlike atoms. The rest of the space is termed as the Interstitial region I [105] as shown below:

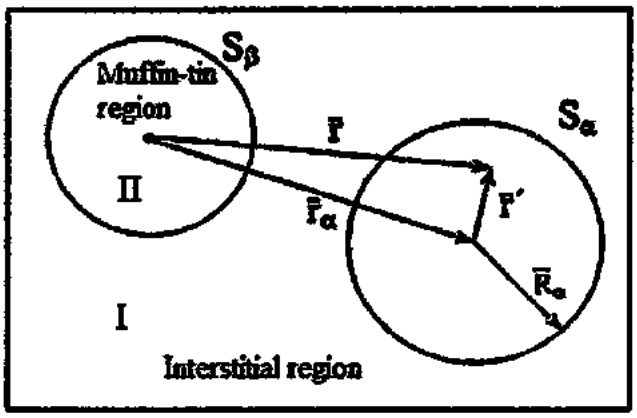

Figure 3.1 - **Muffin-tin and Interstitial regions around an atom [105]**

In an MT sphere, potential can be defined as follows:

$$V_{MT}(r) = \begin{cases} \text{Constant} & r \in I \\ V(r_\alpha) & r \in S_\alpha. \end{cases} \tag{3.4}$$

The plane wave basis set is $e^{i(k,K).r}$ which is joined with the atomic partial waves $\sum_{l,m} A_{lm}^{\alpha,K} u_l^\alpha(r', E) Y_m^l(\hat{r}')$. $u_l^\alpha(r', E)$ are the solutions of the radial SWE for a certain energy E and $A_{lm}^{\alpha,K}$ are the expansion coefficients which are commensurate with the wave functions $\phi_i(\mathbf{r})$ at the boundary between the MT and interstitial regions, which match the PWs as well.

The radial SWE is given by:

$$-\frac{1}{r^2}\frac{d}{dr}\left(r^2 \frac{du_l^\alpha(r',E)}{dr}\right) + \left[\frac{l(l+1)}{r^2} + V(r) - r\right] r u_l^\alpha(r', E) = 0. \tag{3.5}$$

An APW used for the expansion of ψ_k^n in Eq. (3.2) is defined by:

$$\phi_k^k(r, E) = \begin{cases} \frac{1}{\sqrt{V}} e^{i(k+K)\cdot r} & r \in I \\ \sum_{l,m} A_{lm}^{\alpha,k+K} u_l^\alpha(r', E) Y_m^l(\hat{r}') & r \in S_\alpha. \end{cases} \tag{3.6}$$

where

$$A_{lm}^{\alpha,k+K} = \frac{4\pi i^l e^{i(k+K)\cdot r_\alpha}}{\sqrt{V}\, u_l^\alpha(R_\alpha, E)} j_l(|k + K| R_\alpha) Y_m^{l*}(k + K). \tag{3.7}$$

$A_{lm}^{\alpha,k+K}$ is uniquely defined and we will have to contract any value l_{max} as well, called an angular function; $j_l(r)$ is the Bessel function of order l; and V is the volume of the unit cell.

As $u_l^\alpha(r', E)$ are equivalent to the exact MT potential eigenstate of the eigenenergy and as these depend upon E, therefore the eigenvalue problem is non-linear in the energy. It demands an iterative solution to adapt E which bears a high computational price [105] as shown in Figure 3.2.

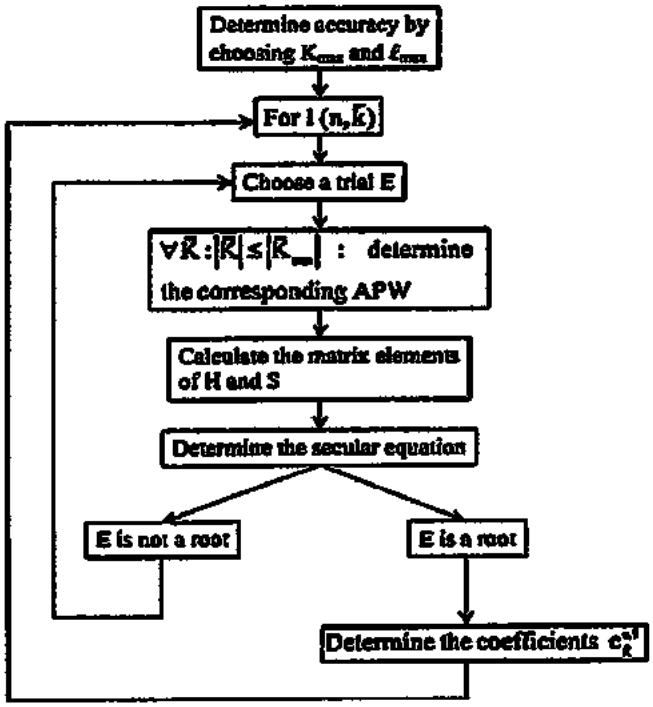

Figure 3.2 - Flow chart for the APW method [105]

It makes the APW method naturally lazy. In order to handle this issue the linearized forms of the APW method were established in which the energy E is adjusted to a static value E_l and the basis functions are reformed to attain the additional flexibility in order to deal with a large region of the energy around the linearization energy.

3.3. Linearized Augmented Plane Wave Method

It was a customary method developed in early 1970s to linearized augmented plane wave (LAPW) method [106]. Basis functions are grown in the same manner as in Eq. (3.6) in the interstitial region I, but within the MT region II. These functions are not only dependent upon $u_l^{\alpha}(r', E)$ but also on its derivative $\dot{u}_l^{\alpha}(r', E) = \frac{\partial u_l^{\alpha}(r', E)}{\partial E}$.

The LAPW method is precise to perform calculations for the electronic structure of crystals. It solves the KS equations for the ground state charge density, total energy and energy bands (the KS eigenvalues) in the many-electron system on introducing a basis set reformed for the problem of dealing with the exchange and correlation

approximations and their uses. An adaptation can be achieved in the MT and the interstitial regions. In these two kinds of regions, distinct basis sets are spent.

Relativistic effects occurring in the valence states may be incorporated either by the scalar relativistic behavior (Koelling and Harmon 1977) [107] or by the second Variational method including the spin-orbit (SO) coupling (Macdonald 1980) [108]. The core states are treated completely by the relativistic fashion (Desclaux 1969) [109].

In literature, there are many descriptions of the LAPW method to linearize the Slater's old APW method and the further programming hints have been given in the references: Andersen 1975 [110]; Koelling and Arbman 1975 [111]; Wimmer et al. 1981 [112]; Weinert et al. 1982 [113]; Blaha et al. 1985 [114]; the Wei et al. 1985 [115]; Mattheiss and Hamann 1986 [116]; Schwarz and Blaha 1996 [117]. There is also an excellent book by D. J. Singh and Lars Nordstrom 2006, which mentions all the details of the PWs, PPs and LAPW method [118]. Here the basics have been discussed only avoiding of the details.

We will review the LAPW method in two ways: the Regular LAPW and LAPW + LO methods described ahead.

3.3.1. Regular LAPW Method

In the APW method, we found a difficulty that we had to set up $u_l^{\alpha}(r', E)$ at the eigenenergy $E = \varepsilon_k^n$ of the determined eigenstate. If we were able to discover $u_l^{\alpha}(r', \varepsilon_k^n)$ from the derived quantities, then it was best and then the method helped us do so [119]. The calculation of $u_l^{\alpha}(r', \varepsilon_k^n)$ at the energy $E = \varepsilon_k^n$ can help us use the Taylor's Series (TS) to determine it at the other energy values (say $E = E_o$) which are not too away from it as given below:

$$u_l^{\alpha}(r', \varepsilon_k^n) = u_l^{\alpha}(r', E_o) + (E_o - \varepsilon_k^n)\frac{\partial u_l^{\alpha}(r', E_o)}{\partial E_o} + O(E_o - \varepsilon_k^n)^2,$$

or writing the derivative in the reduced form:

$$u_l^{\alpha}(r', \varepsilon_k^n) = u_l^{\alpha}(r', E_o) + (E_o - \varepsilon_k^n)\, \dot{u}_l^{\alpha}(r', E_o) + O(E_o - \varepsilon_k^n)^2. \qquad (3.8)$$

If we put the first two terms of series in the APW for the given E_o in Eq. (3.8), then we get the definition of the LAPW. The additive term $O(E_\bullet - \varepsilon_k^n)^2$ allocates the second order error in the wave function and the fourth order ambiguity in the eigenenergy such that $E_\bullet - \varepsilon_k^n$ is to determine first. Now we are adding a coefficient $B_{lm}^{\alpha,k+K}$ in Eq. (3.6) at the given E_o such that it defines an LAPW as:

$$\phi_K^k(r,E) = \begin{cases} \frac{1}{\sqrt{V}} e^{i(k+K)\cdot r} & r \in I \\ \sum_{l,m}\left[A_{lm}^{\alpha,k+K} u_l^\alpha(r',E_\bullet) + B_{lm}^{\alpha,k+K} \dot{u}_l^\alpha(r',E_\bullet)\right] Y_m^l(\hat{r}') & r \in S_\alpha. \end{cases} \quad (3.9)$$

The determination of both the coefficients $A_{lm}^{\alpha,k+K}$ and $B_{lm}^{\alpha,k+K}$ does not happen by the TS but demands that the function should be commensurate with the PWs at the sphere boundary both in value and the slope. It can be achieved by using Eq. (3.7) and its radial derivative. It is an ultimate of a 2 x 2 matrix from which we can get both the coefficients. We still could not get the final definition of an LAPW.

Suppose that we express an eigenstate $\Psi_k^n(r,E_\bullet)$ which already possesses the p-character for atom α at $l = 1$. The expansion of Ψ_k^n in LAPWs gives a large $A_{(l=1)m}^{\alpha,k+K}$. Hence, we benefit if we choose E_o close to the mid of the p-band and the term $O(E_\bullet - \varepsilon_k^n)^2$ in Eq. (3.8) will lie less so that we may surely cut-off after the linear term. This opinion can be repeated for every physically important quantity l up to 3 units, i.e., $s-, p-, d-$ and $f-$states. It can be applied for all the atoms. It also concludes that we should avoid of selecting one E_o and should select a collection of the worthy-selected $E_{1,l}^\alpha$ up to $l = 3$ where the index '1' indicates the highest valence state. We can store a fixed value for a larger l. Then the final definition of the LAPW becomes:

$$\phi_K^k(r,E) = \begin{cases} \frac{1}{\sqrt{V}} e^{i(k+K)\cdot r} & r \in I \\ \sum_{l,m}\left[A_{lm}^{\alpha,k+K} u_l^\alpha(r',E_{1,l}^\alpha) + B_{lm}^{\alpha,k+K} \dot{u}_l^\alpha(r',E_{1,l}^\alpha)\right] Y_m^l(\hat{r}') & r \in S_\alpha. \end{cases} \quad (3.10)$$

Here $u_l^\alpha(r',E_{1,l}^\alpha)$ is the regular solution at the origin of the radial SWE for the energy $E_{1,l}^\alpha$ lying ordinarily at the center of the respective band with the l-like character and inside the sphere $\dot{u}_l^\alpha(r',E_{1,l}^\alpha)$ being a spherical chunk of the potential and reserves at

the identical energy. The functions u_l^α and $\dot{u}_l^\alpha$ are calculated under the numerical integration of the radial SWE over a radial network inside the sphere and their linear combination establishes the linearization of the radial function [119].

3.3.2. LAPW With Local Orbitals Method

Local orbitals are denoted by LO. We construct an LO for a special value of l and m and for a certain atom α and the interstitial regions I and the MT regions II of the spheres of the other atoms having no LO. The LO includes an additional radial function at the new linearization energy E_2 [119].

The regular LAPW method does not reveal which electron states have been computed. It also fails to calculate the electrons in a core state in which the electrons are extremely destined across the nucleus and they act as residing in free atoms. As a core state does not take part in the chemical bonding directly with the other atoms, so it must lie completely in the MT sphere. States which can escape from the MT sphere are termed as the valence states. Since these states join in the chemical bonding, therefore the regular LAPW method is applicable on the valence states. Although the core states are handled like they are in the free atoms, yet they undergo the potential produced by the valence states. During the processing, we find the states which have the same l but the different n and both these states are called the valence states [119].

To enhance the elasticity of the basis, i.e., to improve the linearization and to produce the stable behavior of the semi-core and the valence states in a single energy window to guarantee the orthogonality, the surplus k-independent basis functions may be included which are named the local orbitals (LOs) [120]. We construct an LO for a special value of l and m and for a certain atom α and the interstitial regions I and the MT regions II of the spheres of the other atoms having no Los, thus being called the local orbital. The LO comprises a linear combination of a pair of radial functions, two distinct energy sublevels 3s and 4s, and an energy derivative of one of these energies and an additional radial function at the new linearization energy $E_{2,l}^\alpha$ [119, 120] as expressed in Eq. (3.11):

$$\phi_{\alpha,Lo}^{lm}(r) =$$

$$\begin{cases} 0 & r \notin S_\alpha \\ [A_{lm}^{\alpha,LO} u_l^\alpha(r', E_{1,l}^\alpha) + B_{lm}^{\alpha,LO} \dot{u}_l^\alpha(r', E_{1,l}^\alpha) + C_{lm}^{\alpha,LO} u_l^\alpha(r', E_{2,l}^\alpha)] Y_m^l(\hat{r}') & r \in S_\alpha. \end{cases} \quad (3.11)$$

The same $u_l^\alpha(r', E_{1,l}^\alpha)$ and $\dot{u}_l^\alpha(r', E_{1,l}^\alpha)$ are used in the MT sphere of the atom α with the linearization energy $E_{1,l}^\alpha$ being a value of the higher of two valence states as done in the LAPW basis set. The linearization energies are considered to be identical for two equivalent atoms. The lower valence state is like a free-atom and its sharp peak lies at the energy $E_{2,l}^\alpha$ such that a single radial function $u_l^\alpha(r', E_{2,l}^\alpha)$ is enough to express it. The coefficients $A_{lm}^{\alpha,LO}$, $B_{lm}^{\alpha,LO}$ and $C_{lm}^{\alpha,LO}$ are calculated under the necessity of the LO being normalized and possessing no value and slope at the boundary of the MT sphere which means that the LO can't escape from the MT sphere.

The addition of LOs enlarges the size of the LAPW basis set. If we include more atoms in the unit cell, then we have to add more LOs while contrarily the number of the LAPWs is independent of the quantity of the atoms in the unit cell. The more atoms mean that we just add more sets of coefficients. If we include the LOs in p- and d-states, then the basis set enhances by 3 functions per atom for the p-states and 5 functions per atom for the d-states in the unit cell. Such a basis set is quite smaller than the basis set sizes comprising hundreds of the functions. Although the LOs present slightly larger computational time implying a small increment in the price, yet it yields the better accuracy. This method may also practice the LO to compensate for the linearization errors, especially in case of the narrow d- or f-band [119]. The LAPW + LO method converges like the LAPW method [120].

3.4. APW + lo METHOD

3.4.1. Pure APW + lo Method

We observed that the standard LAPW method with an extended constraint on the PWs which match in value and slope with the solution inside the sphere, could not prove the most competent technique for the linearization of the Slater's APW method as mentioned by Sjöstedt, Nordström and Singh (2000) [121].

In the APW method, the basis set depends upon the energy which creates a problem for us. It should be energy independent. We have removed this energy dependence by applying the LAPW + LO method for the price of a bit larger size of the basis set. Using a standard APW basis, anyone can make it more efficient by keeping $u_l^{\alpha}(r', E)$ at a fixed energy level E for the maintenance of the linear eigenvalue dilemma.

Now we are introducing the APW + lo method [122] whose basis set is energy independent and of equal size like that used in the APW method. It concludes that this method assembles the nice configurations of both the APW and LAPW + LO methods. Actually, the APW + lo basis set comprises two types of the functions in which the first function contains the APWs with a set of the fixed energies $E_{1,l}^{\alpha}$ given by:

$$\phi_K^k(r) = \begin{cases} \frac{1}{\sqrt{v}} e^{i(k+K)\cdot r} & r \in I \\ \sum_{l,m} A_{lm}^{\alpha,k+K} u_l^{\alpha}(r', E_{1,l}^{\alpha})\, Y_m^l(\hat{r}') & r \in S_{\alpha}. \end{cases} \quad (3.12)$$

This basis set with the fixed energies gives a fake expression of the eigenfunctions. So, we are amplifying this basis set with a second kind of the functions, called the local orbital, denoted by 'lo' instead of the LO, and is defined as:

$$\phi_{\alpha,lo}^{lm}(r) = \begin{cases} 0 & r \notin S_{\alpha} \\ [A_{lm}^{\alpha,lo} u_l^{\alpha}(r', E_{1,l}^{\alpha}) + B_{lm}^{\alpha,lo} \dot{u}_l^{\alpha}(r', E_{1,l}^{\alpha})] Y_m^l(\hat{r}') & r \in S_{\alpha}. \end{cases} \quad (3.13)$$

The new lo resembles the old LAPW basis set. The coefficients $A_{lm}^{\alpha,lo}$ and $B_{lm}^{\alpha,lo}$ are k-independent and calculated by the normalization of the lo under the requirement that the lo contains zero value but non-zero slope at the boundary of the Muffin Tin sphere. Therefore, both the APW and the lo are continuous at the sphere boundary but are not continuous for both of their first derivatives. In order to meet this condition, we constitute the basis functions having 'kinks' on the sphere boundary. These basis functions essentially add the surface expressions in the KE part of the Hamiltonian but the ultimate wave function remains flat and differentiable.

The same energies $E_{l,l}^{\alpha}$ have been used here as done in the APWs. The APW + lo basis set size must be similar to that of the APW but is smaller than that used in the LAPW + LO method.

3.4.2. Mixed APW + lo / LAPW Method

The LAPW method requires a bigger K_{max} than that used in the APW + lo method because it fails to determine the valence states of d- and f-orbitals and the states in an atom which comprise a very smaller MT sphere than the other ones in the unit cell.

We will use the APW + lo method for the above states and will keep applying the LAPW method for the other states. The application of the APW + lo method on a single state implies that we add 2l+1 lo,s per atom in its basis set. Hence, the APW + lo basis set becomes significantly larger than that of the LAPW for the same cut-off parameter $R_{\alpha}^{min}K_{max}$ but it is concluded that a compensation can be made by using a smaller value of $R_{\alpha}^{min}K_{max}$ for the accurate outcomes because the addition of these extra basis functions for the purpose to apply on a state where they can be useful is always bad.

Therefore, a new approach came to hand leading us use a mixture of the LAPW and APW + lo basis sets for all the atoms α and all the values of l under Eq. (3.9) [122]. One or more atoms α_o where $r \in S_{\alpha_o}$ and one or more l_o will use Eq. (3.12). Then $\phi_{\alpha_o}^{l_o m}(r)$ obtained from Eq. (3.13) are added to the basis set. This mixed basis set is applicable in WIEN2k. This new criterion converges practically to the desired results but allows the cut-off parameter $R_{\alpha}^{min}\,K_{max}$ reduce by 1 about. It leads to a vividly smaller basis set up to 50% and the respective time for computations is severely lowered to a multiple of a certain value. In a calculation, we can use a "Mixed LAPW / APW + lo basis" for the different atoms and even though for the unique l-values of the same atom as described in the Madsen et al. (2001) [123].

3.4.3. APW + lo + LO Method

We confronted the same problem for the semi-core states on using the APW + lo basis functions like that in the LAPW + LO method. In general, we describe those orbitals from APW + lo which converge extremely slowly with the atoms having the

small spherical sizes or with the certain quantities of the PWs like the transition metals (TM) 3d-states and remaining with the ordinary LAPWs. Now we will add the second type local orbitals (LO) at a diverse energy value to describe both the semi-core and valence states concurrently [122]. The corresponding basis function is defined as:

$$\phi_{\alpha,LO}^{lm}(\mathbf{r}) = \begin{cases} 0 & \mathbf{r} \notin S_\alpha \\ \left[A_{lm}^{\alpha,LO} u_l^\alpha(\mathbf{r}', E_{1,l}^\alpha) + C_{lm}^{\alpha,LO} u_l^\alpha(\mathbf{r}', E_{2,l}^\alpha) \right] Y_m^l(\hat{\mathbf{r}}') & \mathbf{r} \in S_\alpha. \end{cases} \quad (3.14)$$

This APW + lo + LO method does not contain the derivative of $u_l^\alpha(\mathbf{r}', E_{1,l}^\alpha)$ as in the LAPW + LO method. The coefficients $A_{lm}^{\alpha,LO}$ and $C_{lm}^{\alpha,LO}$ are calculated under the ailment of the LO being normalized and preserving zero value but non-zero slope at the boundary of the MT sphere.

3.5. General Considerations about the FP-LAPW Method

1) The general LAPW method expands the potential as follows:

$$V(\mathbf{r}) = \begin{cases} \sum_{lm} V_{lm}(\mathbf{r}) Y_{lm}(\hat{\mathbf{r}}) & \text{Inside the sphere} \\ \sum_K V_K e^{iK\mathbf{r}} & \text{Outside the sphere.} \end{cases} \quad (3.15)$$

The charge densities are expanded analogously. No approximations are made for shapes of the potential and the procedure is called the "Full Potential" method.

2) The Muffin Tin approximation is only for the components $l = 0$ and $m = 0$ in the first expression of Eq. (3.15) and for the $K = 0$ component only in the second expression of this equation. It is a very old method used to take the spherical average in the inner of the MT sphere and the volume average in the interstitial region.

3) The total energy is calculated by using the Weinert et al. (1982) [113].

4) The Rydberg atomic units are applied everywhere excluding the interior of the atomic like programs as LSTART and LCORE in the sub-routine out wins LAPW1 and LAPW2. Although the Hartree units are taken in these regions, yet the output always appears in the Rydberg units.

5) The forces on the atoms are computed by the Yu et al. (2001) [124]. This method is used in WIEN2k according to the Kohler et al. (1996) [125] and the Madsen et al. (2001) [123]. An Alternative method proposed by Soler and Williums (1989) [126], efficient in computations and accurate in numeric, is also equivalently useful but the corresponding code is taken from M. Fahnle in the Krimmel et al. (1994) [127].

6) The Fermi energy and the weights of every energy band are calculated by the Modified Tetrahedron method described in the Blochl et al. (1994) [128]. In this method, the Gaussian or temperature functions are varied according to the requirement. The spin-orbit (SO) interactions are due to a second Variational step when we use the scaler-relativistic eigrnfunctions as the basis [107, 116, 129]. To control this difficulty arising due to the absent $p_{1/2}$ radial basis function equivalent to $p_{3/2}$ in the scalar relativistic basis, we have added an extra $p_{1/2} - LO$ in the standard LAPW basis. This LO is summed in the spin-orbit (SO) calculation at the second Variational step [130].

7) The LDA and GGA methods are not enough precise for a proper portrayal of the localized electrons as in the 4f-states in the Lanthanides or the 3d-states in some TM-oxides. So, we have applied several shapes of the "LDA + U" method along with the Orbital Polarization (OP) method under Novak (2001) [129]. The interactions can be conceived by an applied external magnetic [129] or electric field through the Super cell approach (SPA) under the Stahn et al. (2000) [131].

3.6. Properties of the Full Potential APW Method

1 – The density of states (DOS) is computed by the Modified Tetrahedron method in the Blochal et al. (1994) [128].

2 – The electron density can be analyzed by the Bader's Theory of atoms in molecules using a program of J. Sofo and J. Fuhr (2001) [132].

3 – The X-Ray spectra between a core and a valence or conduction energy band can be viewed by the Fermi's Golden Rule and the elements of the dipole matrix [133].

4 – The Fourier transform of the charge density reveals the structural aspects of X-rays.

5 – The optical properties are grabbed by the Joint density of states (JDOS) modified by the corresponding dipole matrix elements [134, 135]. This modification can also be achieved by the Kramers-Kroning transformation [136].

3.7. Super Cell Approach

It is a universal approach for the study of solids by modeling their surfaces under the periodic boundary conditions. In this approach [137, 138], a superficial periodicity is imposed on the simulation cell for modeling the continuum properties of a solid. Then the Bloch's theorem may be applicable to the wave functions in the solid. A super cell must be large enough to overcome interactions among atoms in the cell.

In principle, we will apply the 2D possible periodicity but we will also use the additional identical constraints to find the deterioration of the PWs in LAPW + lo method. Also, this 2D approach is not essentially useful for the systems absorbing oxygen. Our criterion applied here models the surfaces under the periodic boundary conditions in all the 3D spaces. We express the semi-infinite surfaces with the slabs which are infinite in the xy-plane and comprise many layers along the z-axis. In the z-direction, the periodicity of layers is retained artificially by help of a super cell which consists of a slab and a vacuum region.

A super cell will give the trustworthy outputs if we consider two major parameters as the number of layers in the slab and vacuum thickness. The surfaces which are at the top and bottom of a slab comprise a sufficient number of layers to block the interactions between them. The atoms lying at the center of the slab express the physical properties of the atoms in the bulk phase. There is a large vacuum area between the surfaces of the successive slabs to avoid of the interactions between them. The surface calculations of the solids may become computationally very expensive in the LAPW + lo method because a vacuum region is expressed by the PWs, which enhances the PW basis set significantly as shown in Figure 3.3 [139]:

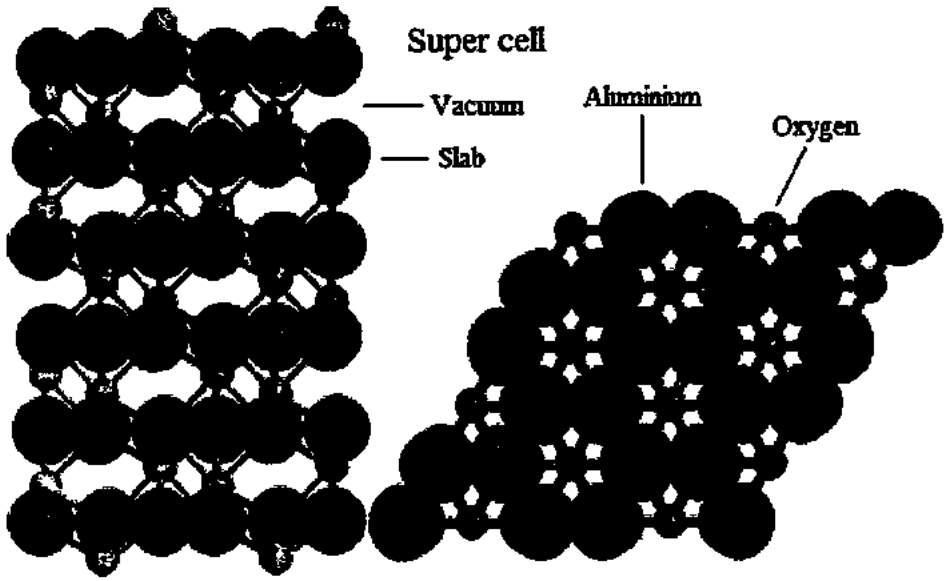

Figure 3.3 - Supercell of Al_2O_3 comprising 2×2×1 hexagonal unit cells with 120 atoms! The left hand figure gives a side view along the *a*-axis and the right hand figure gives the view from top to bottom along the *c*-axis [139].

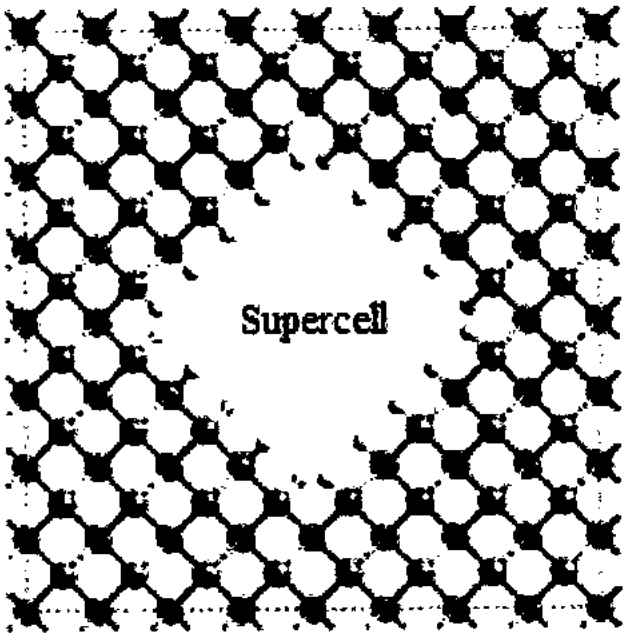

Figure 3.4 - A 128 less 25 atoms super cell for the porous silicon (Si) [140]

To escape from this problem, there is an equivalent approach, not based on periodic boundary conditions, called the Clustering method [141, 142, 143] within which a surface is sculpted by a big cluster. In principle, a solid is approximated by a huge cluster. In such a cluster, Quantum Mechanics of the center-most atoms approximates all the other atoms in a solid. In this approach, the decisive parameter is the cluster size which toughly affects both the accuracy and computational cost. The size which approximates a solid is bigger due to the supremacy of the surface over the bulk atoms in the small and medium clusters. This concept is applicable to all the electronic structure methods (ESM) and the best general solution is obtained by using the restricted repetitions of a primitive cell along with the boundary conditions.

Chapter 4
CALCULATIONS BY WIEN2K

4.1. WIEN2k Software Package

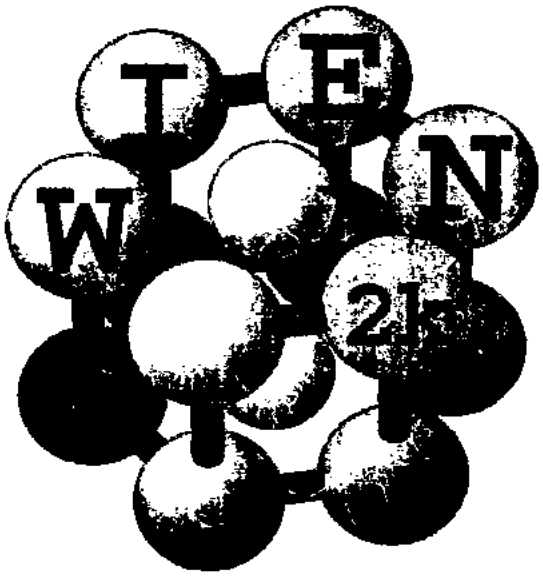

Figure 4.1 - Logo of the WIEN2k software package

4.1.1. Introduction of WIEN2k

The best method to compute the electronic structure of solids, using the density functional theory (DFT), is the linearized augmented plane wave (LAPW) method. More than 25 years ago, a full potential linearized augmented plane wave (FP-LAPW) code was set up for the calculations of the crystalline solids. Its first published legal version was named WIEN [144]. The preceding years displayed the remarkably upgraded and updated versions of the WIEN programming codes as WIEN93, WIEN95, WIEN97 and WIEN2k [145]. The WIEN2k code bases on an alternative basis set. It has been improved in speed, user-friendliness, new features and universality.

This programming software package is used for simulation results obtained from the DFT to make calculations for electronic structure, electrical and optical properties, and energy gaps in the solids. It depends upon the full-potential linearized augmented plane-wave (FP-LAPW) plus local orbitals (lo) method which is the most exact scheme to calculate the band structures of the solid materials. The FP-LAPW + lo basis set is used to solve the Kohn–Sham (KS) equations of the DFT. It is an all-electron arrangement comprising the relativistic effects and has several features. It adds the DFT a new dimension for the calculations of the solids.

4.1.2. Features of WIEN2k

WIEN2k comprises independent programs of the FORTRAN90 programming language. These programs have been connected together via the C-Shell scripts.

WIEN2k can be operated by applying the short special commands and can be run by a web browser and the W2Web (WIEN to WEB) interface. W2Web is a web server. This graphical user interface (GUI) facilitates for producing or adjusting inputs for several applications and it directs to implement many jobs.

The WIEN2k code mainly involves two parts: the initialization and leading self-consistent field (SCF) cycle. Each part is further compiled by various independent programs which have been linked by shell-scripts. Also, several analytical tools have been implemented to calculate the structural, electrical and optical properties of the solids like the band structure, density of states, charge densities, and UV, blue ray, X-ray and infrared spectra, etc.

The current version, WIEN2k_13.1, released on June 25, 2013 is a very important update which fixes many bugs and introduces to many new features. The upgrading is highly recommended. It will be installed in Linux for its working and to get the simulation results.

As the FP-LAPW + lo method is accepted as the most exact one in the DFT, so results received from this method are usually considered as a yardstick. The high accuracy in the results demands a big computational price. To calculate properties of a

solid in the bulk form, WIEN2k performs nicely but the calculations of a solid surface by the super cell approach are too much time consuming.

4.1.3. Registration of WIEN2k

WIEN2k can be had via a minor fee after filling out the Online Request Form at www.wien2k.at. Its license is given to a group, which contains the source code and free updates. Only the group members can run it on many computers as they wish. The group comprises a research leader along with its co-workers. It can't be a whole department, university or company. The license is issued to the person whose name is given on the Registration form. A person can use this license on some other place but can't reuse WEIN2k on the old location.

The WIEN2k registration fee is 4000 Euros for industry and commerce, 1000 € for Govt. institutions / Labs and 400 € for academic institutions. The fee is paid according to the indication on the Registration form. An email is sent to confirm the registration of a user and then the User Id and Password are given the registered user to download the WIEN2k code via the web browser.

There are more than 2000 registered user groups of WIEN2k all over the world.

4.1.4. WIEN2k Workshops

The WIEN2k Workshop is held every year at least once, where the new and experienced users learn more about the WIEN2k code, get the practical training, exchange ideas and share experiences. The conference fee is nominal.

The first workshop was held in 1993 in Vienna, Austria.

The 21st WIEN2k workshop was held at Nantes, France from July 02-09, 2014 with the International conference on advanced materials modeling (ICAMM).

4.1.5. Computer Requirements

1. WIEN2k works under Unix at all the platforms like IBM RS6000 (International Business Machine), Linux-PCs (Personal computers), Compac-Alpha, HP (Hewlett

Packard), Sun and SGI (Soka Gakkai International). It can hopefully be operated on the latest Unix / Linux system.

2. By the passage of time, a most efficient platform changes swiftly and we can imagine that the best cost and performance ratio will be in a Linux PC based on an Intel architecture. We have to install the Intel iFort compiler along with the Intel MKL (Math Kernel Library).

3. The hardware needs change according to the system. A 128 MB RAM is required for smaller computers for processing about 10 atoms per unit cell and for the powerful PCs or workstations with 1GB or a few GBs hard disk space, a 256 MB RAM (preferably 512 MB) is recommended. The workstations with 1-2 GB RAM have processed the systems up to 100 atoms per unit cell about and more than 1000 atoms per unit cell on clusters with 64-1024 cores and a high speed network. 10-1000 GB of hard disk is required for the big cases. Contemporarily, it is recommended a multicore CPU (Central Processing Unit) with 1-2 GB memory per core and the swap space to be the double of the PC memory.

4. If we use a Gbit network on a cluster of PCs comprising a mutual NFS (Network file system) and correctly constructed login RSH (Remote Shell Host) and SSH (Secure Shell Host), then parallelization of k-points is possible and proficient even for the loosely coupled computers connected with a slow network.

5. If we have the fast communication, e.g., the shared memory or the fast networks as InfiniBand, FFTW (Fastest Fourier Transform in the West), MPI (Message Passing Interface) and ScaLAPACK (Scalable Linear Algebra Package), then an adequate grain parallelization for a single k-point can also be obtained. The Gb ethernet is less sufficient.

6. If someone wants to use all the options comprising the GUI or XCrysDen (X Crystalline Structures and Densities), then the packages as Ghost View with PNG (Portable Network Graphics) support; GNU Plot (+ PNG (Portable Network Graphics) support); Acro Read (or similar), Emacs or another editor, Graphical Web Browser, Perl, Octave and OpenDX must be installed on the PC. The MPI (Message Passing Interface)

+ ScaLAPACK (Scalable Linear Algebra Package) is only for the parallel computers for the parallelization of 100 or more than 100 atoms per unit cell.

No principal component of WIEN2k needs these packages and these are required only for the advanced features or for W2Web.

4.1.6. Material Properties Computed by WIEN2k

i. Energy Bands and Total Energy
ii. Electron Density, Density of States (DOS) and Spin Density
iii. Bader's concept of atoms in a molecule
iv. Molecular Dynamics
v. Structure Optimization
vi. Interacting Forces and Equilibrium Geometries
vii. Fermi Surfaces
viii. Electric field gradients, Hyperfine Fields and Isomer Shifts
ix. Spin Polarization, Orbital Polarization and Spin-Orbit Coupling
x. Optical Properties
xi. X-ray Spectra and Electron Energy Loss Spectra
xii. LDA, LDA+U, GGA, Meta-GGA Approximations
xiii. Centro- or Non-centro-Symmetric Cell Analysis
xiv. All the 230 Space Groups

4.2. Running the WIEN2k Program

The WIEN2k package can be run using any web browser and the w2web interface, but at the command line in an xterm program as well. Inputs are created by the init_lapw and StructGen files. W2Web acts as the web server on a user defined port.

4.2.1. Connecting to the W2Web Server

We start w2web on all our hosts and then login a desired host as the Secure shell host (SSH) by inserting the username and password, port-number, (master-) hostname. It generates the ~/.w2web directory. We use our web browser (Firefox) and connect to the

(master-) host: port-number. Every "case" runs in its own directory as ./case. The "master input" directory is termed as case.struct as shown in Figures 4.2 and 4.3.

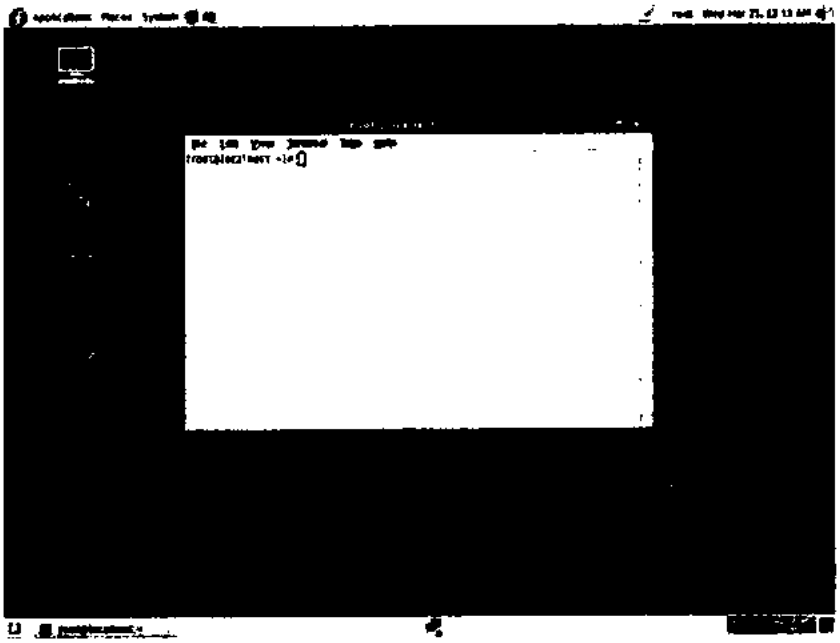

Figure 4.2 - Login desired host

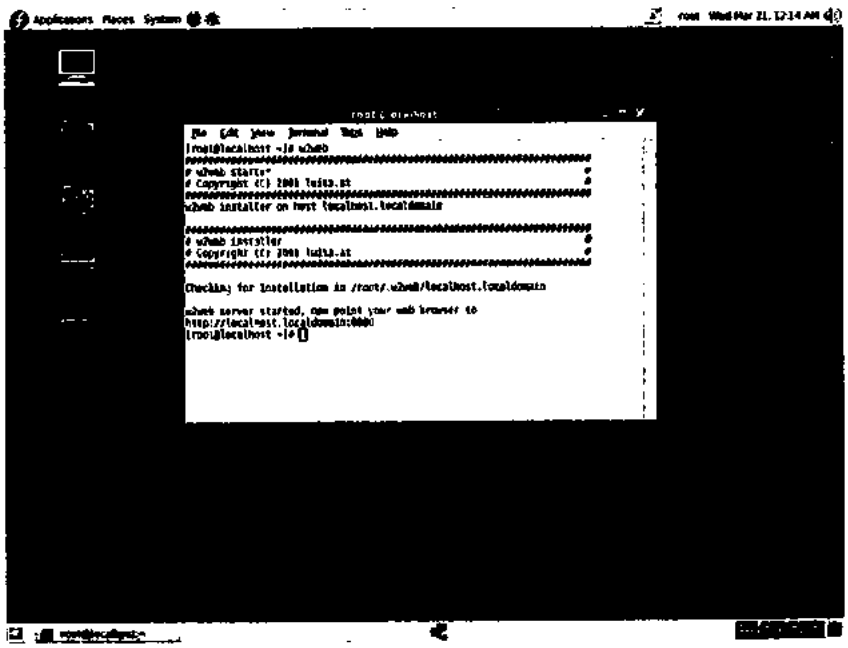

Figure 4.3 - User at the desired host connected to w2web

4.2.2. Creating the New Session

We create a new session at the desired host or select an old session as follows:

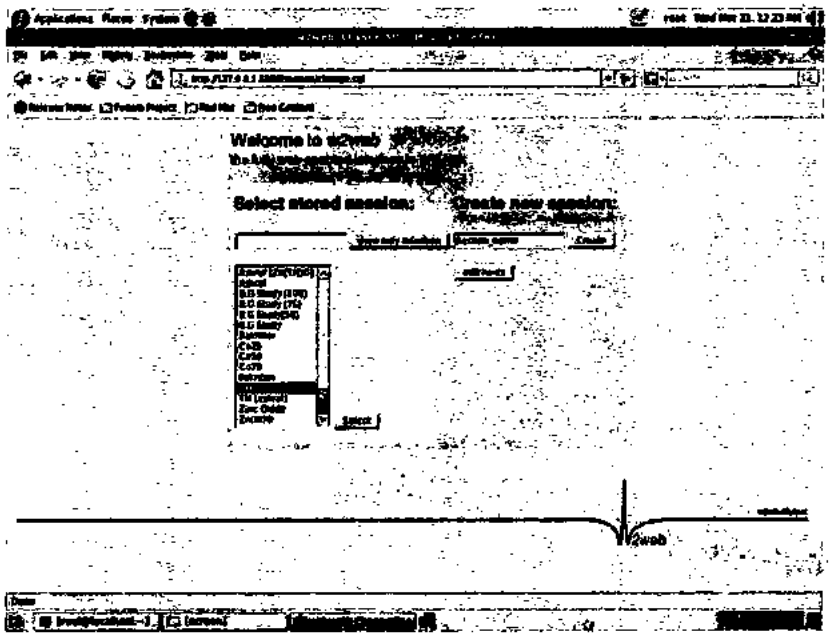

Figure 4.4 - Creation of a new session

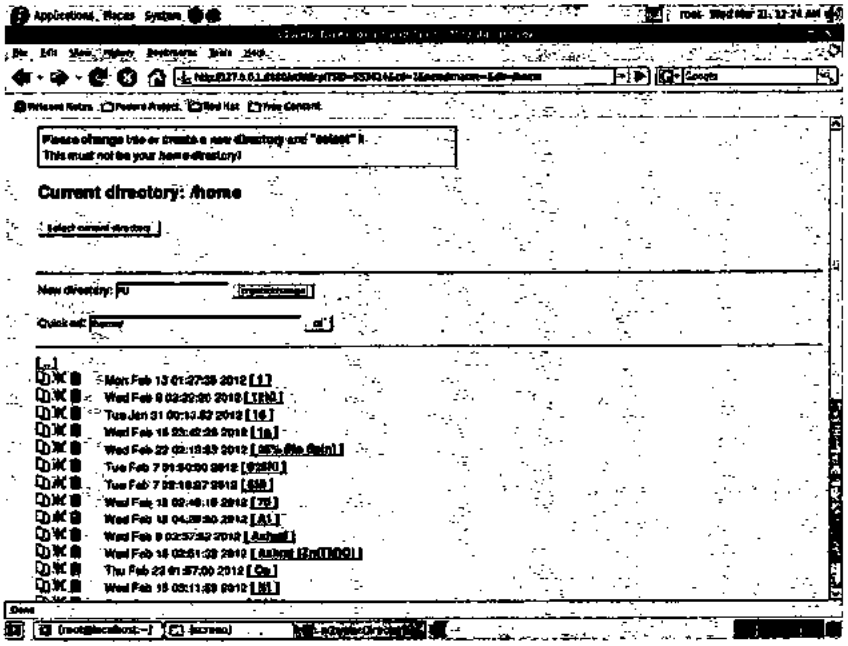

Figure 4.5 - Current working directory of the new / old session

4.2.3. Creating the Structure Generator

Now we set up a structure generator (StructGen) by importing the cif or xyz file for the initial structure. A structure file creates a template in which we will enter the structural data. It is then used to create the y.struct file.

Then we specify the lattice type, space group, lattice parameters, angles, nature and number of atoms, and their atomic positions for a special element or compound. Then we click the "Save Structure" button. The atomic number (Z) will automatically be updated and then we press "Set automatically R_{MT} and continue editing" which will determine the distances among the nearest neighbor atoms by using the nn program and then setrmt_lapw will calculate the optimum values of the Muffin-tin radii (R_{MT}) for the atomic spheres.

Then we specify a suitable reduction of the nn distances, make the non-overlapping as large as possible but not larger than 3 bohrs to save the computational time. We reduce R_{MT} 10-20 % smaller for the sp(d) elements than for the d(f) elements. The largest sphere should not be more than 50% larger than the smallest sphere. We should not change the R_{MT} during a series of calculations. The R_{MT} should be equal for the same atoms. After finishing, we exit the StructGen by pressing the "Save and claen up" button.

It will create the y.struct file displayed in the view-only genre having the distinct colour of the background, which is the Master input file for all the successive programs. This operation also automatically creates the input file for the free atom program LStart dealing with the configurations of the atoms. It updates Z, r_o and the equivalent positions automatically, and also generates the case.inst file for the atomic configurations.

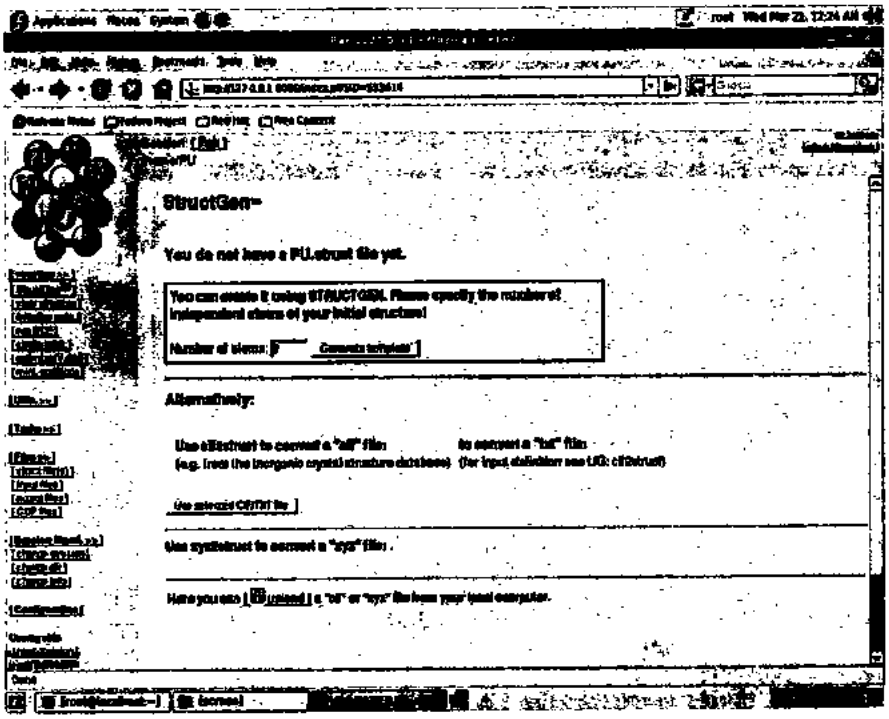

Figure 4.6 - Creation of the structure generator by the import of the xyz file

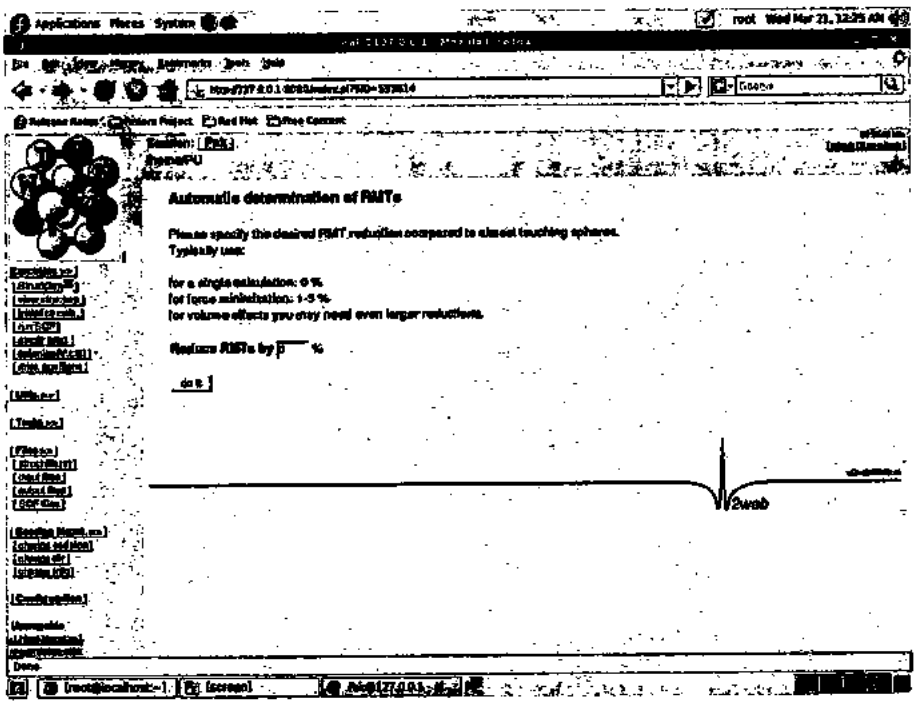

Figure 4.7 - Automatic reduction (10%) in the R_{MT}

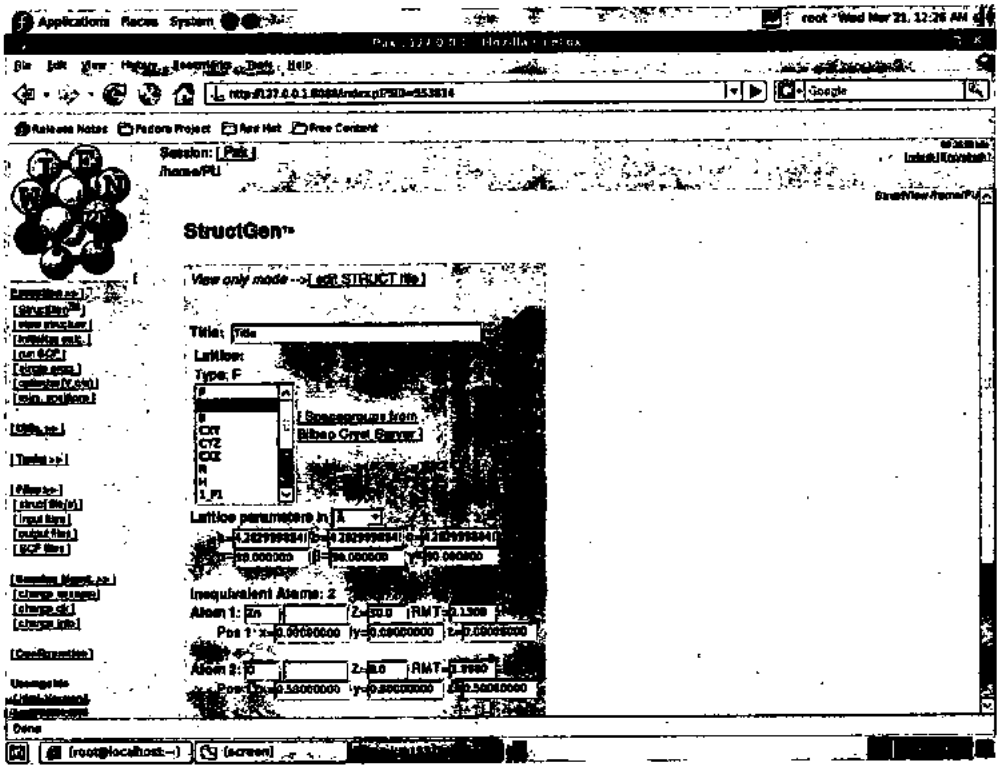

Figure 4.8 - Saving the structure generator

4.2.4. Initialization of A Computation

It is done under the init_lapw program. This program helps us detect symmetry and generates the input file under the defaults. Its cost and calculation time depend on the k-mesh and $R_{MT}K_{max}$ which finds the number of the plane waves (PWs).

X nn

The Xnn program detects the nearest neighbor distances in a certain range described by the distance factor f, and assists us compute radii of the atomic spheres. This program is also beneficial for a surplus check of the case.struct file which describes equivalency of the atoms.

X Sgroup

It is for finding the point group and space group for a certain structure.

Viewing the Y.OutputSGroup File

We can see a structure based on a given point or space group. We either acknowledge the x.struct file created by SGroup or can keep our default file.

X Symmetry

It is created from the raw case.struct file to perform the symmetry operations of a space group. It finds the point group for the distinct atomic sites; yields the LM expansion for the lattice harmonics and defines the local rotation matrices.

X Lstart

It creates densities of the free atoms and finds the manner in which the unlike orbitals are indulged in the band structure computations comprising the core or band states having the local orbitals or not.

X KeyGen

It produces a k-mesh and reduces to the irreducible segment of the Brillouin zone using the symmetry. An inversion is added automatically in the mesh except in the spin orbit (SO) computations of a magnetic material. The time inversion is valid hare, i.e., $E(\mathbf{k}) = E(-\mathbf{k})$. We always shift the k-mesh for the self-consistence field (SCF) cycle because the gaps usually exist at the Γ symmetry point in the mesh but it is not in every k-mesh.

A k-mesh for the small unit cells and metals is large containing 1000-100000 k-points while a k-mesh for the large unit cells and insulators contains 1-10 k-points only. Initially, we should use a fairly rough k-mesh for the SCF cycle and continue later with a fine k-mesh. For the density of states, spectra and optics, we apply an even finer k-mesh.

X DStart

It creates an initial density for the SCF cycle by superposing the densities of the atoms produced in the LStart program.

Initialization

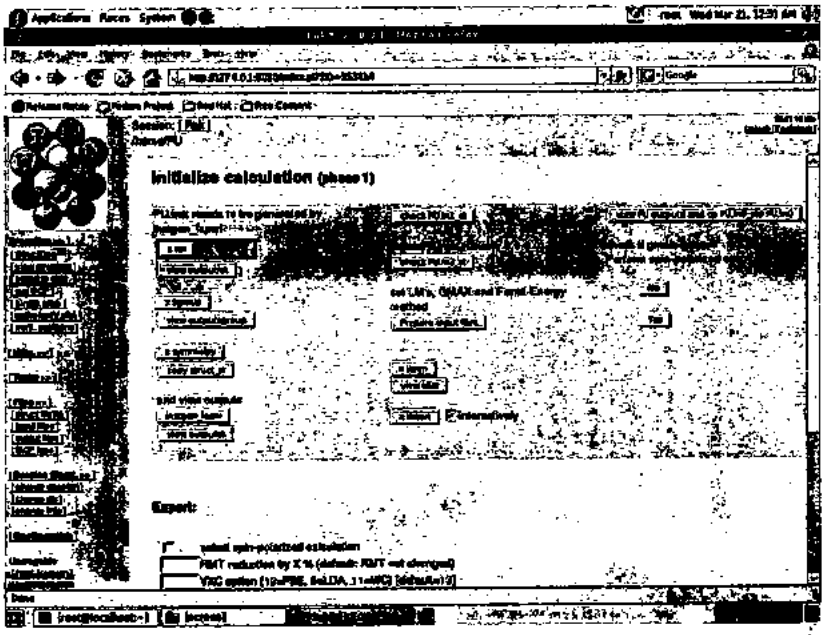

Figure 4.9 - Programs concerning the Initialization

Exchange-Correlation Potential

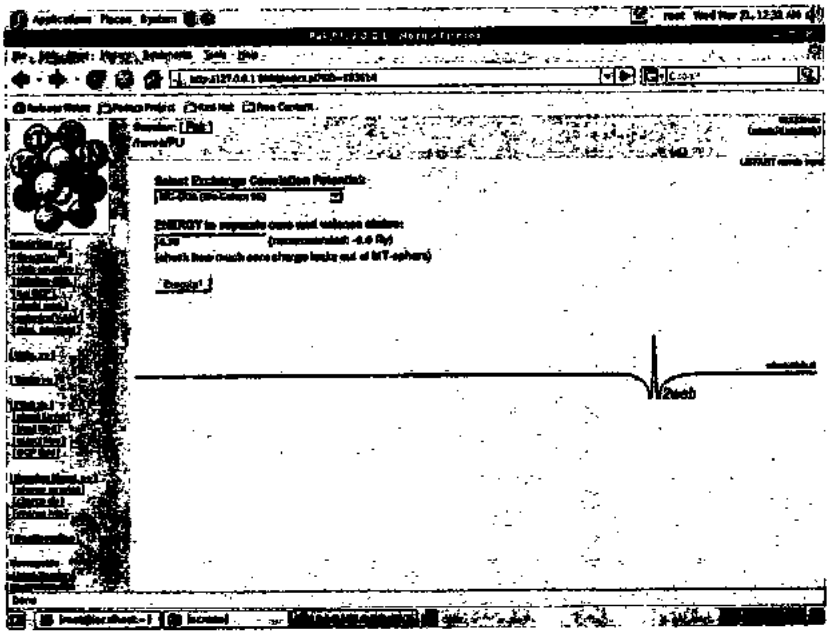

Figure 4.10 - Exchange-correlation potential and the energy in the Wu-Cohen GGA

Volume Optimization

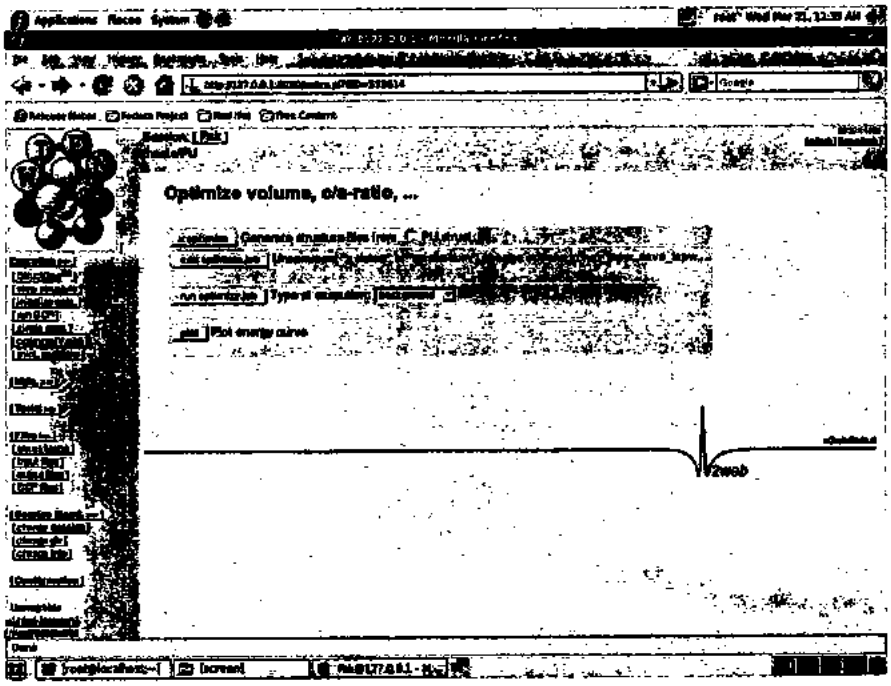

Figure 4.11 - Volume optimization for getting the lattice constant, bulk modulus and its derivative

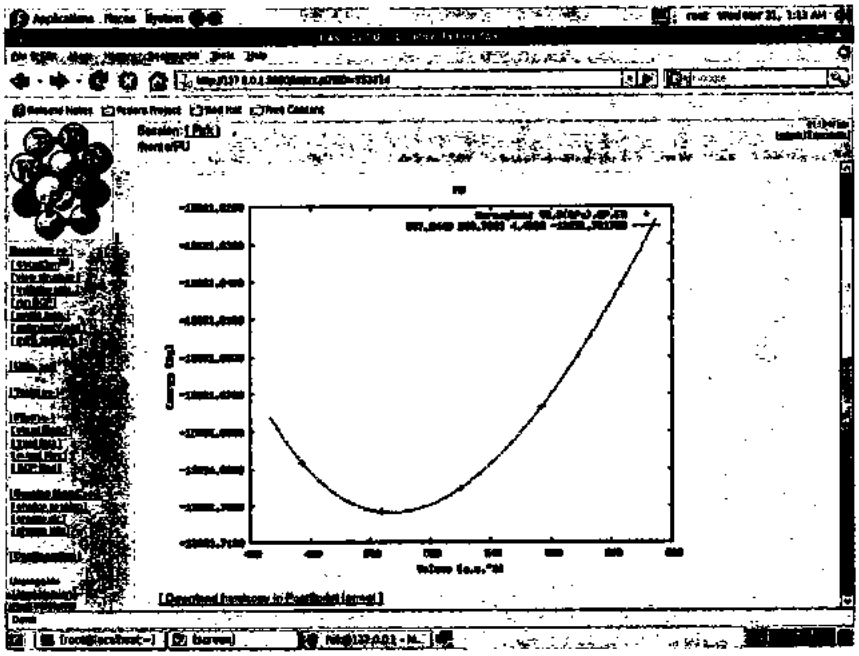

Figure 4.12 - Volume optimization curve

4.2.5. Self-Consistence Field (SCF) Computations

It is a self-consistent field cycle started and repeated to get the convergence criteria (energy, charge, forces). It works under the run_lapw or runsp_lapw programs. We can run the SCF cycle optionally along with the spin-orbit (SO) coupling or the LDA+U approach. case.scf is a master output file, which consists of history of the SCF cycle. We will calculate the band structure, the electron density, the density of states (DOS), the joint density of states (JDOS) and the optical properties, etc.

An SCF cycle is raised up by a script file run_lapw and comprises the steps as follows:

LAPW0 (Potential Generator)

It produces the potential from a certain density. The Lapw0 program calculates the total potential as the addition of the Coulomb potential and the exchange-correlation potential under the total electron spin density taken as the input. It produces the spherical part (l = 0) of the potential as case.vsp and the non-spherical component as case.vns. In the spin polarized systems, case.clmup and case.clmdn represent the spin densities and guide to two couples of the potential files as (case.vspup, case.vnsup) and (case.vspdn, case.vnsdn).

LAPW1 (Eigenvalues And Eigenvectors Finder)

The eigenvalues and the eigenvectors are found by the diagonalization of the Hamiltonian and the overlap matrix elements established by the Lapw1 program. These eigenvalues and eigenvectors are saved in the case.vector file. This program also determines the valence bands specified by the eigenvalues and the eigenvectors. A full potential computation is carried out if the case.vns file occurs.

LAPW2 (Valence Charge Density Expansions Generator)

It calculates the valence densities from the specific eigenvectors. The Lapw2 program uses the case.energy and case.vector files. It calculates the Fermi-energy and directs the expansions of the charge densities for every filled state and every k-point and

the related partial charges are computed inside the atomic spheres by integration. For the systems depriving the inversion symmetry, we use the lapw2c program joined with lapw1c for the complex analysis of the Hamiltonian and overlap matrix elements.

LCore (Core States Generator)

The LCore program is an improved version of the relativistic LSDA atomic code to determine core states comprising SO coupling relativistically or non-relativistically if NREL has been adjusted in the case.struct file for the contemporary spherical portion of the potential specified by the case.vsp file. Lcore generates the case.clmcor file for the relevant core densities, eigenvalues and core contribution to forces concerning the atoms.

Mixer (Charge Densities Adder and Mixer)

It mingles the input and output densities. It uses the LMarks program. In the mixer, the charge densities of the valence and semi-core states are added to produce the total new output densities and their normalization is observed and imposed because the simple new densities cause instabilities in the iterative SCF cycle which is essential to be stabilized by mixing the output densities with the old input densities to yield the new densities for using in the next iteration. Its running cycle is 30-50% less than that of an SCF. It is very stable and gives the real convergence because there is no pseudo-convergence due to the small mixing. In the mixer, the atomic forces and the total energy are determined by the case.scf file and then adding several contributions calculated in the previous steps of the last iteration. Therefore, the case.scf file must be given an iteration number once and it must be less than 999. The spin-polarized systems are automatically perceived by xmixer in the presence of the case.clmvalup file because the l and m values and the K-vectors are always read from the case.clmval file.

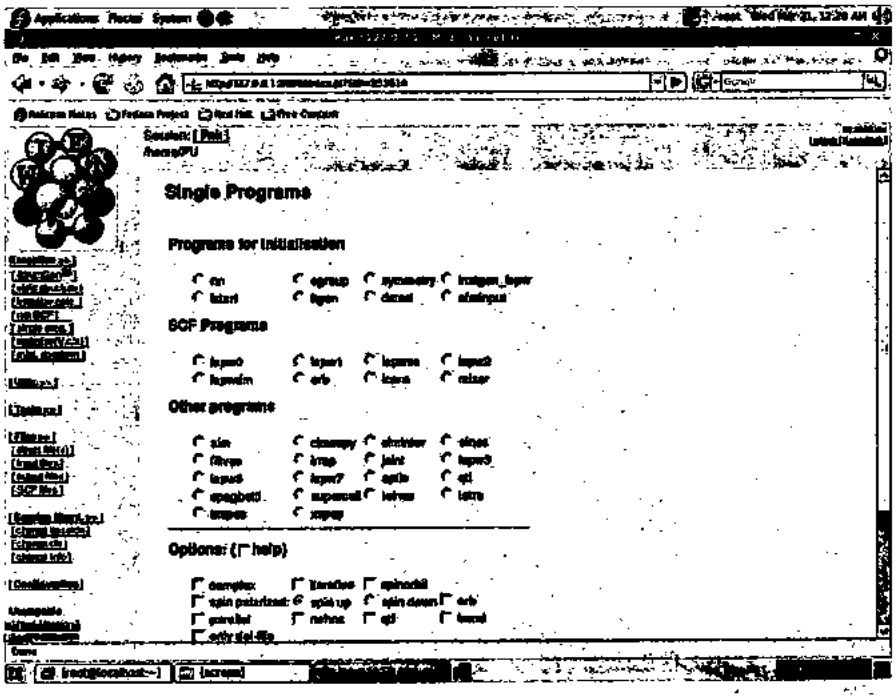

Figure 4.13 - Programs to be executed for the initialization and SCF cycle

4.2.5.1. Band Structure Calculation

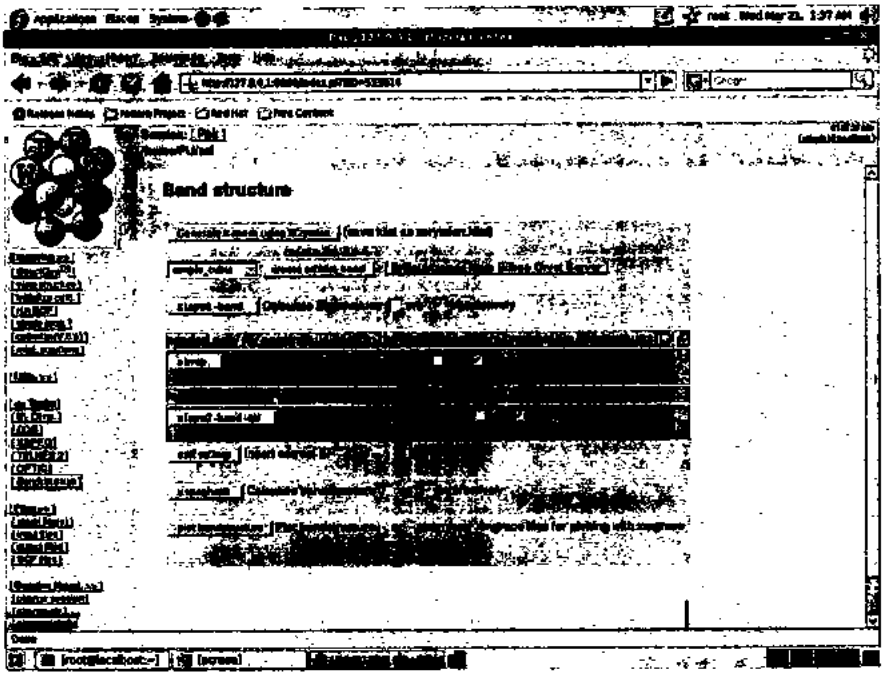

Figure 4.14 - Finding the band structure

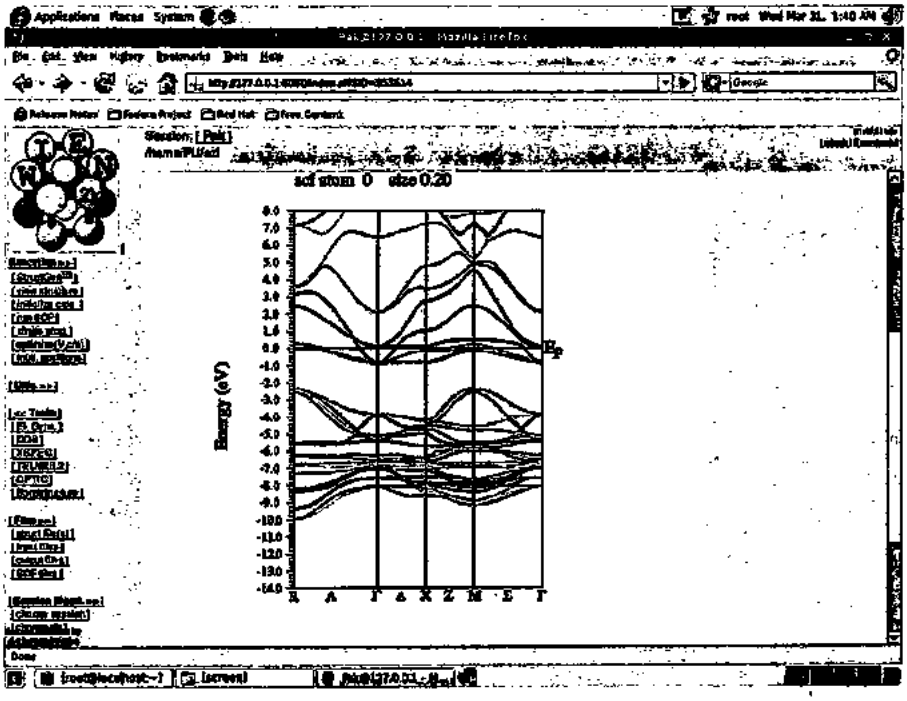

Figure 4.15 - Graph of the band structure

4.2.5.2. Electron Charge Density

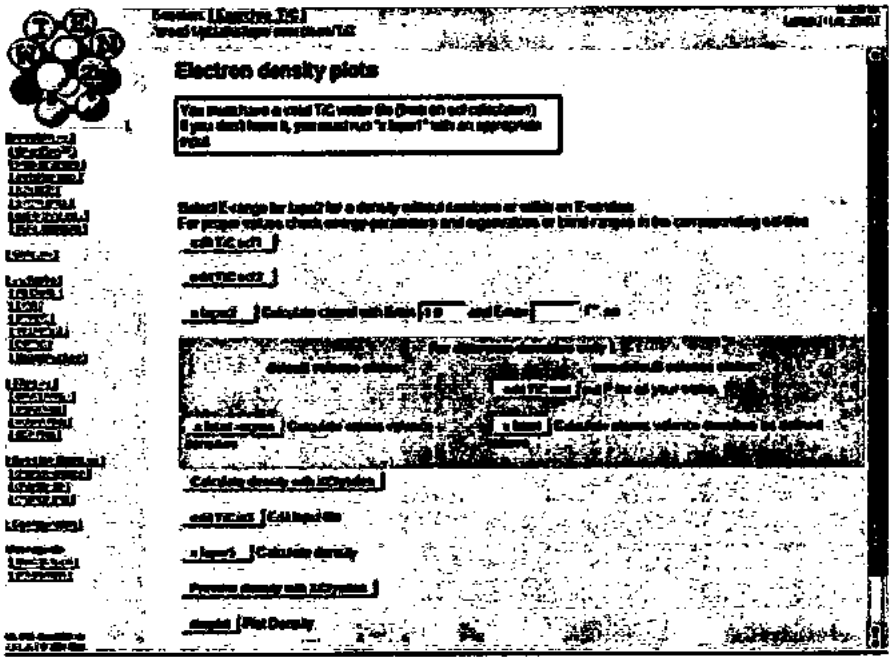

Figure 4.16 - Calculation of the electron charge density [146]

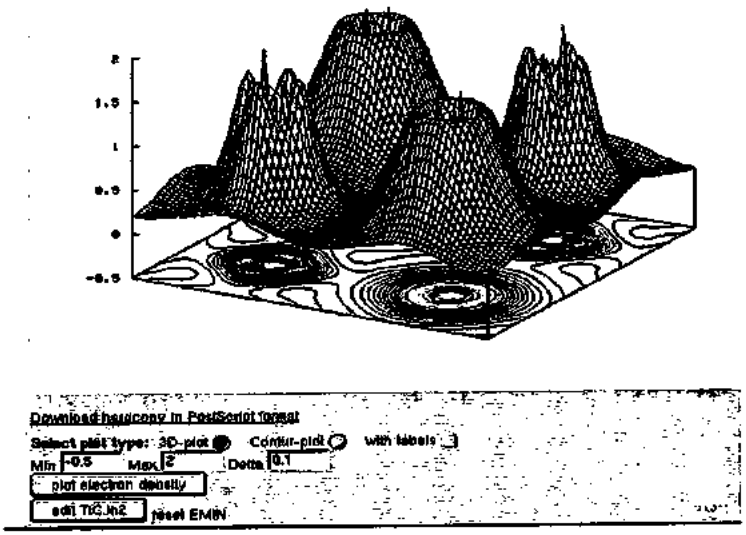

Figure 4.17 - Plot of the electron charge density along with the contour plots [146]

4.2.5.3. Density of States

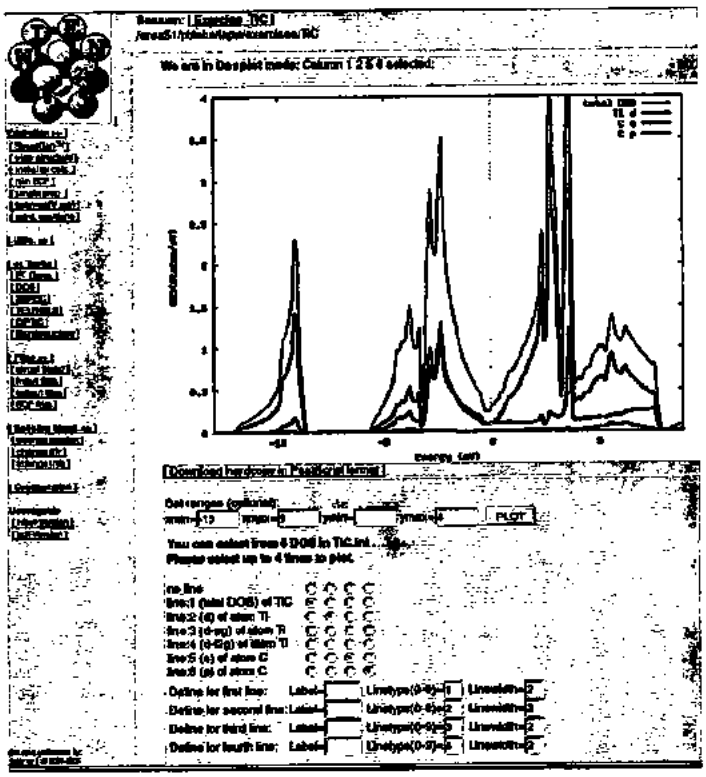

Figure 4.18 - Density of states (DOS) calculation [146]

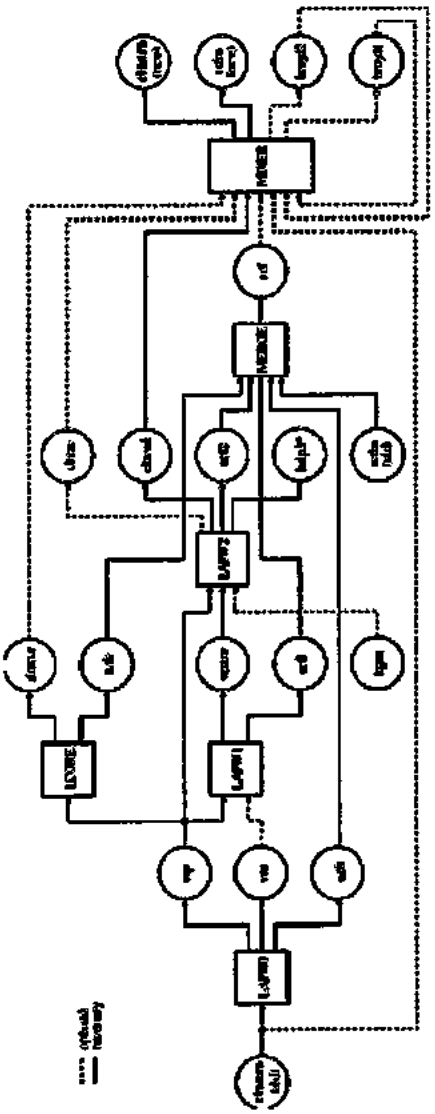

Data flow during a SCF cycle (programX.def, case.struct, case.inX, case.outputX and optional files are omitted)

Figure 4.19 - Data flowing during an SCF cycle [146]

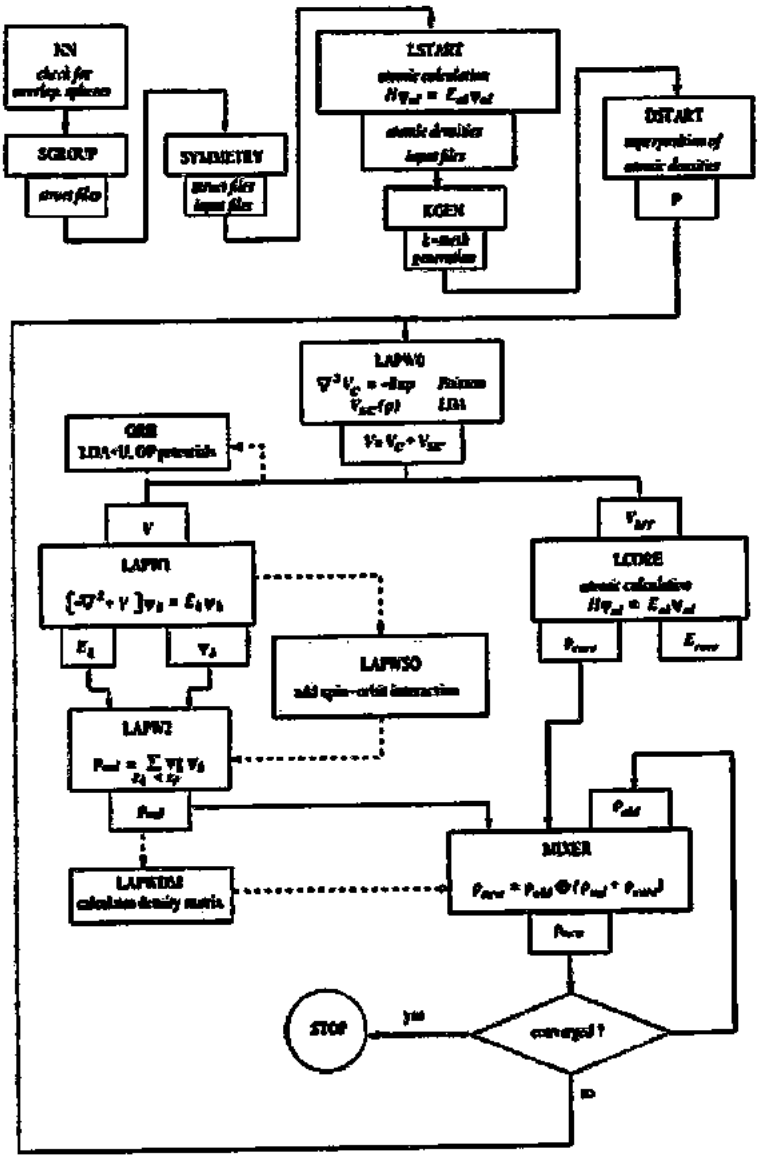

Figure 4.20 - Programs flowing in WIEN2k [146]

Chapter 5

RESULTS, DISCUSSIONS AND CONCLUSIONS

Information Technology has prevailed almost in every field of life comprising the Numerical modeling as an influential tool to understand structures of materials on behalf of the low cost high performance personal computers (PCs). Calculations of the electronic structures of the solids can be carried out through several ways by using the classical to quantum mechanical approaches.

The DFT is a comprehensive technique to determine the ground state properties of the systems of the interacting electrons. It represents an electronic system by its density (one-body problem) rather than its wave function (many-body problem) providing us with the precise results at the low computational price. Initially, the DFT was dealt as an exact theory but later, its practical implementation was based on the approximations known as the exchange and correlation potentials which by their combined application became the exchange-correlation potential. The DFT can handle from a single up to 200 atoms. It can also deal with the transition metals. The DFT approximations are trustworthy and computationally nice techniques to investigate the solids. So, in this concern, we have researched on the structural, electrical and optical properties of zinc oxide (ZnO) and its doping with Cd to form the tertiary compounds $Zn_{1-x}Cd_xO$ depending on the concentration x of cadmium (Cd).

For the computational applications, we used the full potential linearized augmented plane wave (FP-LAPW) method founded on the DFT and executed in WIEN2k software package under the Wu-Cohen GGA scheme [2] to research on the mentioned properties. Under WIEN2k, the Kohn-Sham functions are grown in terms of the spherical harmonic functions inside the non-overlapping Muffin-tin (MT) spheres of the radii R_{MT} which encompass the atomic sites, while the Fourier series (FS) is applied in the interstitial regions. Inside an MT sphere, the l-expansion was made up to $l_{max} = 10$ and the Fourier expansion of the charge density was $G_{max} = 16$. For the convergence of an energy eigenvalue, the wave function in the interstitial region is grown in the form of the plane waves (PWs) with the cut-off value as $R_{MT}K_{max} = 8$ where K_{max} is the maximum

magnitude of the reciprocal lattice vector. The total energy computations were made by taking the energy as the function of the volume of a unit cell. The volume optimization (VO) was done for ZnO and $Zn_{1-x}Cd_xO$ in the zincblende (ZB) phase under the GGA scheme by using a calculated lattice constant *a*. A volume energy curve came to hand on determining the total energy at the volume surrounding the equilibrium and the fitting determined the value of the Marnaghan equation of state [147]. We also evaluated the bulk modulus B in gigapascals (GPa); its derivative with respect to the pressure B', the bond lengths and the bond angles for the ZnO and $Zn_{1-x}Cd_xO$ alloys.

The first step of the procedure comprises VO for the ZnO and $Zn_{1-x}Cd_xO$ alloys in the ZB phase by using the experimental lattice constant under the GGA. Then we determined the electronic charge density ρ, density of states (DOS), band structure and space group for all the compounds.

5.1. Properties Of ZnO-ZB

5.1.1. Structural Properties

For ZnO-ZB, the experimental lattice constant was a = 4.62 Å [148] which on the calculation by the WIEN2k software resulted as 4.54 Å according to the following figure:

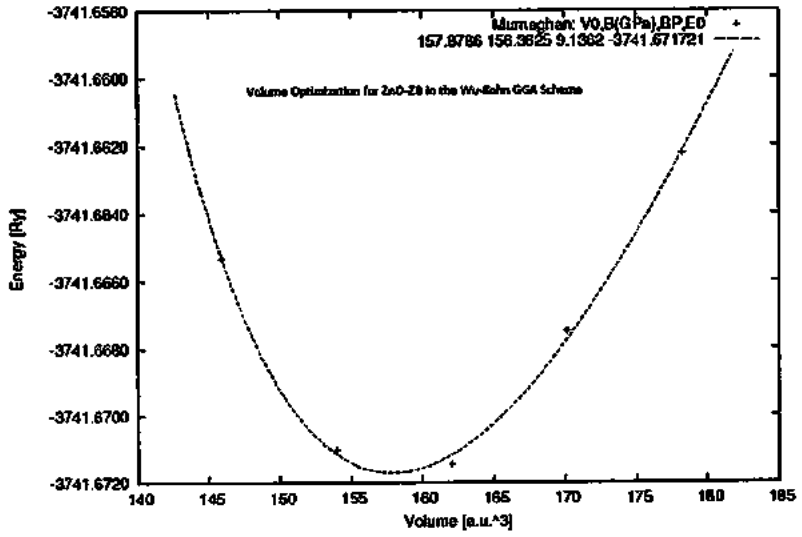

Figure 5.1 - **Volume optimization curve for ZnO in the ZB phase in the Wu-Cohen (WC) GGA**

Optimal volume = $V_o = 136.89\ (au)^3 = 157.88 \times (0.53)^3 = 23.5\ (Å)^3$

$$V_o = \frac{1}{4}\, a^3.$$

Therefore, our calculated lattice constant is:

$$a^{(1)} = (4V_o)^{1/3}.$$

Putting value of V_o, we get:

$$a^{(1)} = (4 \times 157.88)^{1/3} = (631.52)^{1/3} = 8.58\ au.$$

$$= 8.58\ au \times 0.53 = 4.54\ Å$$

5.1.2. Electrical Properties

5.1.2.1. Electronic Charge Density

The 3D charge density $\rho(r)$ has been plotted in the (110) plane for ZnO in the ZB phase. Figure 5.2(a) reveals that Zn atoms have more core electrons near the nuclei giving higher electron charge density in the vicinity of the nuclei while O atoms contain more valence electrons and are more spread out than those of Zn. The electronegativities of the Zn and O atoms are highly different, therefore the charges transfer is also different. The difference in the charge transfer between an anoin and a cation is directly proportional to the difference of the electronegativities of both the atoms. In Figure 5.2(b), the contour plot shows that the bonds between Zn and O atoms are covalent with tense ionic character. The electrons are gathered along a Zn-O bond and then repelled towards the O atom.

A 3-diemnsional plot for ZnOin the ZB phase has been shown in Figure 5.2.

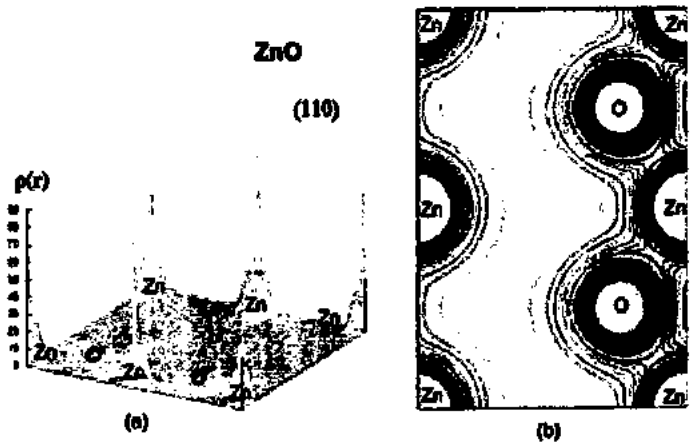

Figure 5.2 - (a) My 3D Plot of ZnO in the ZB phase for the electron density ρ(r) at plane (110) in the Wu-Cohen GGA scheme and (b) Relevant contour plot

5.1.2.2. Density of States

We computed the total density of states (TDOS) at the equilibrium volume 20.38 $(Å)^3$ under the Wu-Cohen GGA scheme for ZnO-ZB. The lowest energy states -16 eV to onward containing O s-orbitals are called the core states, the states ranging from -6.5 to 0 eV (Fermi Level) consisting of O p- and Zn d-states are termed as the semi-core states and the states ranging from 2 eV and above are called valence states. There is small hybridization between Zn 3d- and O 2p-states at about -4.5 eV due to which the band gap (BG) of ZnO increases somewhat. The density of states helps us determine the angular momentum behavior of several structures.

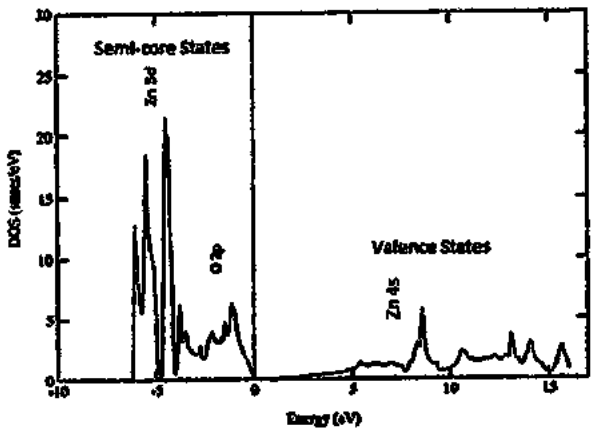

Figure 5.3 - My total density of states (TDOS) spectra for the ZnO-ZB phase in the GGA

5.1.2.3. Band Structure

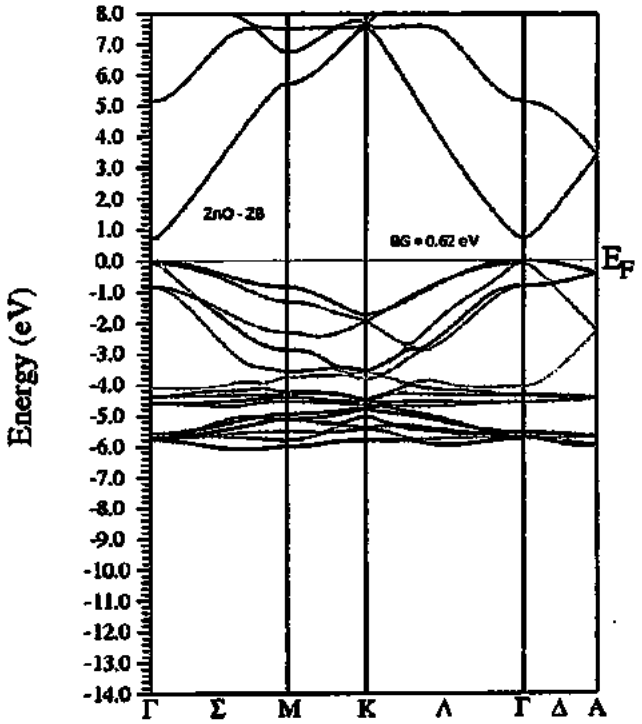

Figure 5.4 - My energy band structure of the ZnO-ZB alloy by the Wu-Cohen GGA scheme

The undermined band gap may be because of the selection of the exchange-correlation energy. The valence band mostly comprises the 2p- and 2s-states of O and 3d- and 4s-states of Zn. In the valence band, the O 2s-states are found from -16 to -19 eV and O 2p-states lie between -4 and 0 eV being very close to the previous results.

It appears from the graph that the Zn 3d-states generate a few bands in the range of 7-9 eV under the valence band maximum (VBM) showing the fragmentation and the dispersion of the wave vector k exterior to the maximum symmetry point Γ. The lowest conduction band is occupied by the Zn 4d-states and it initially emerges out of the O 2p- and Zn-4s states. The huge peak in the valence band at Γ is basically due to the Zn 3d-states. These states affect the band structure unreliably due to the abhorrence of the p- and d-states triggered by the hybridization of the corresponding states. Therefore, the band gap in ZnO is more underestimated because of the hybridization of the Zn 3d- and O 2p-states.

Table 5.1 - My calculated values for ZnO-ZB under the Wu-Cohen GGA scheme

Review Research Work				
ZnO-ZB Compound				
ELEMENT	SYMBOL WITH UNIT	THIS WORK	OTHERS THEORETICAL	EXPERIMENTAL WORKS
Scheme	GGA	Wu-Cohen GGA	GGA	
Phase	ZB / B3	Zincblende		Zincblende
Space Group	SG	216, F-43m		
Muffin-Tin Radius	R_{MT} (au)	Zn = 1.78 O = 1.58		
Optimal Volume	V_o $(Å)^3$	23.5	24.86 [149]	24.65 [148]
Lattice Constant	a (Å)	4.54	4.63 [149]	4.62 [148]
Bulk Modulus	B_o (GPa)	156.36	133.73 [149]	
Derivative of Bulk Modulus	B_o' (GPa)	4.83	4.79 [149]	
Optimal Energy	E_o (Ry)	-3741.67		
Total Density of States	TDOS (e^- states/eV)	Zn 3d = 18.5 at -5.6 eV O 2p = 6.3 at -1.2 eV	Zn 3d = 7.8 at -5.5 eV O 2p = 2.4 at -1.5 eV [150]	
Band Gap	BG/E_g (eV)	0.62	0.65 [149]	3.44 [151]

5.2. Properties of $Zn_{1-x}Cd_xO$ Alloys

We made the volume optimization for the $Zn_{1-x}Cd_xO$ alloys in the ZB phase with help of the Wu-Cohen GGA scheme. We calculated the optimal volume, theoretical lattice parameter, bulk modulus B, derivative of the bulk modulus with respect to pressure B′ and the Muffin-tin radius R_{MT}.

For the investigation of the optical band gap and optical transition of the $Zn_{1-x}Cd_xO$ alloys, it is essential to study the imaginary part of the dielectric function $\varepsilon_2(\omega)$ because it is too significant in describing the optical properties and the photon energies, $E = \hbar\omega$ [152] of a material. We are well-versed by the fact that the photon interaction with the electrons of the material may be expressed in terms of the time-dependent

perturbations of the electrons occupied states at the ground level. The optical transitions between the filled and empty states occur due to the electric field by a photon and the respective spectra may be expressed like the joint density of states (JDOS) between the valence and conduction bands. The momentum matrix elements are determined between the occupied and unoccupied states. The real part of the dielectric function can be determined from the imaginary part with the help of Kramers-Kronig relation [136]. We will study the optical properties of the $Zn_{1-x}Cd_xO$ alloys in energy range from 0 to 50 eV.

Equations to Calculate the Optical Properties

$$\varepsilon(\omega) = \varepsilon_1(\omega) + j\,\varepsilon_2(\omega), \tag{5.1}$$

where

$$\varepsilon_1(\omega) = n(\omega)^2 + k(\omega)^2 \tag{5.2}$$

and

$$\varepsilon_2(\omega) = 2n(\omega)\,k(\omega). \tag{5.3}$$

Here

$$n(\omega) = \sqrt{\frac{[\varepsilon_1(\omega)^2+\varepsilon_2(\omega)^2]^{1/2}+\varepsilon_1(\omega)}{2}} \tag{5.4}$$

and

$$k(\omega) = \sqrt{\frac{[\varepsilon_1(\omega)^2+\varepsilon_2(\omega)^2]^{1/2}-\varepsilon_1(\omega)}{2}}. \tag{5.5}$$

The complex refractive index is defined by:

$$n^*(\omega) = n(\omega) + j\,k(\omega)$$

$$= \sqrt{\varepsilon_1(\omega) + j\,\varepsilon_2(\omega)} = \sqrt{\varepsilon(\omega)}. \tag{5.6}$$

The absorption coefficient is given by:

$$\alpha(\omega) = \sqrt{2}\omega\sqrt{[\varepsilon_1(\omega)^2 + \varepsilon_2(\omega)^2]^{1/2} - \varepsilon_1(\omega)}$$

$$= \frac{4\pi}{\lambda} k(\omega). \tag{5.7}$$

The reflectivity is defined by:

$$R(\omega) = \frac{(n(\omega)-1)^2+k(\omega)^2}{(n(\omega)+1)^2+k(\omega)^2}. \tag{5.8}$$

5.2.1. $Zn_{0.75}Cd_{0.25}O$ Alloy

5.2.1.1. Structural Properties

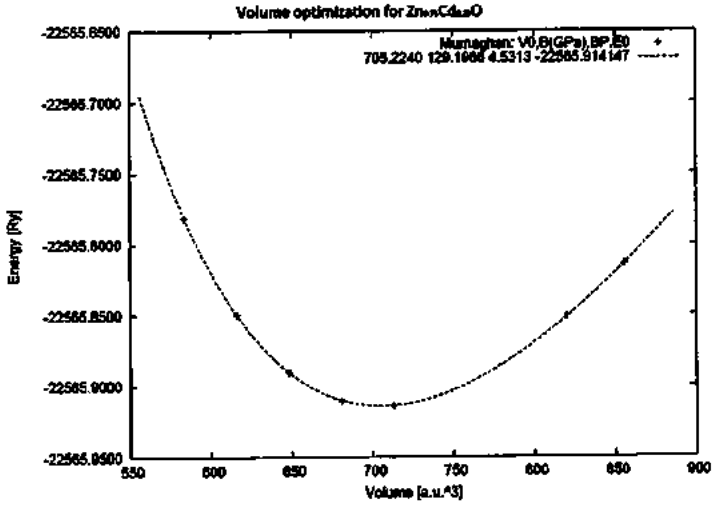

Figure 5.5 - My volume optimization curve of $Zn_{0.75}Cd_{0.25}O$ in the ZB phase in the WC GGA

Lattice constant = $a = (V_o)^{1/3} = (705.22)^{1/3} = 8.901$ au $= 8.901$ au $\times 0.53 = 4.72$ Å

5.2.1.2. Electrical Properties

5.2.1.2.1. Electron Charge Density

We computed the volume charge density for the $Zn_{0.75}Cd_{0.25}O$ alloy in the ZB phase along the (110) plane applying the Wu-Kohn GGA scheme shown in Figure 5.6(a). Figure 5.6(b) gives the contour plot for the $Zn_{0.75}Cd_{0.25}O$ alloy indicating the collection of electrons along the Zn-O and Cd-O bonds and deflect towards the O atom due to electronegativity differences among Zn, Cd and O atoms. The O atoms bond covalently with both the Zn and Cd atoms with strong ionic behavior such that the Zn-O bond is stronger than Cd-O one.

For (110) plane:

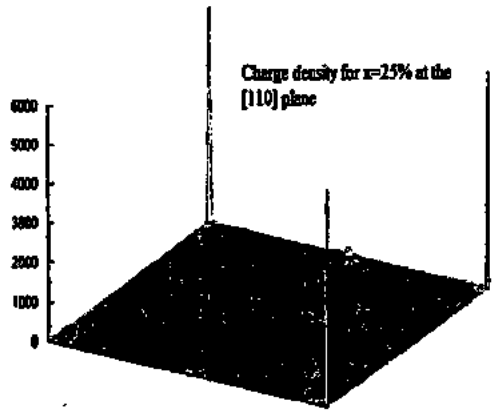

(a)

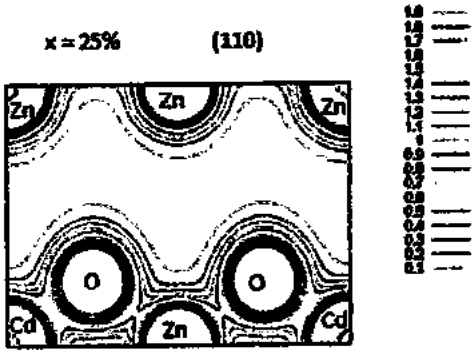

(b)

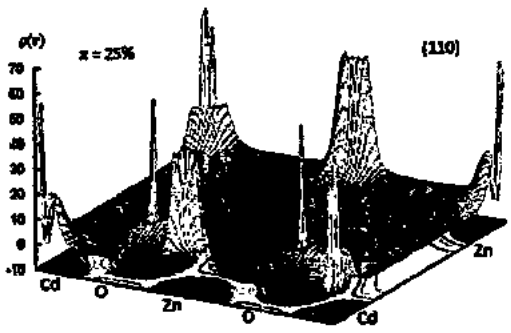

(c)

Figure 5.6 - (a) My 3D plot of $Zn_{0.75}Cd_{0.25}O$ in the ZB phase for electron density ρ(r) at plane (110) in the Wu-Cohen GGA scheme, (b) Relevant contour plot and (c) Combined 3D and contour plots

5.2.1.2.2. Density of States

The density of states (DOS) is computed for observing the bonding character and the orbital hybridization in the $Zn_{0.75}Cd_{0.25}O$ alloy in the ZB phase. The bonding character gives the semiconducting behavior as shown in Figure 5.7. The Cd 4d-states are analyzed in the energy range 12 to 13.5 eV beneath the valance band maximum (VBM) and these states increase gradually with the increasing concentration of Cd for x = 0.0625 to 0.25 while the Zn 3d-states decrease slightly between -5 to -4 eV. The Zn 3d-states have the maximum peak value of 57 at -5 eV. A VBM always lies in the Fermi level having no clear shift and has a magnified spectrum between 0 to 5 eV. For a given range of x at the bottom of the conduction band, this band shifts to the low energy range.

This shift assigns the clear variations in the electronic properties of the $Zn_{1-x}Cd_xO$ alloys. The bottom of conduction band comprises the Zn 4s-states and O 2p-states where the Zn 4s-states are dormant. The O 2p-states have the maximum value of 10 at about -1 eV. There is high orbital hybridization between Zn 3d- and O 2p-states at about -5 eV causing a huge decrease in the band gap (BG) of ZnO. An increase in the Cd concentration increases the s-states and these states go on becoming stronger and stronger resulting in the shift of the conduction band and the narrowing of the band gap due to the increase in x.

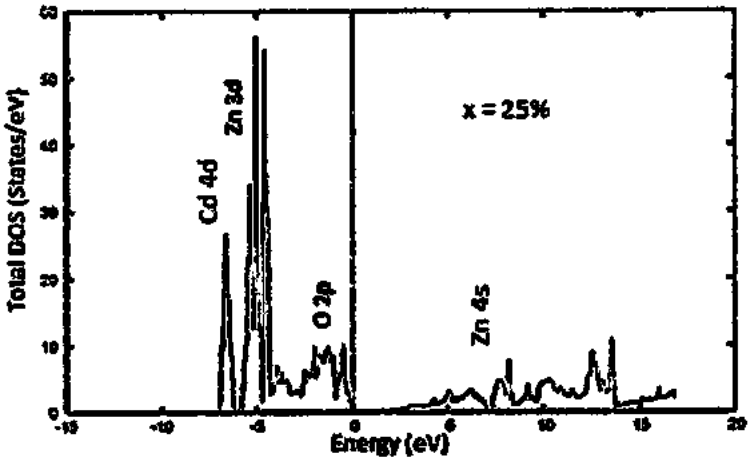

Figure 5.7 - My total density of states (TDOS) of $Zn_{0.75}Cd_{0.25}O$ in the ZB phase in the WC GGA

5.2.1.2.3. Band Structure

The band structure of the $Zn_{0.75}Cd_{0.25}O$ alloy in the ZB phase was calculated by WIEN2k in the Wu-Cohen GGA. We found a band gap of 0.2 eV at the Fermi energy E_F that is less than that of pure ZnO due to the doping of Cd at 25% as shown below:

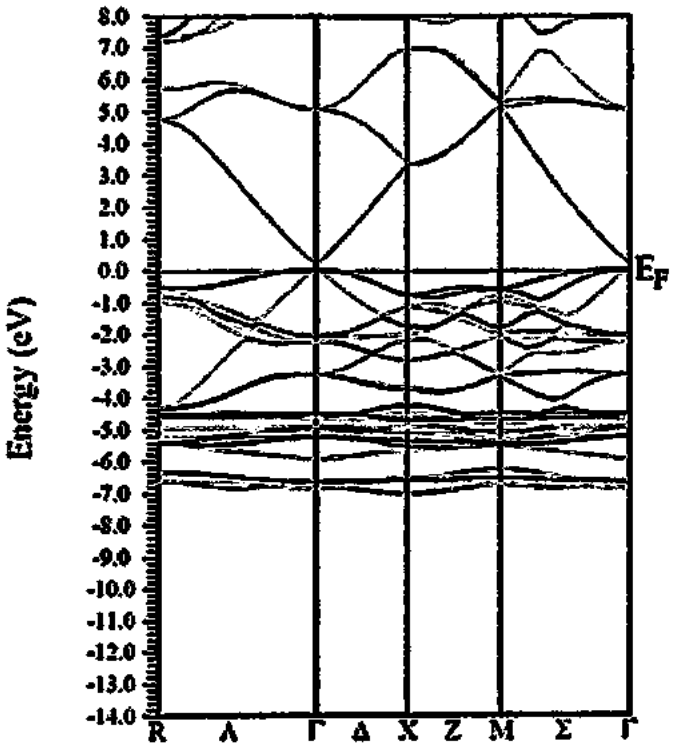

Figure 5.8 - My band structure of $Zn_{0.75}Cd_{0.25}O$ in the ZB phase in the Wu-Cohen GGA

5.2.1.3. Optical Properties

5.2.1.3.1. Dielectric Function

The dielectric function helps us determine the optical properties of the system. The imaginary part $\varepsilon_2(\omega)$ of the dielectric function with the peak value of 2.9 increases from 9.5 to 14.5 eV and then sharply decreases after it. The real part $\varepsilon_1(\omega)$ of the dielectric function has a maximum value of 3.75 at 1.5 eV. Then slightly decreases from 1.5 to 7.5 eV and then quickly decreases after this range for x = 0.25 as shown in Figure 5.9:

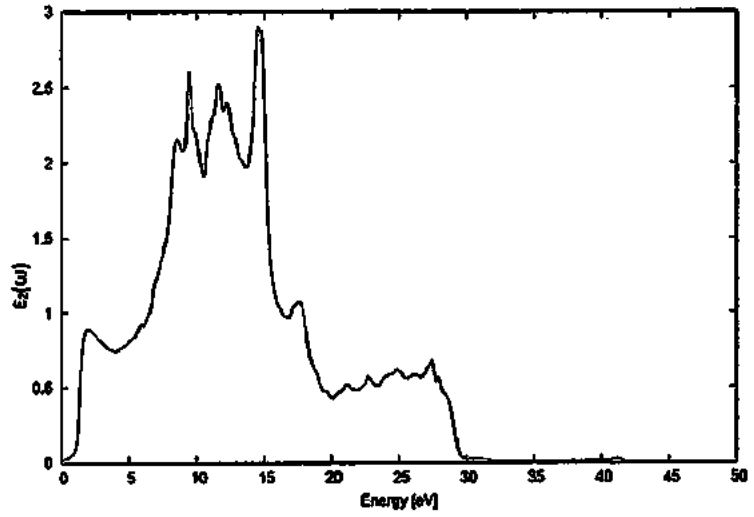

(a)

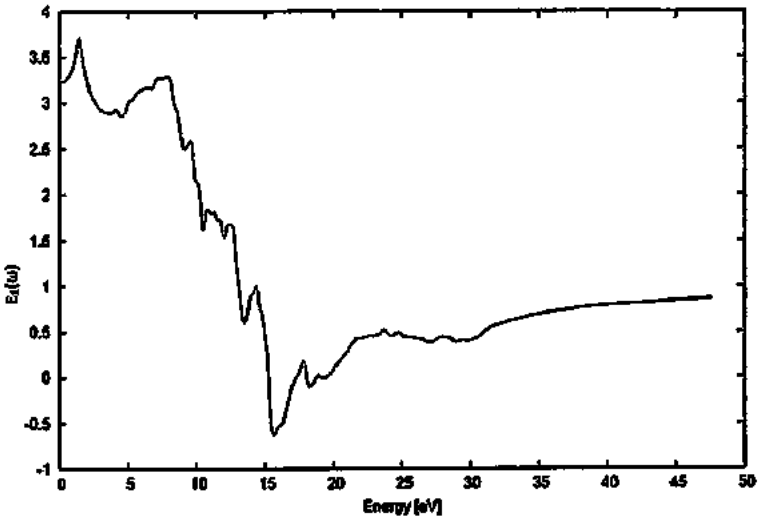

(b)

Figure 5.9 - (a) My Imaginary part $\varepsilon_2(\omega)$ of the dielectric function for $Zn_{0.75}Cd_{0.25}O$ in the ZB phase in the Wu-Cohen GGA scheme and (b) Real part $\varepsilon_1(\omega)$ of the dielectric function

5.2.1.3.2. Joint Density of States

The excited state spectra may be expressed as the joint density of states (JDOS) between the valence and conduction bands of the material. The JDOS increases from 10-15 eV over the low energy range and then sharply decreases after it. Its maximum peak value is 3.8 at 15.2 eV.

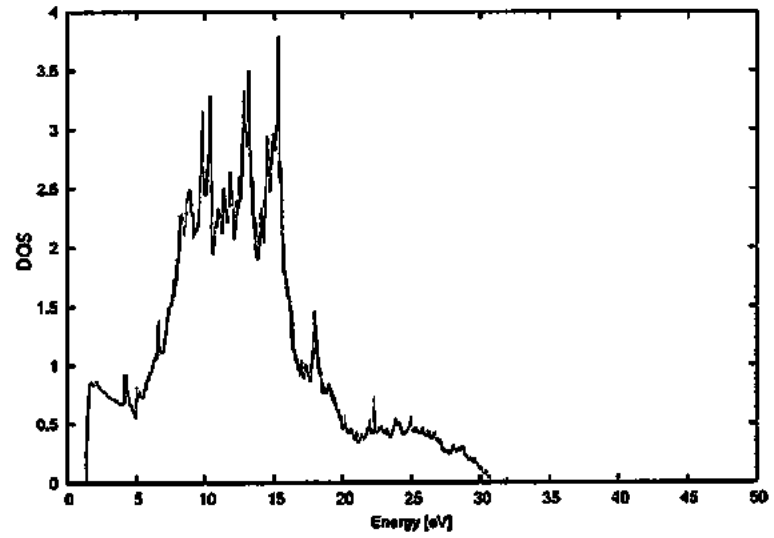

Figure 5.10 - My joint density of states (JDOS) spectra for $Zn_{0.75}Cd_{0.25}O$ in the ZB phase

5.2.1.3.3. Conductivity

The following figure describes the effect on the conductivity C of the $Zn_{0.75}Cd_{0.25}O$ alloy. We see that the Cd incorporation x is faint in the low range of the energy while the conductivity having a maximum peak value of 5.4 $\Omega^{-1}cm^{-1}$ at 15.1 eV quickly reduces above 15 eV corresponding to a change in $\varepsilon_2(\omega)$.

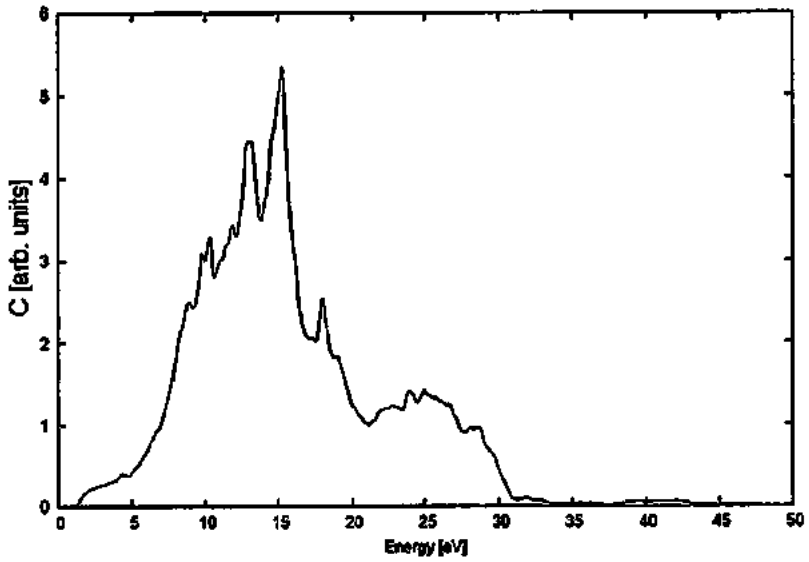

Figure 5.11 - My conductivity spectra for $Zn_{0.75}Cd_{0.25}O$ in the ZB phase in the GGA

5.2.1.3.4. Energy Loss Function

Figure 5.12 shows the energy loss function L that represents the energy loss of a fast electron navigating in $Zn_{0.75}Cd_{0.25}O$ in the ZB phase. The peak values of 1.95 eV at 20.5 eV and 1.3 eV at 27 eV in L describe the plasma resonance peak assigning the points of the transition from the metallic property to the dielectric properties for $Zn_{0.75}Cd_{0.25}O$. The doping of Cd for x = 25% in ZnO persuades the blue shift of 20.3 eV peak with a high fall in the spectra of the energy loss function.

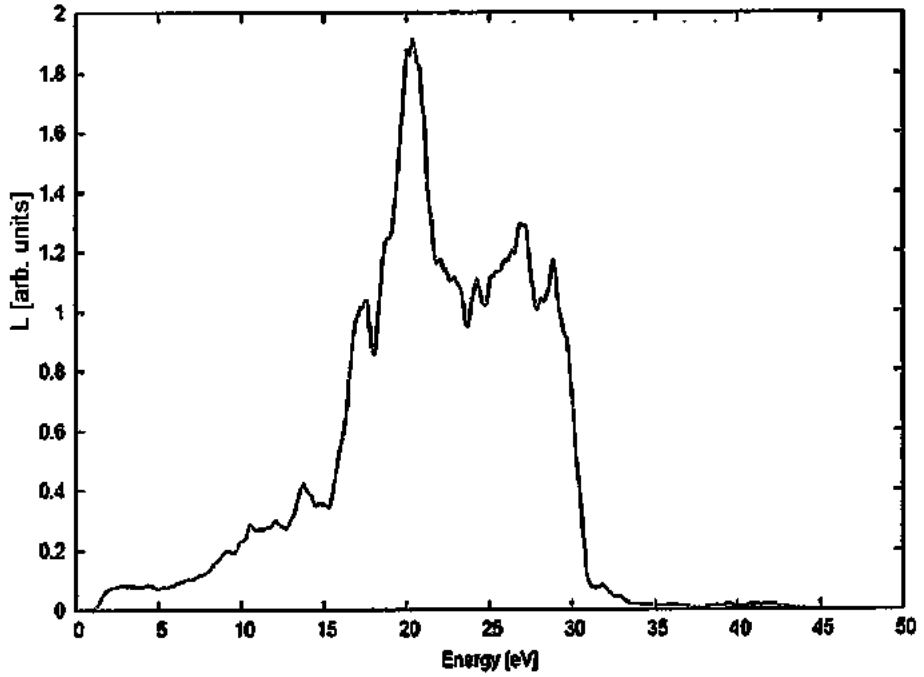

Figure 5.12 - Calculated energy loss function spectra for $Zn_{0.75}Cd_{0.25}O$ in the ZB phase in the Wu-Cohen GGA scheme

5.2.1.3.5. Refractive Index

The refractive index n of the $Zn_{0.75}Cd_{0.25}O$ alloy in the ZB phase helps in modeling and designing devices exactly. We see in the following figure that n enhances in the low energy range indicating a decrease in the band spacing of $Zn_{0.75}Cd_{0.25}O$. It is due to the doping of Cd into ZnO which may lift up the s-states in the conduction band concluding an increase in the optical transition between the highest valence and the

lowest conduction bands in $Zn_{0.75}Cd_{0.25}O$. The maximum value of n comes out to be 1.2 at about 15.3 eV and the corresponding peak concerns with the optical transition close to the band gap as shown below:

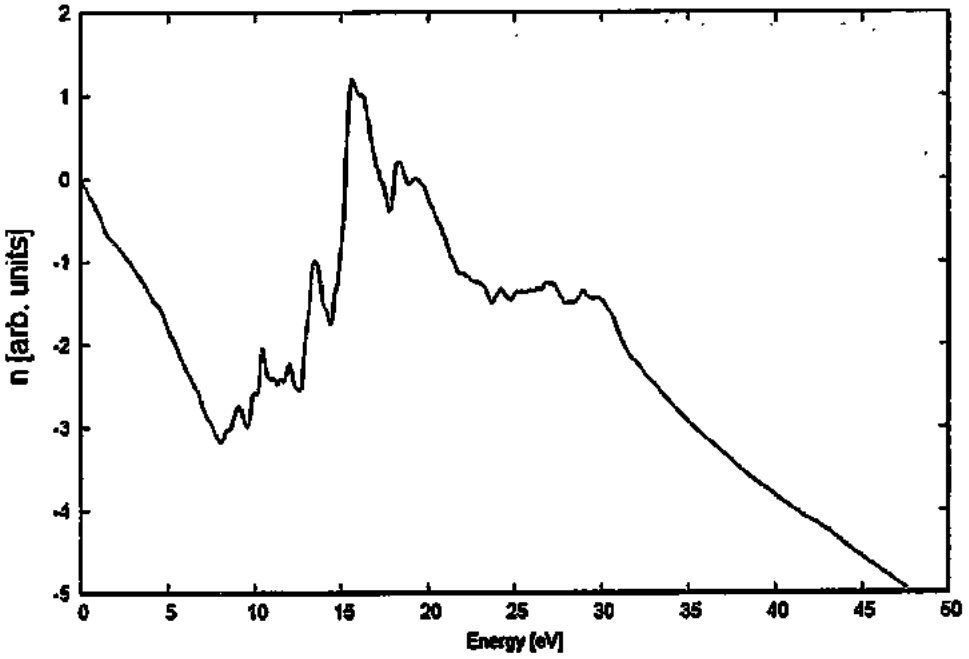

Figure 5.13 - My Refractive index spectra for $Zn_{0.75}Cd_{0.25}O$ in the ZB phase in the Wu-Cohen GGA scheme

Table 5.2 - Measured values for $Zn_{0.75}Cd_{0.25}O$ in the ZB phase by the Wu-Cohen GGA scheme

Recent Research Work			
$Zn_{0.75}Cd_{0.25}O$			
ELEMENT	SYMBOL WITH UNIT	THIS WORK	OTHERS WORK
Scheme	GGA	Wu-Cohen GGA	
Phase	ZB	Zincblende	
Space Group	SG	215, P-43m	
Muffin-Tin Radius	R_{MT} (au)	Zn = 1.78 Cd = 1.78 O = 1.58	
Optimal Volume	V_o $(au)^3$	705.22	
Lattice Constant	a (Å)	4.72	
Bulk Modulus	B_o (GPa)	129.19	
Derivative of Bulk Modulus	B_o' (GPa)	4.52	
Optimal Energy	E_o (Ry)	-22565.92	
Band Gap	BG / E_g (eV)	0.2	0.13 [152]
Dielectric Function	Real Part of DF = $\varepsilon_1(\omega)$ Imaginary Part = $\varepsilon_2(\omega)$	3.74 at 1.3 eV 2.9 at 14.5 eV	2.73 at 1.2 eV [152] 7.4 at 10.3 eV [153]
Total Density of States	TDOS (e^- states/eV)	Cd 4d = 27 at -6.7 eV Zn 3d = 34 at -5.4 eV O 2p = 10.5 at -0.5 eV	Cd 4d = 57 at -8.3 eV Zn 3d = 86 at -6.2 eV O 2p = 28 at -1 eV [152] Cd 4d = 11.2 at -9.3 eV Zn 3d = 9.9 at -9.5 eV O 2p =7.2 at -5.7 eV [153]
Joint Density of States	JDOS (e^- states/eV)	3.8 at 15 eV	
Conductivity	C $(\Omega^{-1}cm^{-1})$	5.4 at 15 eV	1.3 at 6.6 eV [152]
Energy Loss Function	L (eV)	1.95 at 21 eV	1.96 at 12.7 eV [152]
Refractive Index	n	1.2 at 15.3 eV	2.48 at 0.02 eV [152]

5.2.2. $Zn_{0.50}Cd_{0.50}O$ Alloy

5.2.2.1. Structural Properties

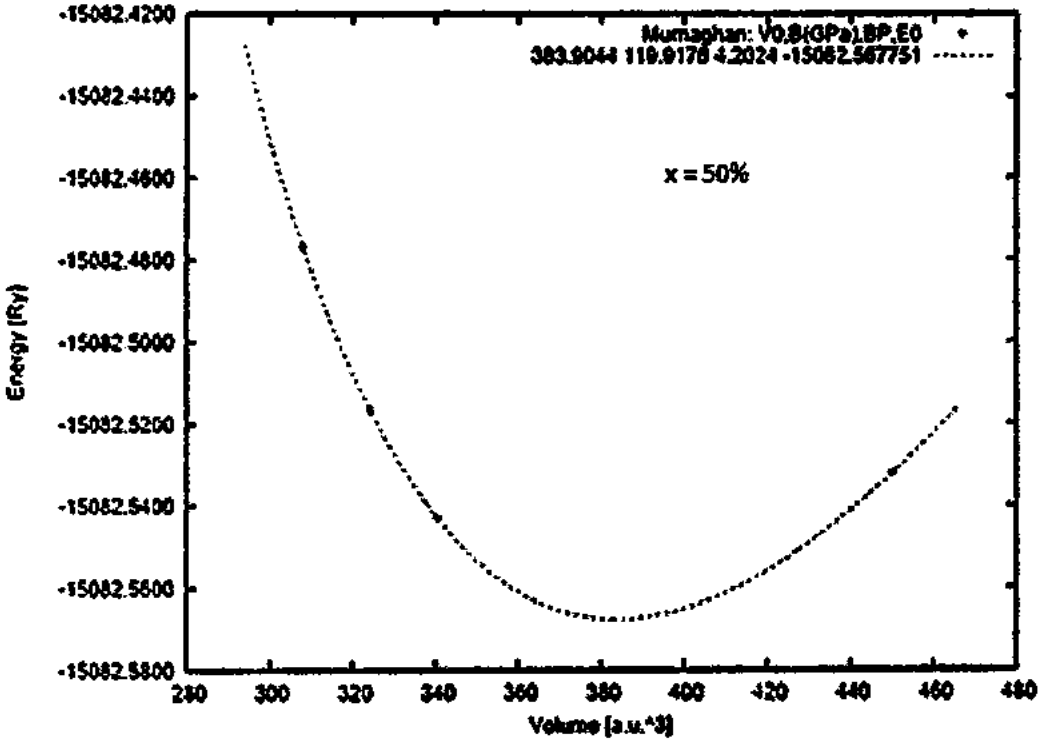

Figure 5.14 - Volume optimization for the $Zn_{0.50}Cd_{0.50}O$-ZB in the Wu-Cohen GGA

5.2.2.2. Electrical Properties

5.2.2.2.1. Charge Density

We computed the volume charge density for the $Zn_{0.75}Cd_{0.25}O$ alloy in the ZB phase along the (110) plane applying the Wu-Cohen GGA scheme shown in Figure 5.15(a). Figure 5.15(b) gives the contour plot for $Zn_{0.50}Cd_{0.50}O$ indicating the collection of electrons along the Zn-O and Cd-O bonds and deflect towards the O atom due to electronegativity differences among Zn, Cd and O atoms. The O atoms bond covalently with both the Zn and Cd atoms with strong ionic character such that the Zn-O and Cd-O bonds are almost equally stronger. Both the figures are combined in Figure 5.15(c).

Plane (110):

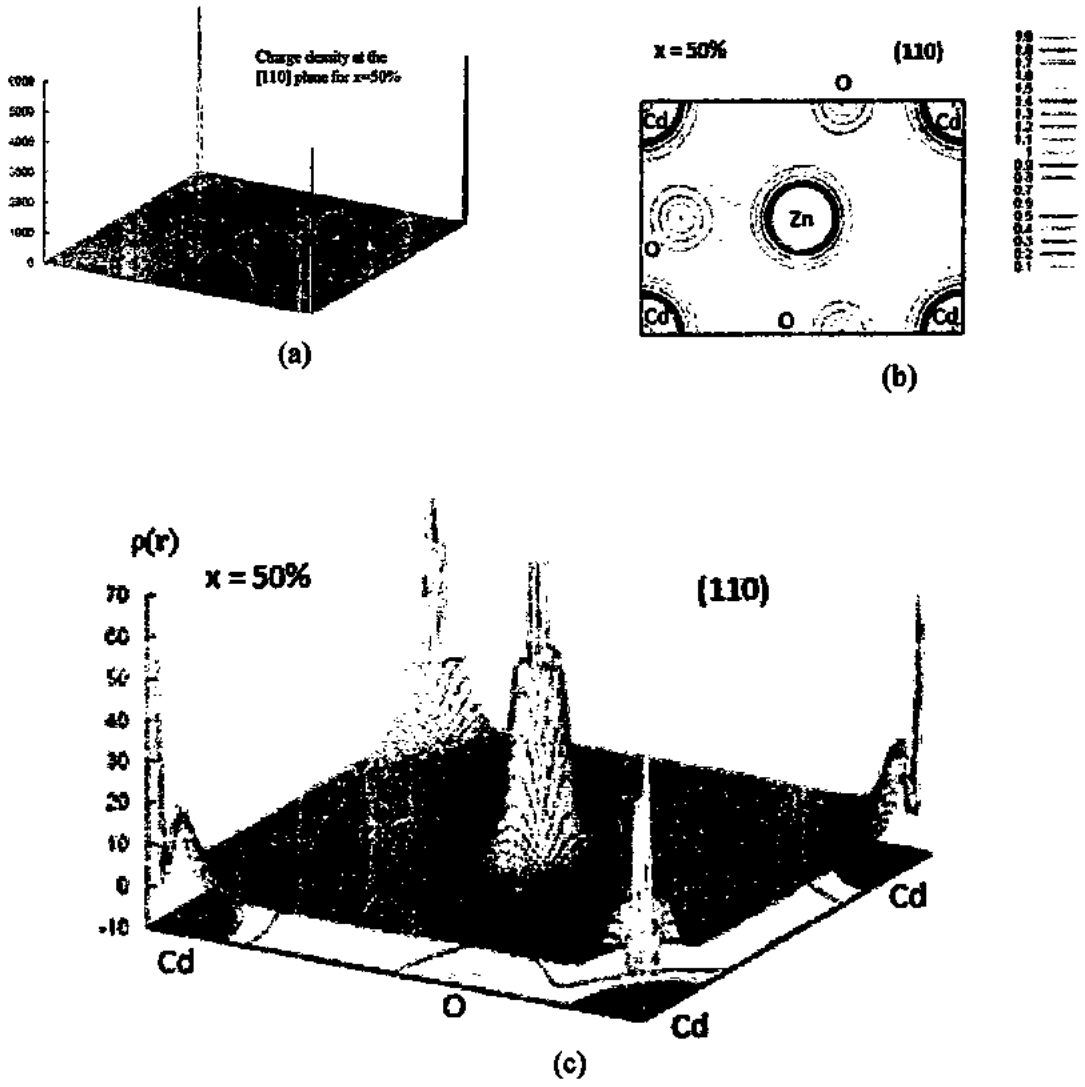

Figure 5.15 - **(a) My 3D plot of $Zn_{0.50}Cd_{0.50}O$ in the ZB phase for the electron density ρ(r) at plane (110) in the Wu-Kohn GGA scheme, (b) Relevant contour plot and (c) Combined 3D and contour plots**

5.2.2.2.2. Density of States

The density of states (DOS) is computed for watching bonding character and hybridization in the $Zn_{0.50}Cd_{0.50}O$-ZB alloy. This bonding character provides the metallic behavior. The Zn d-states have maximum peak value of 62 at -5.7 eV and that of the O-p states is 17.5 at -0.3 eV. No orbital hybridization occurs between Zn 3d- and O 2p-states.

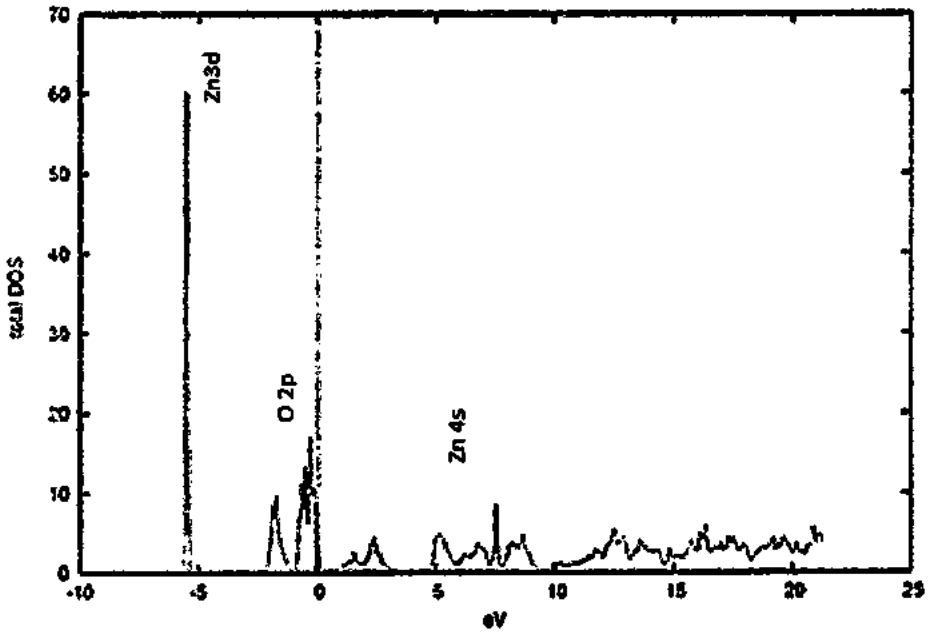

Figure 5.16 - TDOS of the $Zn_{0.50}Cd_{0.50}O$-ZB alloy in the Wu-Cohen GGA scheme

5.2.2.2.3. Band Structure

The band structure of the $Zn_{0.50}Cd_{0.50}O$-ZB alloy was computed by the WIEN2k program applying the Wu-Kohn GGA scheme. We determined an overlapping of the valence and conduction bands at the Fermi energy E_F, which shows that $Zn_{0.50}Cd_{0.50}O$ possesses metallic properties as shown in Figure 5.17:

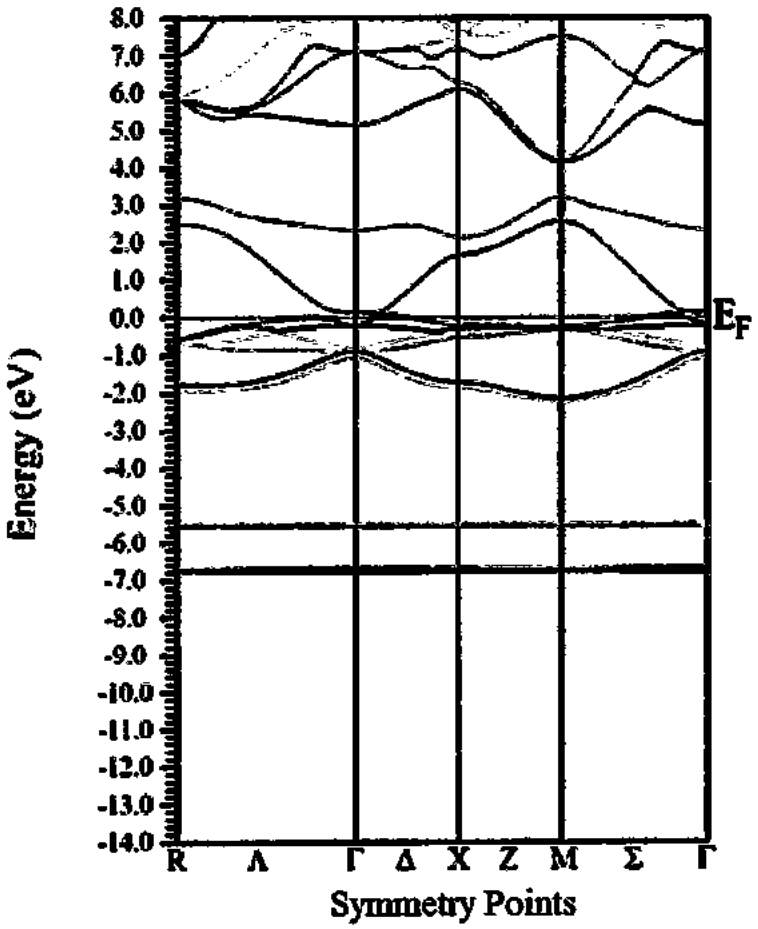

Figure 5.17 - **Band structure of the $Zn_{0.50}Cd_{0.50}O$-ZB alloy in the Wu-Cohen GGA scheme**

5.2.2.3. Optical Properties

5.2.2.3.1. Dielectric Function

The optical properties of the $Zn_{0.50}Cd_{0.50}O$-ZB alloy are determined by the dielectric function. The imaginary part $\varepsilon_2(\omega)$ of the dielectric function has a maximum value of 2.5 at 5 eV and then falls immediately after it. The real part $\varepsilon_1(\omega)$ of the dielectric function has the maximum peak value of 3.7 at 2 eV and then quickly decreases after it for x = 50% as shown in Figure 5.18.

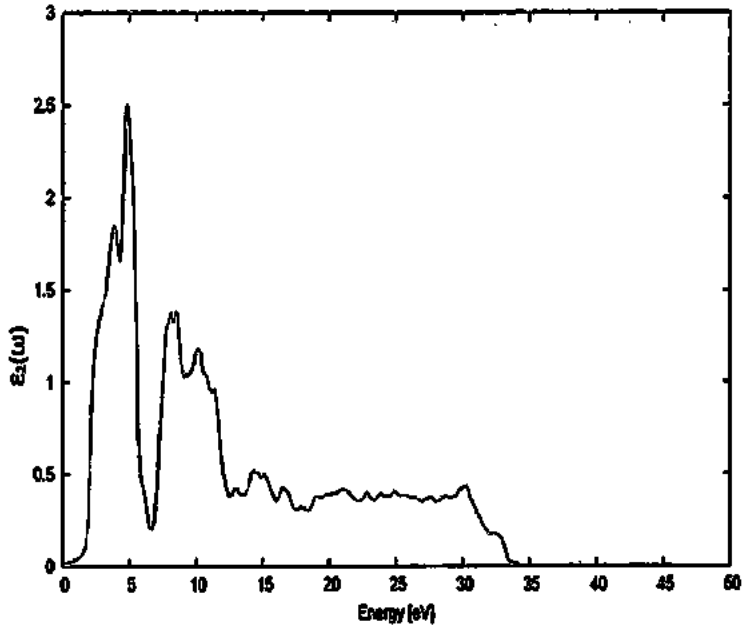

(a)

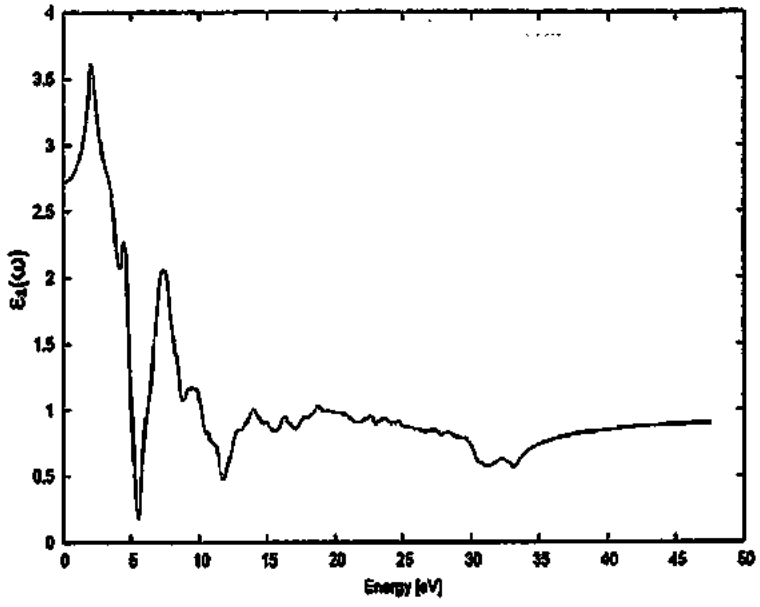

(b)

Figure 5.18 - (a) My Imaginary part $\varepsilon_2(\omega)$ of the dielectric function for $Zn_{0.50}Cd_{0.50}O$ in the ZB phase in the Wu-Cohen GGA and (b) Real part $\varepsilon_1(\omega)$ of the dielectric function

5.2.2.3.2. Conductivity

Figure 5.19 expresses the effect on the conductivity C of the $Zn_{0.50}Cd_{0.50}O$-ZB alloy. We find that the Cd impurity x is apparent in the low energy range. Its maximum value is 1.6 $\Omega^{-1}cm^{-1}$ at 30 eV. It slightly increases from 5-30 eV and then quickly decreases over 30 eV corresponding to the deviation of $\varepsilon_2(\omega)$.

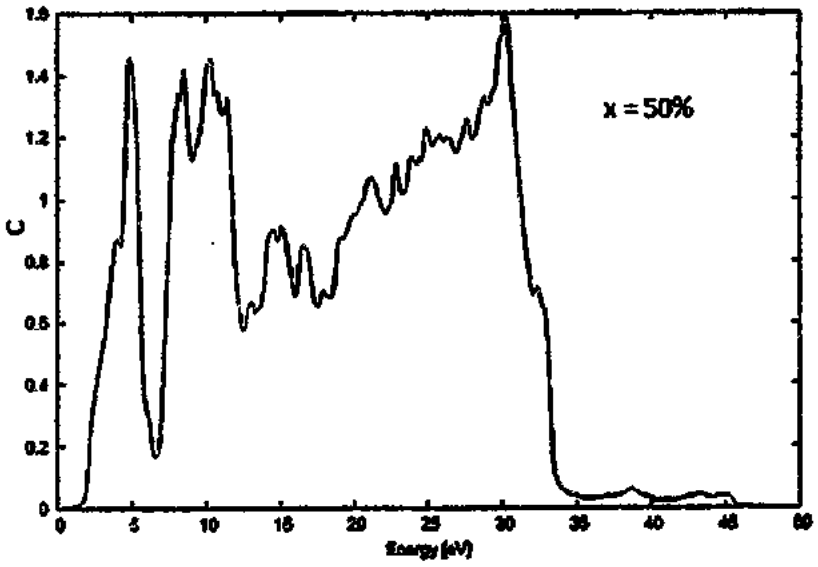

Figure 5.19 - **My conductivity spectra for the $Zn_{0.50}Cd_{0.50}O$-ZB alloy in the Wu-Cohen GGA**

5.2.2.3.3. Energy Loss Function

The energy loss function L that describes the energy loss of a fast electron passing through $Zn_{0.50}Cd_{0.50}O$-ZB. The peaks of 1.18 eV at 5.6 eV and 1.0 eV at 12 eV in L are the plasma resonance peak assigning the points of the transition from the metallic property to the dielectric properties of the system. The doping of Cd for x = 50% in ZnO causes a blue shift of 30 eV peak with a higher decrease in the loss function spectrum as expressed in Figure 5.20.

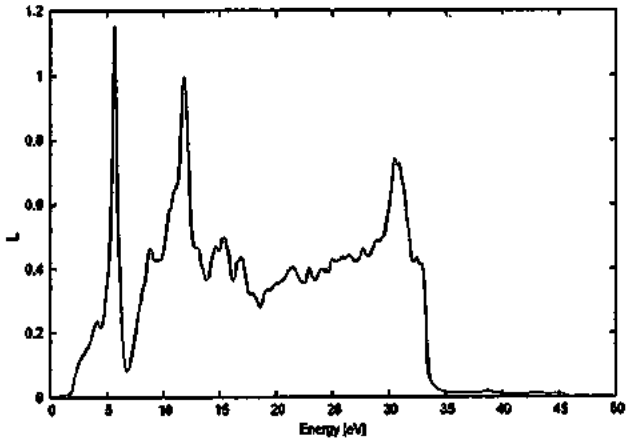

Figure 5.20 - My energy loss function spectra for the $Zn_{0.50}Cd_{0.50}O$-ZB alloy in the GGA

5.2.2.3.4. Refractive Index

The refractive index n of the $Zn_{0.50}Cd_{0.50}O$-ZB alloy helps in sculpting and manipulating instruments precisely. We see in the following figure that n enhances in the low energy range indicating a decrease in the band interval of the system. It is because of the doping of Cd into ZnO which may lift up the s-states in the conduction band resulting in an increase in the optical transition between the uppermost valence band and lowest conduction band in the $Zn_{0.50}Cd_{0.50}O$-ZB alloy. The maximum value of n comes out to be -0.1 at 5.5 eV about and the equivalent peak is linked with the optical transition close to the band spacing.

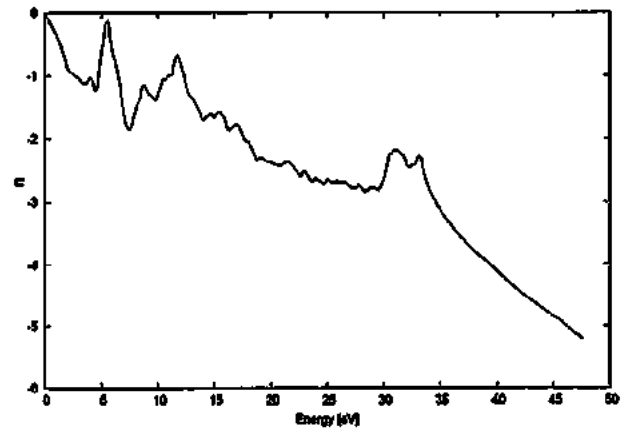

Figure 5.21 - My Refractive index spectra for $Zn_{0.50}Cd_{0.50}O$-ZB in the Wu-Cohen GGA scheme

Table 5.3 - My statistics for $Zn_{0.50}Cd_{0.50}O$-ZB in the Wu-Cohen GGA scheme

Contemporary Research Work			
$Zn_{0.50}Cd_{0.50}O$-ZB Compound			
ELEMENT	SYMBOL WITH UNIT	THIS WORK	OTHERS WORK
Scheme	GGA	Wu-Cohen GGA	
Phase	ZB	Zincblende	
Space Group	SG	115_P-43m	
Muffin-Tin Radius	R_{MT} (au)	Zn = 1.78 Cd = 1.78 O = 1.58	
Optimal Volume	V_o $(au)^3$	383.90	
Lattice Constant	a (Å)	4.84	
Bulk Modulus	B_o (GPa)	119.92	
Derivative of Bulk Modulus	B_o' (GPa)	4.20	
Optimal Energy	E_o (Ry)	-15082.57	
Band Gap	BG / E_g (eV)	0.09	1.65 [153] 0.0 [154]
Dielectric Function	Real Part of DF = $\varepsilon_1(\omega)$ Imaginary Part = $\varepsilon_2(\omega)$	3.65 at 2.2 eV 2.5 at 4.9 eV	5.3 at 9.7 eV [153]
Total Density of States	TDOS (e^- states/eV)	Zn 3d = 60 at - 5.8 eV O 2p = 16 at -17 eV	Zn 3d = 7.2 at -9.1 eV O 2p = 6.6 at -5.6 eV [153]
Joint Density of States	JDOS (e^- states/eV)		
Conductivity	C $(\Omega^{-1}cm^{-1})$	1.6 at 31 eV	
Energy Loss Function	L (eV)	1.18 at 5 eV	
Refractive Index	n	-2.8 at 28.3 eV	

5.2.3. $Zn_{0.25}Cd_{0.75}O$ Alloy

5.2.3.1. Structural Properties

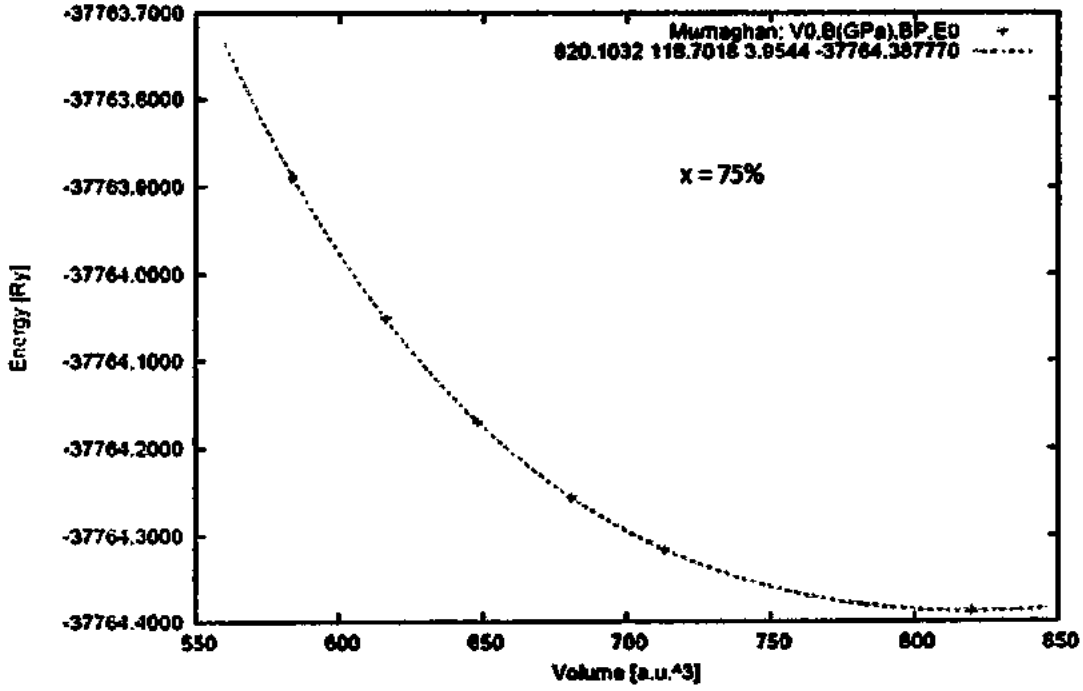

Figure 5.22 - Volume optimization for the zinc blende $Zn_{0.25}Cd_{0.75}O$ compound

5.2.3.2. Electronic Properties

5.2.3.2.1. Charge Density

We computed the volume charge density for the $Zn_{0.75}Cd_{0.25}O$ alloy in the ZB phase along the (110) plane applying the Wu-Cohen GGA scheme shown in Figure 5.23(a). Figure 5.23(b) gives the contour plot for the $Zn_{0.25}Cd_{0.75}O$ alloy indicating the collection of electrons along the Zn-O and Cd-O bonds and deflect towards the O atom due to electronegativity differences among Zn, Cd and O atoms. The O atoms bond covalently with both the Zn and Cd atoms with strong ionic behavior such that the Zn-O bond is weaker than Cd-O one. Both the figures have been combined in Figure 5.23(c).

At plane (110):

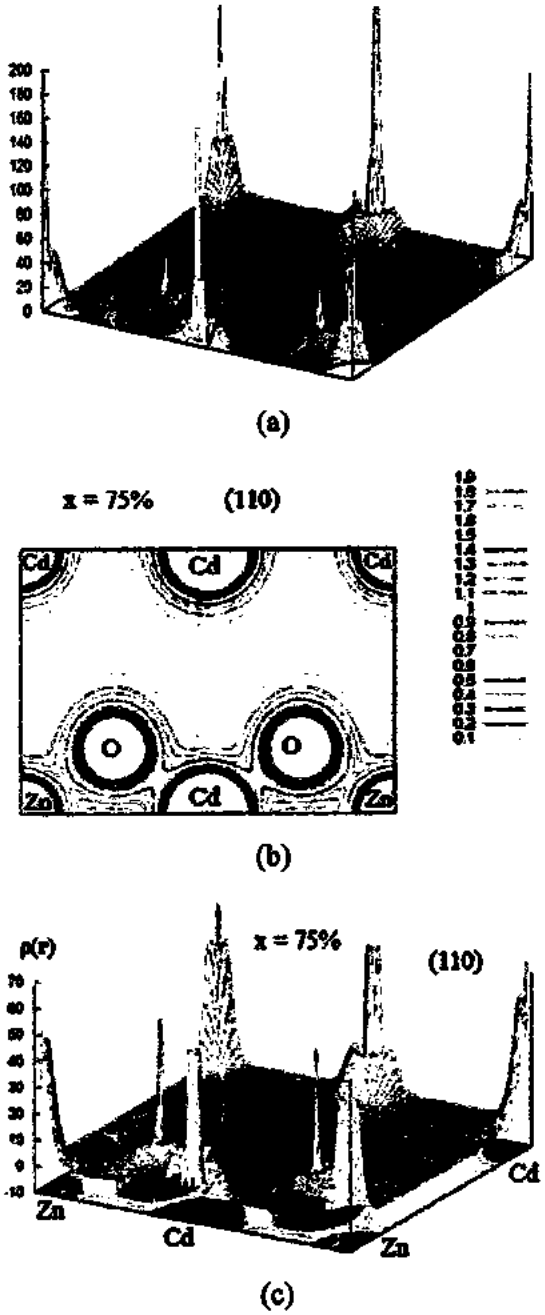

Figure 5.23 - (a) My 3D plot of $Zn_{0.25}Cd_{0.75}O$ in the ZB phase for the electron density ρ(r) at plane (110) in the Wu-Cohen GGA, (b) Relevant contour plot and (c) Combined 3D and contour plots

5.2.3.2.2. Density of States

The density of states (DOS) is computed for analyzing the bonding character and hybridization in zinc blende $Zn_{0.25}Cd_{0.75}O$. The bonding character offers the semiconducting behavior as shown in the figure below. The maximum peak value of the Zn-d states is 44.7 at -4.8 eV while that of the O-p states is 44.5 at -2 eV. There is negligible orbital hybridization at -0.49 eV between Zn 3d- and O 2p-states which had no effect on the band gap (BG) value of $Zn_{0.50}Cd_{0.50}O$ due to increase in x.

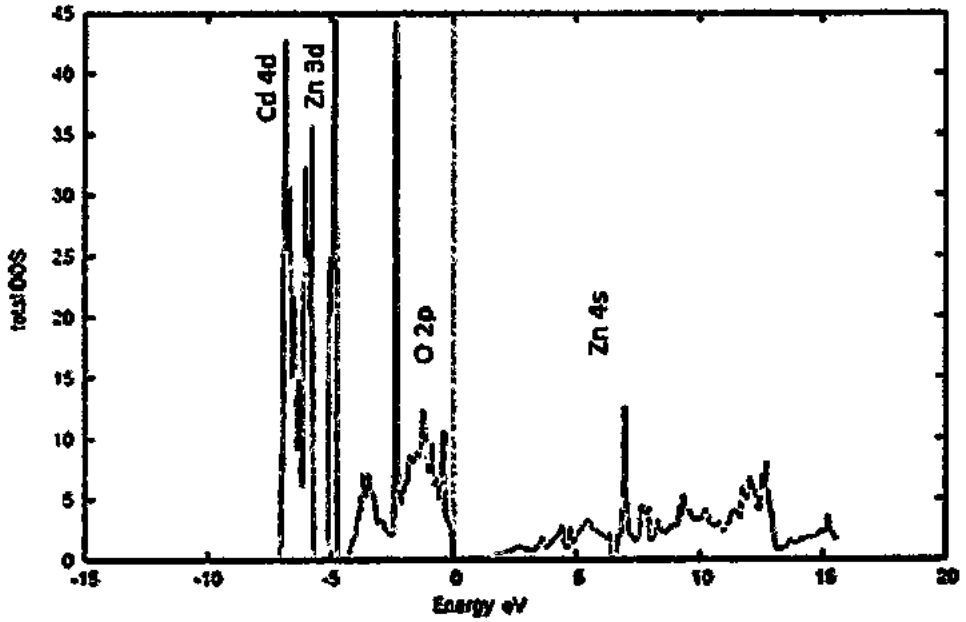

Figure 5.24 - My computed total density of states (TDOS) of the zinc blende $Zn_{0.25}Cd_{0.75}O$ compound in the Wu-Cohen GGA scheme

5.2.3.2.3. Band Structure

The band structure of the zinc blende $Zn_{0.25}Cd_{0.75}O$ alloy was determined by the WIEN2k program applying the Wu-Cohen GGA scheme. The valence and conduction bands overlap at the Fermi energy E_F in the GGA scheme due to the doping of Cd at 75% in ZnO showing that the $Zn_{0.25}Cd_{0.75}O$ alloy is of the metallic nature according to Figure 5.25.

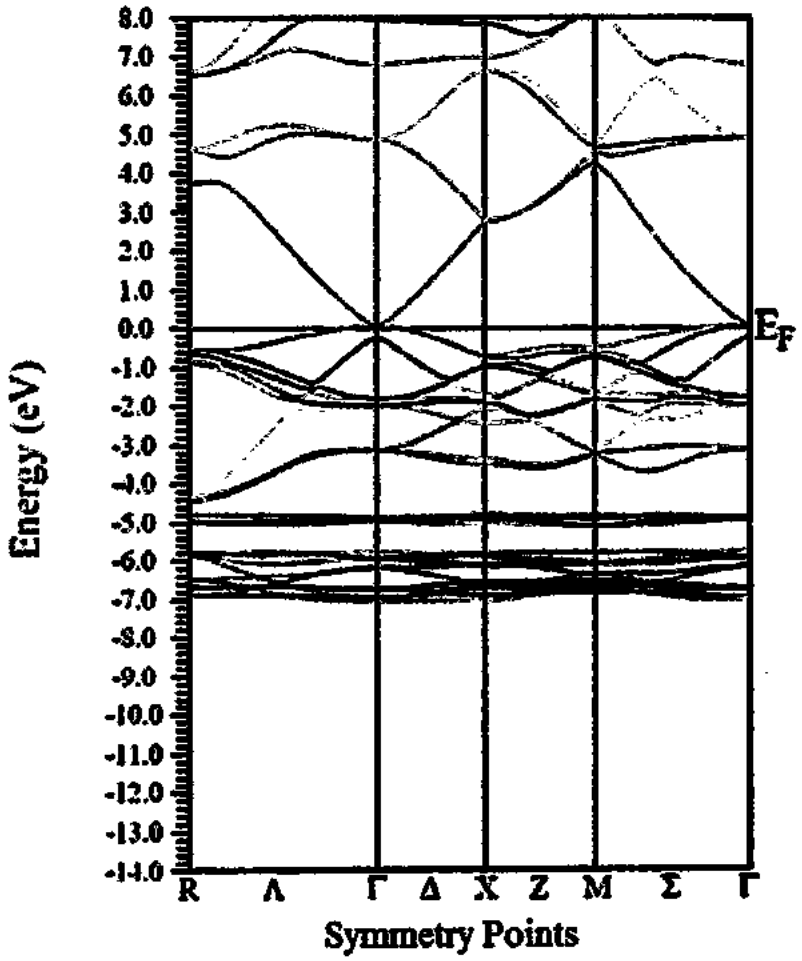

Figure 5.25 - My computed band structure of the zinc blende $Zn_{0.25}Cd_{0.75}O$ compound in the Wu-Cohen GGA scheme

5.2.3.3. Optical Properties

5.2.3.3.1. Dielectric Function

The dielectric function helps us determine the optical properties of the zinc blende $Zn_{0.25}Cd_{0.75}O$ compound. The imaginary part $\varepsilon_2(\omega)$ of the dielectric function increases slightly in the energy range of 9-14.7 eV. It has the maximum value of 2.83 at 14.6 eV and then falls immediately after it. The real part $\varepsilon_1(\omega)$ of the dielectric function has the extreme value of 3.77 at 1.5 eV and then quickly decreases after it up till the minimum value of -0.8 for x = 75% as shown in Figure 5.26.

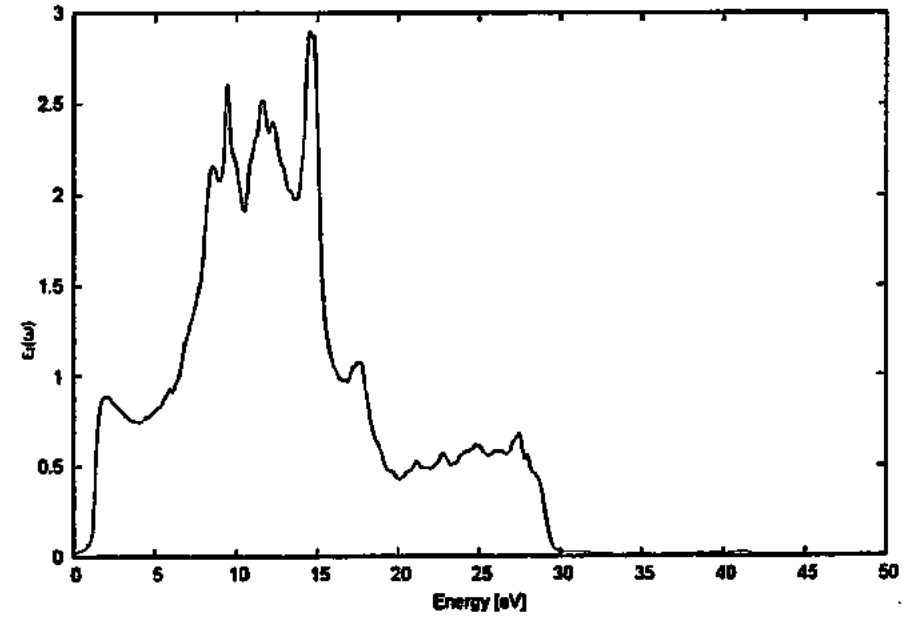

(a)

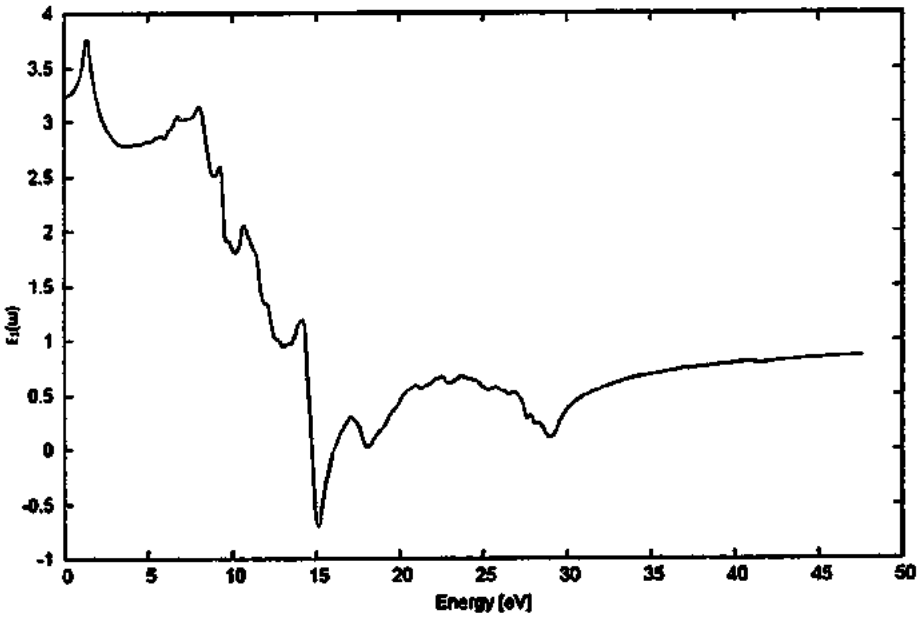

(b)

Figure 5.26 - (a) Imaginary part $\varepsilon_2(\omega)$ of the dielectric function for $Zn_{0.50}Cd_{0.75}O$ in the ZB phase in the Wu-Cohen GGA scheme and (b) Real part $\varepsilon_1(\omega)$ of the dielectric function

5.2.3.3.2. Joint Density of States

The excited state may be expressed as the joint density of states (JDOS) between the valence and conduction bands of the zinc blende $Zn_{0.25}Cd_{0.75}O$ compound. The maximum peak value of the JDOS is 3.5 at 14.5 eV. Then it slightly increases from 9-14.5 eV in the low energy range and then sharply decreases after it for x = 0.75 as in the following figure:

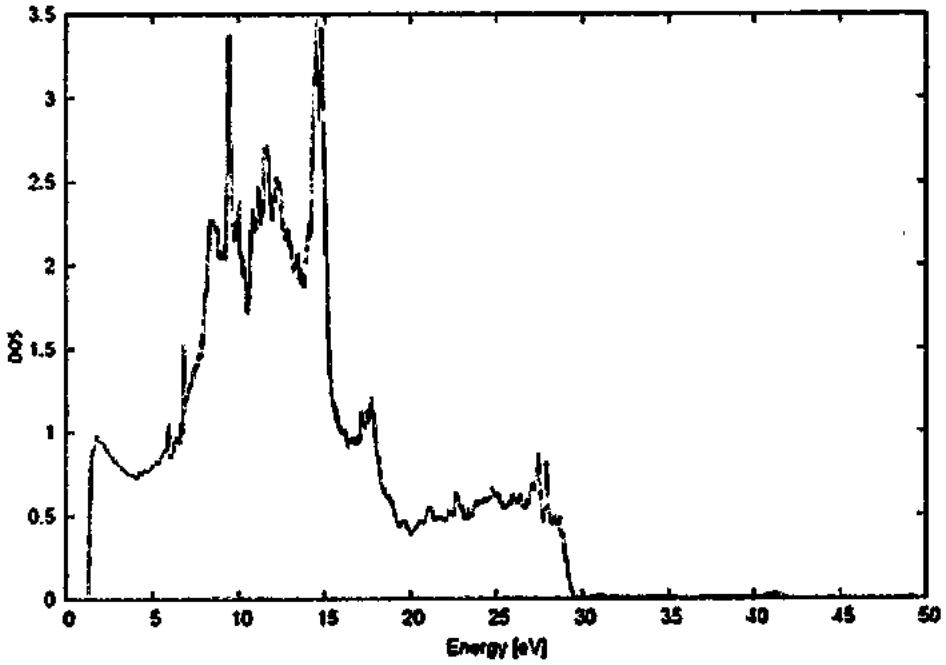

Figure 5.27 - My joint density of states (JDOS) for the zinc blende $Zn_{0.25}Cd_{0.75}O$ compound in the Wu-Cohen GGA scheme

5.2.3.3.3. Conductivity

Figure 5.28 describes the effect on the conductivity C of the zinc blende $Zn_{0.25}Cd_{0.75}O$ alloy. We see that the cadmium (Cd) concentration x is invisible in the low energy range. The conductivity slightly increases from 9-15 eV and then quickly decreases after it with respect to the variation of $\varepsilon_2(\omega)$. The maximum peak value is 5.2 at 14.7 eV as displayed in Figure 5.28:

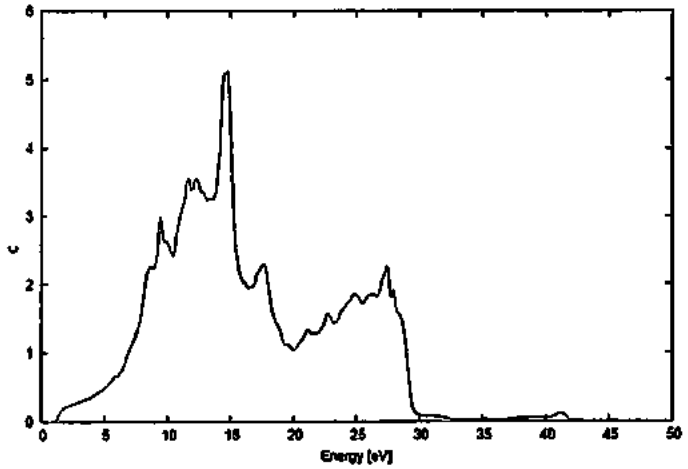

Figure 5.28 - **My computed conductivity for the zinc blende $Zn_{0.25}Cd_{0.75}O$ alloy in the WC GGA**

5.2.3.3.4. Energy Loss Function

The energy loss function L describes the loss of energy when a fast electron moves in the zinc blende $Zn_{0.25}Cd_{0.75}O$ alloy. The peaks of 1.65 eV at 18.7 eV and 3.85 eV at 29 eV in L are the plasma resonance peaks assigning the points of the transition from the metallic property to the dielectric properties of the system. The doping of Cd for x = 75% in ZnO induces the blue shift of the 29 eV peak with a slight decrease in L as shown in the following figure:

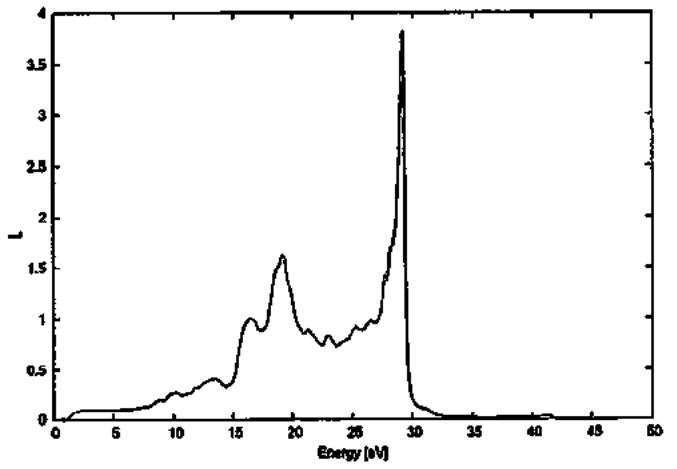

Figure 5.29 - **My computed energy loss function for the zinc blende $Zn_{0.25}Cd_{0.75}O$ compound in the Wu-Cohen GGA scheme**

5.2.3.3.5. Refractive Index

The refractive index n of zinc blende $Zn_{0.25}Cd_{0.75}O$ alloy helps in modeling and designing devices exactly. We analyze in the following figure that refractive index n enhances in the low energy range indicating decrease in band gap of the system. It is due to the doping of Cd into ZnO which may raise s-states in conduction band resulting in increase in optical transition between the uppest valence and the lowest conduction bands in $Zn_{0.25}Cd_{0.75}O$. The maximum value of n comes out to be 1.35 at 15 eV. The peak relates to the optical transition near the band gap.

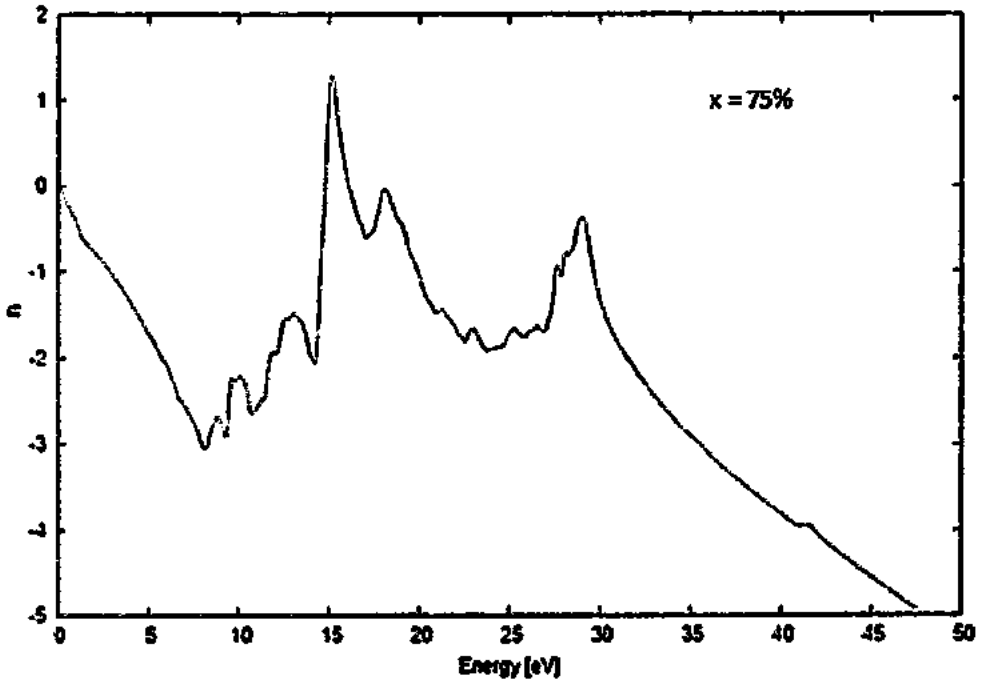

Figure 5.30 - **My computed refractive index spectra for the zinc blende $Zn_{0.25}Cd_{0.75}O$ compound by the Wu-Cohen GGA scheme**

Table 5.4 - My data for the zinc blende $Zn_{0.25}Cd_{0.75}O$ compound in the Wu-Kohn GGA scheme

Current Research Work			
$Zn_{0.25}Cd_{0.75}O$-ZB			
ELEMENT	SYMBOL WITH UNIT	THIS WORK	OTHERS WORK
Scheme	GGA	Wu-Cohen GGA	
Phase	ZB	Zincblende	
Space Group	SG	215, P-43m	
Muffin-Tin Radius	R_{MT} (au)	Zn = 1.78 Cd = 1.78 O = 1.58	
Optimal Volume	V_o $(au)^3$	820.10	
Lattice Constant	a (Å)	4.96	
Bulk Modulus	B_o (GPa)	118.70	
Derivative of Bulk Modulus	B_o' (GPa)	3.95	
Optimal Energy	E_o (Ry)	-37764.39	
Band Gap	BG / E_g (eV)	0.0	1.28 [153]
Dielectric Function	Real Part of DF = $\varepsilon_1(\omega)$ Imaginary Part = $\varepsilon_2(\omega)$	3.77 at 1.5 eV 2.8 at 14.2 eV	 2.7 at 9.3 eV
Total Density of States	TDOS (e^- states/eV)	Cd 4d = 48 at -7 eV Zn 3d = 36 at -6 eV O 2p = 17 at -1.5 eV	Cd 4d = 3.7 at -10.4 eV Zn 3d = 3.8 at -8.4 eV O 2p = 3.74 at -6.2 eV [153]
Joint Density of States	JDOS (e^- states/eV)	3.45 at 14.3 eV	
Conductivity	C $(\Omega^{-1}cm^{-1})$	5.2 at 14 eV	
Energy Loss Function	L (eV)	3.85 at 28 eV	
Refractive Index	n	1.35 at 15 eV	

5.3. CONCLUSIONS

We applied the FP-LAPW method under the DFT to investigate the structural, electrical and optical properties of the $Zn_{1-x}Cd_xO$ tertiary compounds in the zinc blende (ZB/B_3) phase fabricated from zinc oxide (ZnO) by its doping with cadmium (Cd) under the GGA scheme, especially the Wu-Cohen GGA scheme by considering the 3d-states of zinc (Zn) as the valence states of the electrons.

The first-principles formalism was applied to investigate the mentioned properties of the ZnO binary compound and the $Zn_{1-x}Cd_xO$ ternary alloys. We find that the structural parameters are in nice accordance with the experimental results. The values of our calculated band structure are in good agreement with the experimental and theoretical calculations.

Our calculated value of the volume optimization $V_o = 23.5$ $(Å)^3$ computed by the Wu-Cohen GGA is 5.47% and 4.66% less than the theoretical and experimental values of 24.86 and 24.65 $(Å)^3$ respectively. The lattice constant a = 4.54 Å is 1.94% and 1.73% less than the theoretical and experimental ones as 4.63 and 4.62 Å respectively, which is very accurate. The corresponding value of the bulk modulus $B_o = 156.36$ GPa is 16.92% greater than the theoretical value of 133.73, and its derivative $B_o' = 4.83$ GPa is 0.83% larger than the theoretical value of 4.79 GPa for ZnO, which are in enough accordance with the theoretical results. The density of states (DOS) and the corresponding direct band gap (BG) of 0.62 eV which is 4.61% and 81.98% less than the theoretical and experimental values of 0.65 and 3.44 eV respectively, very close to the theoretical value reveal that ZnO is a semiconductor.

We also observe that the lattice constant *a* in the $Zn_{1-x}Cd_xO$ compounds went on increasing with the increase in the concentration x of Cd while the bulk modulus was monotonically decreasing and its derivative as well. As we increased x from 25% to 75% in the ZnO compound, the band gap of the $Zn_{1-x}Cd_xO$ compounds decreased from 0.62 eV to 0.0 eV.

Then we studied the electron charge density $\rho(r)$, DOS and BG of the $Zn_{1-x}Cd_xO$ alloys to observe the bonding character and orbital hybridization. The bonding character of $Zn_{1-x}Cd_xO$ alloys revealed that the $Zn_{0.75}Cd_{0.25}O$ alloy possesses the semiconductor behavior while the BG indicates that the $Zn_{0.50}Cd_{0.50}O$ and $Zn_{0.25}Cd_{0.75}$ alloys are metallic in nature. The orbital hybridizations happen in the $Zn_{1-x}Cd_xO$ compounds.

In the optical analysis of the $Zn_{1-x}Cd_xO$ alloys, we found that the imaginary part of the dielectric function first decreased for x = 50% and then increased for x =75% with the increase in the energy with respect to the increase in x while the real one happened correspondingly; the total density of states (TDOS) first increased for x = 50% and then decreased for x = 75% shifting the curves towards the low energy range; joint density of states (JDOS) decreased with the decrease in the energy; the conductivity fell down for x = 50% and then enhanced for x = 75% with the fall of the energy; the energy loss function decreased for x = 50% and then enhanced for x =75% with an increment in the energy; and the refractive index increased first decreased for x = 50% and then increased with the decrease in the energy.

The optical transition between the uppermost valence band and the lowest conduction band was found to be shifted to the low energy range with the increasing concentration x of cadmium. Also, the $Zn_{1-x}Cd_xO$ compounds proved metastable

REFERENCES

[1]. B. Amrani, Rashid Ahmed and F. El Haj Hassan; "Structural, electronic and thermodynamic properties of wide band gap $Mg_xZn_{1-x}O$ alloy", Computational Material Science; Vol. 40; PP. 66-72; 2007.

[2]. H. S. Kang, J. W. Kim, J. H. Kim, S. Y. Lee, Y. Li, Jang Sik Lee, J. K. Lee, M. A. Nastasi, S. A. Crooker and Q. X. Jia; "Optical properties and Stoke's shift of $Zn_{1-x}Cd_xO$ thin films depending on Cd content", Journal of Applied Physics; Vol. 99; Issue No. 6; Id. No. 066113; PP. 1-3; 2006.

[3]. A. Schleife, F. Fuchs, J. Furthmüller and F. Bechstedt; "First-principles study of ground- and excited-state properties of MgO, ZnO and CdO polymorphs", Physical Review B; Vol. 73; Id. No. 245212; PP. 1-14; 2006.

[4]. A. Hernandezbattez, R. Gonzalez, J. Viesca, J. Fernandez, J. Diazfernandez, A. Mac Hado, R. Chou and J. Riba; "CuO, ZrO_2 and ZnO nanoparticles as antiwear additive in oil lubricants", Wear; Vol. 265; P. 422; 2008.

[5]. C. Palache, H. Berman and C. Frondel; "For ZINC in the composition", Dana's System of Mineralogy, Ver. I; 7th Ed.; PP. 504-506; 1944.

[6]. Windholz M.; "Occupational Safety and Health Guideline for Zinc Oxide", Windholz M. Ed. 1983; Windholz Index 10th Ed.; P. 1457; NLM; 1992.

[7]. Kiyoshi Takahashi, Akihiko Yoshikawa and Adarsh Sandhu; "Wide bandgap semiconductors: fundamental properties and modern photonic and electronic devices" Springer; P. 357; 2007.

[8]. Fierro, J. L. G.; "Metal Oxides: Chemistry & Applications", ChemPhysChem; Vol. 8; Iss. No. 4; PP. 617-618; March 2007.

[9]. Claus F. Klingshirn, Bruno K. Meyer, Andreas Waag, Axel Hoffmann and Johannes M. Geurts; "Zinc Oxide: From Fundamental Properties Towards Novel Applications Series", Springer Series in Materials Science; Vol. 120; PP. 9-10; July 2011.

[10]. Baruah, S. and Dutta, J.; "Hydrothermal growth of ZnO nanostructures", Sci. Techno. Adv. Mater.; IOP Science; Vol. 10; Iss. No. 1; Id. No. 13001; PP. 1-19; 2009.

[11]. François Cardarelli; "Strukturbericht, the original crystallographic reports from 1919-1939 (Volumes 1-8) published in Germany", Materials Handbook: A Concise Desktop Reference; 2nd Ed.; Springer; P. 878; 2008.

[12]. O. Madelung, U. Rossler and M. Schulz; "Semiconductors: II-VI and I-VII Compounds, Semimagnetic Compounds", Landolt-Bornstein's New Series; Group III: Condensed Matter; Vol. 41B; P. 357; Springer; 1999.

[13]. Deore, S. and Navrotsky, A.; "Oxide melt solution calorimetry of sulfides: Enthalpy of formation of sphalerite, galena, greenockite, and hawleyite", American Mineralogist; Vol. 91; PP. 400-403; 2006.

[14]. L. Kantorovich; "Quantum Theory of the Solid State", An Introduction Series: Fundamental Theories of Physics; Vol. 136; Springer; P. 32; 2004.

[15]. J. K. Cockcroft and A. N. Fitch; "The solid phases of sulphur hexafluoride by powder neutron diffraction", Journal of Crystallography; Vol. 184; PP. 123-145; 1988.

[16]. Özgür, Ü.; Alivov, Ya. I.; Liu, C.; Teke, A.; Reshchikov, M. A.; Doğan, S.; Avrutin, V. and Cho, S. J.; "A comprehensive review of ZnO materials and devices", J. Appl. Phys.; Vol. 98; Issue 4; Id. No. 041301; PP. 4; 2005.

[17]. Abrahams, S. C. and Bernstein, J. L.; "Accuracy of an automatic diffractometer. Measurement of the sodium chloride structure factors", Acta Cryst.; Vol. 18; No. 5; PP. 926-932; 1965.

[18]. D. C. Look, J. W. Hemsky and J. R. Sizelove; "Residual Native Shallow Donor in ZnO", Physical Review Letters; Vol. 82; Issue 12; PP. 2552-2555; 1999.

[19]. A. Janotti and C. G. Van De Walle; "Hydrogen 112tilizing112112 bonds", Nature Materials; Vol. 6; No. 1; P. 44; 2007.

[20]. Kato, H.; "Growth and characterization of Ga-doped ZnO layers on a-plane sapphire substrates grown by molecular beam epitaxy", Journal of Crystal Growth; Vols. 237–239; Part 1; PP. 538-543; 2002.

[21]. Takeshi Ohgaki, Naoki Ohashi, Shigeaki Sugimura, Haruki Ryoken, Isao Sakaguchi, Yutaka Adachi and Hajime Haneda; "Positive Hall coefficients obtained from contact misplacement on evident n-type ZnO films and crystals", Journal of Materials Research; Vol. 23; No. 9; PP. 2293-2295; 2008.

[22]. Wagner, P. and Helbig, R.; "Hall effect and anisotropy of the electron mobility in ZnO", Journal of Physics and Chemistry of Solids; Vol. 35; P. 327; 1974.

[23]. Y. R. Ryu, T. S. Lee and H. W. White; "Properties of arsenic-doped p-type ZnO grown by hybrid beam deposition", Applied Physics Letters; Vol. 83; P. 87; 2003.

[24]. Robert F. Service; "Will UV Lasers Beat the Blues?", Science; Vol. 276; No. 5314; P. 895; 1997.

[25]. W. I. Park, S. J. An, G. C. Yi and H. M. Jang; "Metal-organic vapor phase epitaxial growth of high-quality ZnO films on $Al_2O_3(00{\cdot}1)$", Journal of Materials Research; Cambridge University Press; Vol. 16; Issue 5; PP. 1358-1362; 2001.

[26]. Bakin, A. et al.; "ZnO – GaN Hybrid Heterostructures as Potential Cost Efficient LED Technology", Proceedings of the IEEE; Vol. 98; No. 7; PP. 1281–1287; 2010.

[27]. Look, D.; "Recent advances in ZnO materials and devices", Materials Science and Engineering B; Vol. 80; P. 383; 2001.

[28]. Kucheyev, S. O. et al.; "Ion-beam-produced structural defects in ZnO", Phys. Rev. B; Vol. 67; Issue 9; No. 094115; PP. 1-11; 2003.

[29]. R. H. Dicke; "Coherence in Spontaneous Radiation Processes", Phys. Rev.; Vol. 93; P. 99; Jan. 1954.

[30]. R. Bonifacio, P. Schwendimann and F. Haake; "Quantum Statistical Theory of Superradiance I", Phys. Rev. A; Vol. 4; P. 302; Jul. 1971.

[31]. Byeong-Yun Oh, Min-Chang Jeong, Tae-Hyoung Moon, Woong Lee, Jae-Min Myoung, Jeoung-Yeon Hwang and Dae-Shik Seo; "Transparent conductive Al-doped ZnO films for liquid crystal displays", J. Appl. Phys.; Vol. 99; Issue 12; No. 124505; PP. 1-4; 2006.

[32]. Porter, Frank C.; "Zinc metal is produced using extractive metallurgy", Zinc Handbook; CRC Press; PP. 8-29; 1994.

[33]. Y. B. Li, Y. Bando and D. Golberg,; "ZnO nanoneedles with tip surface perturbations: Excellent field emitters", Applied Physics Letters; Vol. 84; Issue 18; No. 3603; PP. 1-3; 2004.

[34]. Y. W. Heo, L. C. Tien, Y. Kwon, D. P. Norton, S. J. Pearton, B. S. Kang and F. Ren; "Depletion-mode ZnO nanowire field-effect transistor", Applied Physics Letters; Vol. 85; Issue 12; Id. No. 2274; PP. 1-3; 2004.

[35]. A. Che Mofor, A. El-Shaer, A. Bakin, A. Waag, H. Ahlers, U. Siegner, S. Sievers and M. Albrecht; "Magnetic property investigations on Mn-doped ZnO Layers on sapphire", Applied Physics Letters; Vol. 87; Issue 6; Id. No. 062501; PP. 1-3; 2005.

[36]. Andrea Dal Corso, Michel Posternak, Raffaele Resta and Alfonso Baldereschi; "Ab initio study of piezoelectricity and spontaneous polarization in ZnO", Physical Review B; Vol. 50; Issue 15; PP. 10715-10721; 1994.

[37]. Keim, Brandon; "Piezoelectric Nanowires Turn Fabric Into Power Source", Wired; Wired Science Tab; Uncategorized Report; February 13, 2008.

[38]. Y. Qin, X. Wang, and Z. L. Wang; "Editor's summary: Nanomaterial: power dresser", Nature; Vol. 451; PP. 809-813; 2008.

[39]. Kumar, S. Ashok and Chen, Shen-Ming; "Nanostructured Zinc Oxide Particles in Chemically Modified Electrodes for Biosensor Applications", Analytical Letters; Vol. 41; No. 2; PP. 141-158; 2008.

[40]. David R. Lide; "Magnetic susceptibility of the elements and inorganic compounds", Handbook of Chem. and Phys.; 81st Ed; CRC Press; PP. 130-135; 2000.

[41]. Arnold F. Holleman, Egon Wiberg and Nils Wiberg; "Cadmium (in German)", Textbook of Inorganic Chemistry; 91st - 100th Ed.; PP. 1056-1057; 1985.

[42]. D. A. Edwards, W. E. Wallace and R. S. Craig; "Magnesium-Cadmium Alloys. IV. The Cadmium-Rich Alloys; Some Lattice Parameters and Phase Relationships between 25 and 300°. Structure of the $MgCd_3$ Superlattice. Schottky Defects and the Anomalous Entropy[1]", J. Am. Chem. Soc.; Vol. 74; P. 5256-61; 1952.

[43]. Juame Duch Guillot, Richard Freedman and Sarah Donohoe; "Battery collection; recycling, nature protected", European Union Parliament Directive; PP. 24-25; 2006.

[44]. Scoullos, Michael J.; "Mercury, Cadmium, Lead: Handbook for Sustainable Heavy Metals Policy and Regulation", Environment & Policy Series; Springer; Vol. 31; PP. 104-116; 2001.

[45]. C. J. E. Smith, M. S. Higgs and K. R. Baldwin; "Advances to Protective Coatings and their Application to Ageing Aircraft", PP. 1-8; April 1999; RTO MP-25; Retrieved May 2011.

[46]. David Robarge; "Breaking Through Technological Barriers – Finding The Right Metal", Archangel: CIA's Supersonic A-12 Reconnaissance Aircraft; 2nd Ed.; Center for the Study of Intelligence (CSI) Publ.; P. 11-17; Jan. 2012.

[47]. Nambiar, K. R.; "Helium-cadmium Laser", LASERS: Principles, Types and Applications; PP. 488-490; 2006.

[48]. Tokunaga M., et al.; "Single molecule imaging of fluorophores and enzymatic reactions achieved by objective-type total internal reflection fluorescence microscopy" Biochem. Biophys. Res. Commun.; Vol. 235; PP. 47-53; 1997.

[49]. Bill von Ofenheim; "Cadmium Selenium Testing for Microbial Contaminants", NASA; Id. No. MSFC-0601303; P. 1; 2003.

[50]. Lee, Ching-Hwa and I, C. S.; "Recycling of Scrap Cathode Ray Tubes", Environmental Science and Technology; Vol. 36; No. 1, PP. 69-75; 2002.

[51]. Miller, L. S. and Mullin, J. B.; "Crystalline Cadmium Sulfide", Electronic materials: from silicon to organics; Springer; P. 273; 1991.

[52]. Fthenakis, V.; "Life Cycle Impact Analysis of Cadmium in CdTe PV Production", Renewable and Sustainable Energy Reviews; Vol. 8; No. 4; PP. 303-334; 2004.

[53]. Jennings, Thomas C.; "Cadmium Environmental Concerns", PVC Handbook; Hanser Verlag Publ.; P. 149; 2005.

[54]. D. W. Ma, Z. Z. Ye and Y. S. Yang; "Photoluminescent analysis of $Zn_{1-x}Cd_xO$ alloys" Appl. Phys. B; Vol. 82; PP. 85-87; 2006.

[55]. Irina A. Buyanova et al.; "Optical Characterization of ZnCdO Alloys Grown by Molecular-Beam Epitaxy", ECS Transactions; Vol. 3; Issue 5; PP. 391-398; 210th ECS Meeting: Mexico; Abstr. No. 1325; 2006.

[56]. M. H. N. Assadi et al.; "Theoretical study on copper's energetics and magnetism in TiO2 polymorphs", J. Appl. Phys.; Vol. 113; No. 23; P. 233913; 2013.

[57]. Tanja Van Mourik and Robert J. Gdanitz; "A critical note on density functional theory studies on rare-gas dimers", J. Chemic. Phys.; Vol. 116; No. 22; PP. 9620–9623; 2002.

[58]. Jiří Vondrášek, Lada Bendová, Vojtěch Klusák and Pavel Hobza; "Unexpectedly strong energy stabilization inside the hydrophobic core of small protein rubredoxin mediated by aromatic residues: correlated ab initio quantum chemical calculations", J. Am. Chemic. Soc.; Vol. 127; No. 8; PP. 2615-2619; 2005.

[59]. Grimme, Stefan; "Semiempirical hybrid density functional with perturbative second-order correlation", J. Chemic. Phys.; Vol. 124; Issue No. 3; Id. No. 034108; PP. 1-16; 2006.

[60]. Urs Zimmerli, Michele Parrinello and Petros Koumoutsakos; "Dispersion corrections to density functionals for water aromatic interactions", J. Chemic. Phys.; Vol. 120; No. 6; PP. 2693-2699; 2004.

[61]. Grimme, Stefan; "Accurate description of van der Waals complexes by density functional theory including empirical corrections", Journal of Computational Chemistry; Vol. 25; No. 12; PP. 1463-1473; 2004.

[62]. O. A. Von Lilienfeld, Ivano Tavernelli, Ursula Rothlisberger and Daniel Sebastiani; "Optimization of effective atom centered potentials for London dispersion forces in density functional theory", Phys. Rev. Letts.; Vol. 93; Issue 15; Id. No. 153004; PP. 1-4; 2004.

[63]. N. Argaman and G. Makov; "Density functional theory: An introduction", Am. J. Phys.; Vol. 68; Iss. No. 1; PP. 69-79; 2000.

[64]. Max Born and J. Robert Oppenheimer; "On the Quantum Theory of Molecules", Annals of Physics; Vol. 389; Iss. No. 20; PP.457-484; 1927.

[65]. P. Hohenburg and W. Kohn; "Inhomogeneous Electron gas" Phys. Rev.; Vol. 136; Issue 3B; PP. B864-B871; 1964.

[66]. M. Levy and J. P. Perdew; "The Constrained Search Formalism for Density Functional Theory, in Density Functional Methods in Physics", R. M. Dreisler and J. da Providencia Ed.; Plenum: New York; PP. 11-30; 1985.

[67]. Wilson, E. B. Jr.; "Four-dimensional electron density function", J. Chemic. Phys.; Vol. 36; PP. 2232-33; 1962.

[68]. Emili Besalú and Josep Martí; "Exploring the Rayleigh-Ritz Variational Principle", J. Chemic. Edu.; Vol. 75; No. 1; P. 105; 1998.

[69]. W. Kohn and L. J. Sham; "Self-Consistent Equations including Exchange and Correlation Effects", Phys. Rev.; Vol. 140; No. 4A; PP. A1133-A1138; 1965.

[70]. S. Cottenier; "The Kohn-Sham Equations", Density Functional Theory and the Family of (L) APW-methods: a step-by-step introduction; Institute for Kern and Radiation Physics; Catholic University of Louvain; Belgium; PP. 5-7; 2002.

[71]. N. M. Harrison; "An Itroduction to Density Functional Theory", Computational Materials Science; Richard Catlow and Eugene Kotomin Ed.; NATO Science Series III; IOS Press: Ohmsha; P. 197; 2003.

[72]. March, N. H; "Self-consistent fields in atoms; Hartree and Thomas-Fermi atoms", Pergamon Press: New York; PP.162-164; 1975.

[73]. P. A. M. Dirac; "Note on exchange phenomena in the Thomas-Fermi atom", Proc. Cambridge Phil. Roy. Soc.; Vol. 26; PP. 376-385; 1930.

[74]. R. G. Parr and W. Yang; "Density-Functional Theory of Atoms and Molecules", Oxford; Oxford University Press, New York; PP. 7-16; 1989.

[75]. E. H. Lieb; "Thomas-fermi and related theories of atoms and molecules", Rev. Mod. Phys.; Vol. 53; PP. 603-641; 1981.

[76]. B. L. Hammond, W. A. Lester Jr. and P. J. Reynolds; "Monte Carlo Methods in Ab Initio Quantum Chemistry", World Scientific; Singapore; 1994.

[77]. D. M. Ceperley and B. J. Alder; "Ground State of the Electron Gas by a Stochastic Method", Phys. Rev. Letts.; Vol. 45; PP. 566-569; 1980.

[78]. J. P. Perdew and A. Zunger; "Self-interaction correction to density-functional approximations for many-electron systems", Physical Review B; Vol. 23; Issue No. 10; PP. 5048-5079; 1981.

[79]. Von Barth, U. and Hedin, L.; "A local exchange-correlation potential for the spin polarized case", J. Phys. C: Solid State Phys.; Vol. 5; PP. 1629-1642; 1972.

[80]. S. H. Vosko; L. Wilk and M. Nusair; "Accurate spin-dependent electron liquid correlation energies for local spin density calculations: a critical analysis", Can. J. Phys.; Vol. 58; No. 8; PP. 1200-1211; 1980.

[81]. J. P. Perdew and Wang Yue; "Accurate and Simple Density Functional for the Electronic Exchange Energy: Generalized Gradient Approximation", Physical Review B Vol. 33, PP. 8800-8802; 1986.

[82]. E. K. U. Gross, C. A. Ullrich and U. J. Gossmann ; "Density functional theory of time-dependent systems", Density Functional Theory; Vol. 337; NATO ASI Series B; E. K. U. Gross and R. M. Dreizler Ed.; Plenum Press, New York; P. 149; 1995.

[83]. D. C. Langreth and M. J. Mehl; "Beyond the local-density approximation in calculations of ground-state electronic properties", Phys. Rev. B; Vol. 28; Issue 4; PP. 1809-1834; 1983.

[84]. J. P. Perdew; "Unified Theory of Exchange and Correlation Beyond the Local Density Approximation", Electronic Structure of Solids 91; P. Ziesche and H. Eschrig Ed.; Verlag Acad.; Berlin; PP. 11-20; 1991.

[85]. A. D. Becke; "Density-functional exchange-energy approximation with correct asymptotic behavior", Phys. Rev. A; Vol. 38; Issue 6; PP. 3098-3100; 1988.

[86]. C. Lee, W. Yang and R. G. Parr; "Development of the Colle-Salvetti correlation-energy formula into a functional of the electron density", Physical Review B; Vol. 37; Iss. No. 2; PP. 785-789; 1988.

[87]. R. O. Jones and O. Gunnarsson; "The density functional formalism, its applications and prospects", Rev. Mod. Phys.; Vol. 61; PP. 689-746; 1989.

[88]. M. D. Segall et al.; "First principles calculation of the activity of cytochrome P450", Phys. Rev. E; Vol. 57; PP. 4618-4621; 1998.

[89]. R. Shah, M. C. Payne, M. H. Lee and J. D. Gale; "Understanding the catalytic behavior of zeolites — a first-principles study of the adsorption of methanol", Science; Vol. 271; PP. 1395–1397; 1996.

[90]. M. J. Rutter and V. Heine; "Phonon free energy and devil's staircases in the origin of polytypes", J. Phys.: Cond. Matter; Vol. 9; PP. 2009-2024; 1997.

[91]. W. S. Zeng, V. Heine and O. Jepsen, "The structure of barium in the hexagonal close-packed phase under high pressure", J. Phys.: Cond. Matter; Vol. 9; PP. 3489-3502; 1997.

[92]. F. Kirchhoff et al.; "Structure and bonding of liquid Se", J. Phys.: Cond. Matter; Vol. 8; PP. 9353-9357; 1996.

[93]. R. Car and M. Parrinello; "Unified approach for molecular dynamics and density–functional theory", Phys. Rev. Letts.; Vol. 55; PP. 2471-2474; 1985.

[94]. Cramer, Christopher J.; "The Configuration Interaction Method", Essentials of Computational Chemistry; Chichester: John Wiley & Sons Ltd.; PP. 191–232; 2002.

[95]. W. Kohn, A. D. Becke and R. G. Parr; "Density functional theory of electronic structure", J. Phys. Chem.; Vol. 100; PP. 12974-12980; 1996.

[96]. V. L. Moruzzi, J. F. Janak, and A. R. Williams; "Density Functional Theory", Calculated Electronic Properties of Metals; Pergamon: New York; PP. 3-10; 1978.

[97]. G. Makov and M. C. Payne; "Periodic boundary conditions in ab initio calculations", Phys. Rev. B; Vol. 51, P. 4014-4022; 1995.

[98]. Z. Y. Zhang, D. C. Langreth and J. P. Perdew; "Planar-surface charge densities and energies beyond the local-density approximation", Phys. Rev. B; Vol. 41; PP. 5674-5684; 1990.

[99]. W. Kohn, Y. Meir and D. E. Makarov; "Van der Waals energies in density functional theory", Phys. Rev. Lett.; Vol. 80; PP. 4153-4156; 1998.

[100]. R. M. Dreizler and E. K. U. Gross; "Density Functional Theory for Relativistic Systems", Density Functional Theory: An Approach to the Quantum Many-Body Problem; Springer: Berlin; P. 245-269; 1990.

[101]. C. Speicher, R. M. Dreizler and E. Engel; "Density functional approach to quantum hadrodynamics: Theoretical foundations and construction of extended Thomas-Fermi models", Ann. Phys.; Vol. 213, Issue 2; PP. 312-354; 1992.

[102]. P. Blaha, K. Schwarz, G. Madsen, D. Kvasnicka and J. Luitz; "WIEN2k: An Augmented Plane Wave Plus Local Orbitals Program for Calculating Crystal Properties", User's Guide; Inst. of Phys. and Theor. Chem; Vienna University of Technology; Austria; PP. 8-10; Nov 2001; Revised Ed. 2002.

[103]. S. Cottenier; "The Pseudopotential Method (in brief)", Density Functional Theory and the Family of (L) APW-methods: a step-by-step introduction, Institute for Kern and Radiation Physics; Catholic University of Louvain; Belgium; PP. 11-13; 2002.

[104]. Slater, J. C.; "Wave Functions in a Periodic Potential", Physical Review; Vol. 51; No. 10; PP. 846-851; 1937. (Ref. 2) Slater, J. C.; "Energy Band Calculations by the Augmented Plane Wave Method", Advances in Quant. Chem.; Vol. 1, PP. 35-58, 1964.

[105]. S. Cottenier; "The APW Method", Density Functional Theory and the Family of (L)APW-methods: a step-by-step introduction; Institute for Kern and Radiation Physics; Catholic University of Louvain; Belgium; PP. 15-19; August 6, 2004.

[106]. S. Cottenier; "The LAPW Method", Density Functional Theory and the Family of (L)APW-methods: a step-by-step introduction; Institute for Kern and Radiation Physics; Catholic University of Louvain; Belgium; PP. 21-23; August 6, 2004.

[107]. Koelling D. D. and Harmon B. N.; "A technique for relativistic spin-polarised calculations", J. Phys. C: Sol. St. Phys.; Vol. 10; No. 16; P. 3107; 1977.

[108]. Mac Donald A. H., Pickett, W. E. and Koelling, D. D.; "A 120tilizing120 relativistic augmented-plane-wave method 120tilizing approximate pure spin basis functions", J. Phys. C; Vol. 13; No. 14; P. 2675; 1980.

[109]. J. P. Desclaux, N. Bessis and J. Picart; "Hyperfine-Structure Calculations for Atoms with the $(4p)^N$ Ground-State Configuration", Phys. Rev.; Vol. 187, Iss. No. 1; PP. 88-96; 1969.

[110]. O. K. Andersen; "Linear methods in band theory", Phys. Rev. B; Vol. 12; Iss. No. 8; PP. 3060-3083; 1975.

[111]. Koelling D. D. and Arbman G. O.; "Use of energy derivative of the radial solution in an augmented plane wave method: application to copper", J. Phys. F: Met. Phys.; Vol. 5; No. 11; P. 2041; 1975.

[112]. E. Wimmer, H. Krakauer, M. Weinert and A. J. Freeman; "Full Potential Self-consistent Linearized Augmented Plane Wave Method for Calculating the Electronic Structure of Molecules and Surfaces: O_2 Molecule," Phys. Rev. B; Vol. 24, Iss. 2; PP. 864-875; 1981.

[113]. Weinert M., Wimmer E. and Freeman A. J.; "Total-energy all-electron density functional method for bulk solids and surfaces", Phys. Rev. B; Vol. 26; Iss. No. 8; PP. 4571-4578; 1982.

[114]. Blaha P., Schwarz K. and Herzig P.; "First-Principles Calculation of the Electric Field Gradient of Li_3N", Phys. Rev. Letts.; Vol. 54; Issue 11; PP. 1192-1195; 1985.

[115]. Wei S. H., Krakauer H. and Weinert M.; "Linearized augmented-plane wave calculation of the electronic structure and total energy of tungsten", Phys. Rev. B; Vol. 32; Iss. No. 12; PP. 7792-7797; 1985.

[116]. L. F. Mattheiss and D. R. Hamann; "Linear-Augmented Plane-Wave Calculation of the Structural Properties of Bulk Cr, Mo and W", Physical Review B; Vol. 33; Iss. No. 2; PP. 823-840; 1986.

[117]. K. Schwarz and P. Blaha; "Description of an LAPW DF program (WIEN95)", Lecture Notes in Chemistry; Vol. 67; P. 139; 1996.

[118]. D. J. Singh and L. Nordstrom; "Plane waves, Pseudopotentials and the LAPW method", 2nd Ed.; Springer Inc.; NY: USA; PP. 1-134; 2006.

[119]. S. Cottenier; "The LAPW Method", Density Functional Theory and the Family of (L) APW-methods: a step-by-step introduction; Institute for Kern and Radiation Physics; Catholic University of Louvain; Belgium; Ch. 4; PP. 21-23; 2004.

[120]. Singh, D. J.; "Ground-state properties of lanthanum: Treatment of extended-core states", Phys. Rev. B; Vol. 43; Iss. No. 8; PP. 6388-6392; 1991.

[121]. E. Sjöstedt, L. Nordström and D. J. Singh; "An alternative way of linearizing the augmented plane-wave method", Solid State Commun.; Vol. 114; Iss. No. 1; PP. 15-20; 2000.

[122]. S. Cottenier; "The APW + lo Method", Density Functional Theory and the Family of (L) APW-methods: a step-by-step introduction; Institute for Kern and Radiation Physics; Catholic University of Louvain; Belgium; PP. 25-26; 2004.

[123]. Madsen G. K. H., Blaha P., Schwarz K., Sjöstedt E. and Nordström L.; "Efficient linearization of the augmented plane-wave method", Phys. Rev. B; Vol. 64; Iss. No. 19; Id. No. 195134; PP. 1-9; 2001.

[124]. Yu R., Singh D. and Krakauer H.; "All-electron and pseudopotential force calculations using the linearized-augmented-plane-wave method", Phys. Rev. B; Vol. 43; Iss. No. 8; PP. 6411-6422, 1991.

[125]. Kohler B., Wilke S., Scheffler M., Kouba R. and Ambrosch-Draxl C.; "Force calculation and atomic-structure optimization for the full-potential linearized augmented plane wave code WIEN", Comp. Phys. Commun.; Vol. 94; No. 1; PP. 31-48; 1996.

[126]. J. M. Soler and A. R. Williams; "Simple formula for the atomic forces in the augmented-plane-waves method", Phys. Rev. B; Vol. 40; Iss. No. 3; PP. 1560-1564; 1989.

[127]. Krimmel H. G., Ehmann J., Elsässer C., Fähnle M. and Soler J. M.; "Calculation of atomic forces using the linearized-augmented-plane-wave method", Phys. Rev. B; Vol. 50; Iss. No. 12; PP. 8846-8848; 1994.

[128]. Blöchl P. E., Jepsen O. and Andersen O. K.; "Improved tetrahedron method for Brillouin-zone integrations", Phys. Rev B; Vol. 49; Iss. No. 23; PP. 16223-16233; 1994.

[129]. Novák P., Boucher F., Gressier P., Blaha P. and Schwarz K.; "Electronic structure of the mixed valence system $(YM)_2BaNiO_5$ (M=Ca,Sr)", Phys. Rev. B; Vol. 63, Iss. No. 23; Id. No. 235114; PP. 1-8; 2001.

[130]. Kuneš J., Novák P., Schmid R., Blaha P. and Schwarz K.; "Electronic structure of fcc Th: Spin-orbit calculation with $6p_{1/2}$ local orbital extension", Phys. Rev. B; Vol. 64; Iss. No. 15; Id. No. 153102; PP. 1-3; 2001.

[131]. Stahn J., Pietsch U., Blaha P and Schwarz K.; "Electric-field-induced charge-density variations in covalently bonded binary compounds", Phys. Rev. B; Vol. 63; Iss. No. 16; Id. No. 165205; PP. 1-10; 2001.

[132]. Sofo J. and Fuhr J.; "Implementation of Bader theory in WIEN package", PP. 1-6; 2000...$WIENROOT/SRC/aim_sofo_notes.ps --- (Ref. 2) W. H. Press, S. A. Teuklosky, W. T. Vetterling and B. P. Flannery; "Numerical Recipes in C: The Art of Scientific Computing", Cambridge University Press, UK; P. 252; 1992.

[133]. Peter Weinberger; "Theoretical interpretation of the valence X-ray photoelectron spectrum of TiC", Theoreti. Chimica Acta; Springer; Vol. 44; No. 3; PP. 315-320; 1977.

[134]. Ambrosch-Draxl C., Majewski J. A., Vogl P. and Leising G.; "First-principles studies of the structural and optical properties of crystalline poly (para-phenylene)", Phys. Rev. B; Vol. 51; Iss. No. 15; PP. 9668-9676; 1995.

[135]. Abt R.; Ambrosch-Draxl C. and Knoll P.; "Optical response of high temperature superconductors by full potential LAPW band structure calculations", Physica B: Cond. Matter; Vol. 194; PP. 1451-1452; 1994.

[136]. F. Wooten; "Linear Response Functions and the Kramers-Kronig Relations", Optical Properties of Solids; Academic Press, NY and London; P. 173; 1972.

[137]. M. P. Allen; "Practical implementation of a DF-MD scheme: Basis set for the electronic orbitals and MD super cell", Computer Simulation in Chemistry and Physics; Kluwer Acad. Publ.; PP. 278-280; 1993.

[138]. N. Marzari, I. Souza and D. Vanderbilt; "An introduction to maximally-localized Wannier functions", Psi-K Sci. Highlight of the Month; Vol. 57; No. 12; PP. 138-141; 2003.

[139]. N. D. M. Hine, K. Frensch, W. M. C. Foulkes, and M. W. Finnis; "Supercell size scaling of density functional theory formation energies of charged defects", Phys. Rev. B; Vol. 79, P. 024112; Jan. 2009.

[140]. M. Cruz, M. R. Beltrán, C. Wang, J. Tagüeña-martínez and Yuri G. Rubo; "Supercell Approach to the Optical Properties of Porous Silicon", Phys. Rev. B; Vol. 59, PP. 15381-387; June 1999.

[141]. V. Luaña, M. Flórez, E. Francisco, A. M. Pendás, J. M. Recio, M. Bermejo and L. Pueyo; "Quantum Mechanical Cluster Calculations of Solids: The ab initio Perturbed Ion Method", Cluster Models for Surface and Bulk Phenomena; NATO ASI Series; Springer; Vol. 283, PP. 605-618; 1992.

[142]. R. Jones; "Ab initio cluster calculations of defects in solids", Philosophical Transactions: Physical Sciences and Engineering; Royal Society; Vol. 341; No. 1661; PP. 351-360; Nov. 1992

[143]. D. S. Mebane and J. H. Wang; "A General Method of Solution for the Cluster Variation Method in Ionic Solids, with Application to Diffusionless Transitions in Yttria-Stabilized Zirconia", J. Stat. Phys.; Vol. 139; No. 4; PP. 727-742; 2010.

[144]. P. Blaha, K. Schwarz, P. I. Sorantin and S. B. Trickey; "Full-potential, linearized augmented plane wave programs for crystalline systems", Comput. Phys. Commun.; Vol. 59; Iss. No. 2; PP. 399-415; 1990.

[145]. K. Schwarz and P. Blaha; "Solid state calculations using WIEN2k", Comput. Mater. Sci.; Vol. 28; No. 259; PP. 259-273; 2003.

[146]. P. Blaha, K. Schwarz, G. Madsen, D. Kvasnicka and J. Luitz; "WIEN2k - An Augmented Plane Wave Plus Local Orbitals Program for Calculating Crystal Properties", User's Guide; WIEN2k-13.1; Inst. of Physical and Theoretical Chemistry; Vienna University of Technology; Vienna: Austria; PP. 24-45; 26-06-2013.

[147]. F. D. Murnaghan; "The Compressibility of Media under Extreme Pressures", Proc. Natl. Acad. Sci.; USA; Vol. 30; PP. 244-247; 1944.

[148]. W. H. Bragg and J. A. Darbyshire "First Principles Study of Structural and Electronic Properties of $O_xS_{1-x}Zn$ Ternary Alloy", Joint Management Entrance Test; Vol. 6; P. 238; 1954.

[149]. Z. Charifi, H. Baaziz and A. H. Reshak; "Ab-initio investigation of structural, electronic and optical properties for three phases of ZnO compound", Physica Status Solidi (B); Vol. 244; Issue 9; PP. 3154-3167; September 2007.

[150]. A. S. Mohammadi et al.; "Density Functional Approach to Study Electronic Structure of ZnO Single Crystal", World Appl. Sci. Jour.; Vol. 14; No. 10; PP. 1530-1536; 2011.

[151]. K. Hummer; "Interband magnetoreflection of ZnO", Phys. Stat. Soli. B: Basic Solid State Physics; Vol. 56; 249-260; 1973.

[152]. X. D. Zhang, M. L. Guo, W. X. Li and C. L. Liu; "First-principles study of electronic and optical properties in wurtzite Zn1−xCdxO", J. Appl. Phys.; Vol. 103; No. 063721; PP. 1-6; 2008.

[153]. A. Schleife, C. Rödl, J. Furthmüller and F. Bechstedt; "Electronic ans optical propereties of $Mg_xZn_{1-x}O$ and $Cd_xZn_{1-x}O$ form ab initio calculations", New J. Phys.; IOP Science; Vol. 13; Id No. 085012; PP. 1-24; 2011.

[154]. Wang Zhi-Jun et al., "First-principles study of structure and corrected band properties of wurtzite Zn1-xCdxO and Zn1-xMgxO systems", Chinese Physics B; IOP Publ.; Vol. 18; No. 7; PP. 2992-96; 2009.